

Major Project Report

on

Optogenetic Modulation of Neural Activity in Alzheimer's
Disease Using Channelrhodopsin-2

Submitted in partial fulfillment of the requirements
of the degree of

MASTER OF ELECTRONICS

by

Aftab Anwar
22MEL002

Under the Supervision of
Dr Mukesh Pratap Singh



Department of Applied Sciences & Humanities
Faculty of Engineering & Technology
Jamia Millia Islamia
New Delhi-110025

June 2024

Major Project Report

on

Optogenetic Modulation of Neural Activity in Alzheimer's
Disease Using Channelrhodopsin-2

Submitted in partial fulfillment of the requirements
of the degree of

MASTER OF ELECTRONICS

by

Aftab Anwar
22MEL002

Under the Supervision of
Dr Mukesh Pratap Singh



Department of Applied Sciences & Humanities
Faculty of Engineering & Technology
Jamia Millia Islamia
New Delhi-110025

June 2024

CANDIDATE'S DECLARATION

I, AFTAB ANWAR, hereby, declare that the work which is being presented in this dissertation entitled "Optogenetic Modulation of Neural Activity in Alzheimer's Disease Using Channelrhodopsin-2" submitted in partial fulfillment of the requirements for the award of Degree of M.Sc. (Electronics), to the Department of Applied Sciences and Humanities, Faculty of Engineering and Technology, Jamia Millia Islamia, New Delhi- 110025, is an authentic record of my own work carried out during the project work under the supervision of Dr. Mukesh Pratap Singh.

I have presented the work/idea in my own words and where ever others ideas or words have been included; I have adequately cited and referenced the original sources. To the best of my knowledge, the matter embodied in this dissertation has not been submitted for the award of any other degree or diploma in any other Institute/University.

I also declare that I have adhered to all principles of academic honesty and integrity and have not misrepresented or fabricated or falsified any idea/data/fact/source in my submission. I understand that any violation of the above will be cause for disciplinary action by the Institute and can also evoke penal action from the sources which have thus not been properly cited or from whom proper permission has not been taken when needed. It is further stated that if at any later stage any plagiarism or any material of this dissertation found copied from the other's work/source, I will be solely responsible for that and I will abide by the rules of Intellectual Property Act, Govt. of India.

Date: 10 June 2024

Place: New Delhi

Aftab Anwar

CERTIFICATE

This is to certify that "AFTAB ANWAR" student of final semester of "MSc (Electronics)" has submitted MAJOR PROJECT REPORT entitled "Optogenetic Modulation of Neural Activity in Alzheimer's Disease Using Channelrhodopsin-2" in partial fulfillment for the requirements of the degree of Master of Science in electronics, Department of Applied Science & Humanities, Faculty of engineering & technology, JAMIA MILLIA ISLAMIA, NEW DELHI, in Session 2022-24. It has been found to be satisfactory and hereby approved for submission.

Dr Zishan Hussain Khan
Head of the Department

Dr. Mukesh Pratap Singh
Supervisor
Associate Professor

Acknowledgements

I would like to express my deepest gratitude to all those who have supported and guided me throughout the course of my research and the writing of this thesis.

First and foremost, I would like to thank my supervisor, Dr. Mukesh Pratap Singh, for his invaluable guidance, and encouragement, and for suggesting the fascinating field of optogenetics for my research. His insights and expertise have been instrumental in shaping this work.

I am also profoundly grateful to Dr. Sanjeev Kumar Mahato from the School of Biomedical Engineering at IIT BHU. His support and the opportunity he provided to study computational biology have been crucial to my academic development and the successful completion of this project.

A special thanks goes to Dr. Navaid Zafar Rizvi, whose guidance and advice have been essential in navigating the complexities of my project. His mentorship has been a constant source of inspiration and knowledge.

I would also like to express my sincere appreciation to Dr. Prabhash Mishra for his motivation and work support. His encouragement and practical assistance have significantly contributed to the progress and completion of this research.

I would also like to acknowledge all my colleagues and friends for their encouragement and support. Finally, I owe my deepest thanks to my family for their unwavering support and patience throughout my academic journey.

Thank you all for your contributions and belief in my work.

Aftab Anwar
22MEL002

Abstract

This thesis investigates the potential of channelrhodopsin-2 (ChR2) ion channels as a therapeutic intervention for Alzheimer's disease (AD) using computational modeling techniques. The study meticulously examines the dynamics of ChR2 under continuous light stimulation, employing a sophisticated four-state model. Enhancements to the model's accuracy are achieved through empirical adjustments, facilitating its application in AD research. The research explores the use of optogenetics, particularly ChR2, to modulate neuronal activity and restore synaptic plasticity, thereby addressing the synaptic dysfunction associated with AD. By integrating computational simulations with experimental data, the study provides insights into the mechanisms underlying synaptic dysfunction in AD and highlights the potential of optogenetic techniques to mitigate cognitive deficits. Additionally, the thesis incorporates a model that elucidates the impact of specific genetic factors on axonal spheroids and network defects in AD. By combining this model with simulations of ChR2 dynamics, the research aims to uncover the mechanisms of synaptic dysfunction in AD and explore novel therapeutic strategies. This comprehensive approach underscores the promise of ChR2 and optogenetic techniques in advancing our understanding and treatment of Alzheimer's disease.

Table of contents

Certificate	ii
Declaration	ii
Acknowledgement	iii
Abstract	iv
List of figures	viii
List of tables	xii
Nomenclature	xiii
1 Introduction	1
2 Optogenetic Toolbox	5
2.1 Intricacies of Neurons	6
2.1.1 Structure of Neurons	8
2.1.2 Types of Neurons	9
2.2 Ion Channels in Neurons	11
2.2.1 Voltage-Gated Ion Channels	12
2.2.2 Ligand-Gated Ion Channels	12
2.2.3 Mechanosensitive Ion Channels	12
2.2.4 Transient Receptor Potential (TRP) Channels	12
2.2.5 Light-Gated Ion Channels	12
2.3 Light-Sensitive Proteins in Optogenetics	13
2.3.1 Excitatory opsins	16
2.3.2 Inhibitory opsins	20
2.3.3 Step-function opsins	22
2.3.4 Ion selectivity	22

2.3.5	Opsin Pairs for Bidirectional Optogenetic Control	23
2.4	Gene expression	24
2.5	Illumination	25
2.6	Neuronal Signaling	26
2.6.1	Types of Neuronal Signaling	27
2.6.2	Signaling Pathways and Cellular Mechanisms	27
2.6.3	Integration of Signals and Network Dynamics	28
2.6.4	Implications for Neuroscience and Medicine	28
2.7	The clinical translation	28
2.7.1	Application	29
2.7.2	Apart from the brain	31
2.8	Hurdles and Challenges	32
3	Neuronal Modeling	36
3.1	Cell electrophysiology	37
3.1.1	The trans-membrane current	39
3.1.2	The axial current	43
3.2	The Dynamics of Neuronal Action Potentials	44
3.2.1	Voltage gated ion channels	45
3.3	The Hodgkin and Huxley model	46
4	Modeling of Channelrhodopsin-2	51
4.1	Photocycle Dynamics of Channelrhodopsin-2 (ChR2)	52
4.1.1	Initial Light Absorption	53
4.1.2	Intermediate States and Ion Channel Gating	54
4.1.3	Thermal Relaxation	57
4.1.4	Additional Points	58
4.2	Photocycle models	60
4.3	The 3-State ChR2 Model	63
4.4	The 4-State ChR2 Model	67
4.5	The 6-State ChR2 Model	71
4.5.1	ChR2 Model Implementation	75
4.6	Double Two-State ChR2 Model	77
5	Model Simulation and Results	84
5.1	ChR2 Model Simulation	86
5.1.1	Four-state model's simulation	87

5.1.2	Discussion	89
5.2	ChR2 H134R application in Alzheimer's disease	93
5.2.1	Methodology and Parameters	94
5.2.2	Results	97
5.3	Discussion	101
Conclusion		103
Future Work		105
Appendix A NEURON Simulator		107
Appendix B Python Environment for Computational Neuroscience		109
References		111

List of figures

2.1	Crystal structure determined by Kato in (2012)[92] provided the basis for the structural model of C1C2. The closed dark adapted conformation is reflected in the model. While helices H6 and H7 come from ChR2, helices H1–H5 come from ChR1. (a) the framed regions of interest within the overall protein structure. The green molecule in (b), which shows the retinal binding pocket, is the retina. (c) the pathway of ion permeation. (d) the inner gate. (f) the location of N a+ accumulations and (e) the central gate. The protein’s cavities, which may contain cations and water molecules, are shown in the grey wireframes. Reproduced from Schneider and colleagues (2015)[146].	14
2.2	Summary of various opsins including their activation peak wavelength, decay kinetics, and associated benefits, taken from Gerits and Vanduffel (2013).[49]	18
2.3	An illustration of a viral vector. Reproduced from Gerits and Vanduffel (2013)[49]	25
2.4	strategies for lighting that improve spatial specificity. (A) scanning using galvos. (b) using a digital micromirror for direct projection. (c) the projection of holography. (d) Activation by one or two photons. Reproduced from (Packer et al., 2013)[129].	26
3.1	Taken from Abbott and Dayan[2], this schematic illustration shows a portion of the cell membrane with two ion channels.	38
3.2	An electrotonically compact cell’s electric equivalent. Arrows are used to show different conductance levels.[145]	41
3.3	Neuronal Action Potential	45

3.4 Ion channels that are voltage-dependent are crucial for the operation of neurons. (a) The current-voltage ($I - V$) relationship for potassium (K^+) and sodium (Na^+) currents in these channels is non-linear. (a) They also show how transient and persistent current properties differ from one another. (c) Gate probabilities for K^+ and Na^+ currents provide additional insight into the behavior of these channels. The Hodgkin-Huxley model in MATLAB R2032b was used to construct these visualisations[2].	46
3.5 Action potential in accordance with the giant squid axon Hodgkin and Huxley model[82]. (A) APD. (b) single currents. (c) gate probabilities of matching currents, produced by MatlabR2023b and color-coded.	49
4.1 Figure 4.1(a) shows a model of the ChR2 photocycle, suggesting the photoactivation of two separate dark states (D480 and D470) with differing retinal geometries. This model includes five states each cycle and is based on results from differential infrared and UV/Vis spectroscopy. To allow for electrical measurements, an additional cycle is incorporated, and the transition between the two cycles takes place when late P480 photointermediates are present. Blue arrows indicate when the light is on. Figure 4.1(b), which was taken from Biophysics of Channelrhodopsin (Annual Review of Biophysics), 2015[146], depicts the retinal isomers.	59
4.2 The channelrhodopsin-2 photocurrent is depicted in Figure 4.2. (a), illustrating the response to a single 0.5-second light pulse. In Figure 4.2. (b), the peak recovery kinetics are shown, with light pulses represented by blue bars. These figures were generated using MatlabR2023b, with the model described in section 4.3.	60

4.3	The proposed models of the Channelrhodopsin-2 (ChR2) photocycle are depicted in Figure 4.3, each offering unique insights into the dynamics of ChR2 activation and deactivation. (a) A simplified three-state cycle model illustrates the transition from closed to open state, capturing the essential kinetics of ChR2 activation[77]. (b) An alternative model illustrates the desensitised state as an incidental response, elucidating the intricate relationship between desensitisation and channel opening[?]. (c) A cycle incorporating partial recovery through the desensitized state (D) offers a nuanced understanding of the transient and steady-state behaviors observed in ChR2 photocurrents[77]. (d, e) Additional models introduce a second light-dependent step, providing alternative mechanisms for ChR2 photoactivation with reduced efficiency[154]. (f, g) Four-state models, depicted as circular and branching structures, respectively, offer comprehensive representations of ChR2 dynamics, accounting for multiple intermediate states and transitions[125]. (h) A six-state model introduces two additional activation intermediates, providing further granularity to the ChR2 photocycle[67, 125].	61
4.4	Three-state model of ChR-2 photocycle.[124]	64
4.5	The cell's response to a light pulse is depicted as a time-dependent series, illustrating the number of open ion channels activated by light (i.e., light-activated currents) across various light intensities. The duration of the light pulse is set to 50 time units, equivalent to 1 second when considering a time unit of 20 ms (1/Pmax). Different relative light intensities are examined: 0.1, 0.2, 0.4, 0.6, and 1. Parameters $\Gamma_d = 1$ and $\Gamma_r = 0.15$ are utilized for the simulations[124].	66
4.6	The experimental results from Ishizuka et al.[86] and the theoretical predictions from Nikolic et al. 2006[124] are depicted in Figure 4.6, showcasing both the peak (open squares) and plateau currents (closed squares). The parameters were set to $g_d = 3$ and $g_r = 0.2$ [124].	67
4.7	The six-state model of the ChR2 photocycle.[66]	72

4.8	The graph presents the experimental validation of the six-state ChR2 model, implemented within the NEURON simulation environment by Grossman[66]. Experimental data is depicted in black, accompanied by error bars indicating standard deviation, while simulation results are highlighted in red. Panel (a) showcases photokinetic insights of ChR2 conductance, normalized to values acquired at 90 mW/mm ² . This includes the peak ChR2 current plotted against light intensity (top left), peak current recovery concerning inter-pulse interval (top right), and steady-state (plateau) ChR2 current relative to light intensity (bottom left). Additionally, the correlation between action potential (AP) latency and irradiance is explored in the bottom right panel. Panel (b) illustrates ChR2 photocurrent waveforms under diverse illumination scenarios, encompassing constant and pulsed illuminations across varying intensities. The scale bar denotes a long pulse lasting 50 ms at 0.25 nA and a pulse train lasting 200 ms at 0.5 nA.[66]	78
4.9	The proposed double two-state opsin model (22OM) with separation of open-closing mechanism and conductance change due to dark-light adaptation. The latter is captured in the mathematical R and S model state pair. DA and LA indicate dark and light adapted molecule states, respectively. O means open, C is closed and D is desensitized. Blue arrows indicate light dependent rates.[147]	80
5.1	Experimental traces in response to S1–S2 protocol, 3 s inter-pulse interval, the irradiance of 1.6 mW/mm ² , and holding voltages of 240 and 280 mV. Figure adapted from William et al [176].	90
5.2	Current response of ChR2 H134R model with a stimulus duration of 400 ms and an irradiance of 5.5 mW/mm ² shown for (a) MATLAB and (b) Python implementations.	91
5.3	A and B Light dependence of τ_R across four voltage values. C and D Voltage dependence of tR across three irradiance levels.	91
5.4	Schematic Diagram of the Axon in NEURON Simulator	96
5.5	Current propagation from one end to another end of the axon.	97
5.6	(a) In normal case when a neuron fires as in Alzheimer's case. (b) Increasing the signal frequency by activating the ChR2 ion channel causes an increase in frequency at the end of the Axon.	99
5.7	Increased frequency of the axon potential over a long period of 1500 ms for three stages of Alzheimer's.	100

List of tables

2.1	Benefits and obstacles for conversion to clinical use, along with potential solutions	35
3.1	Ion Concentrations and Equilibrium Potentials. Numbers adapted from An Introductory course in computational neuroscience book[117].	38
4.1	Parameter values for ChR2(H134R) model[176]	70
4.2	Empirical expressions for the flux-dependent transition rates[66]	76
4.3	Fitting parameters[66]	76
4.4	Parameters[147]	83
4.5	Parameters[147]	83
5.1	Simulation Parameters	87
5.2	Simulation Parameters	96

Nomenclature

Greek Symbols

α_n	Opening rate (1/s)
α_w	Opening rate (1/s)
β_n	Closing rate (1/s)
β_w	Closing rate (1/s)
γ	Ratio of high and low conductance states (O_2/O_1)
λ	Optical stimulation protocol $\Theta = 100I$
λ^{-1}	Inverse calcium decay time constant (1/s)
λ_{max}	Wavelength of maximal absorption for retinal (m)
μ	Length constant
σ_{ret}	Absorption cross-section for retinal (m^2)
τ	Time constant (s)
τ_{ChR2}	Time constant of ChR2 activation (s)
τ_{chron}	Chronaxie (s)
τ_{inact}	Inactivation time constant (s)
τ_{off}	Deactivation time constant (s)
τ_{on}	Activation time constant (s)
τ_r	Recovery time constant (s)

- τ_w Gating variable time constant (s)
 Θ Quantum efficiency for photon absorption

Other Symbols

- $[A^-]$ Concentration anion (μM)
 $[X]_i, [X]_{in}$ Intracellular concentration ion X (μM)
 $[X]_o, [X]_{out}$ Extracellular concentration ion X (μM)
 A Surface area (m^2)
 A^- Concentration anion (μM)
 C_m Membrane capacitance (F)
 c_m, c_A, c_S Specific capacitance (membrane, Axon, Soma in F/m^2)
 d Specific depth (m)
 e_1 ChR2 light dependent equilibrium, transition rates (1/s)
 e_2 ChR2 light dependent equilibrium, transition rates (1/s)
 E_l ChR2 light dependent equilibrium, transition rates (1/s)
 E_m Membrane equilibrium potential (mV)
 E_{ChR2} ChR2 reversal potential (mV)
 $E_{Na^+}, E_{K^+}, E_{Ca^{2+}}$ Ion specific Nernst potential (mV)
 E_{Na}, E_K, E_{Ca} Ion specific Nernst potential (mV)
 F Faraday's constant (C/mol)
 $G(V)$ Rectification function
 g_A Potassium type channel specific membrane conductance (S/m^2)
 g_h Calcium type channel specific membrane conductance (S/m^2)
 g_L Leakage channel specific membrane conductance (S/m^2)
 g_l Leakage channel specific membrane conductance (S/m^2)

g_m	Specific membrane conductance (S/m^2)
G_r	ChR2 deactivation transition rates ($1/\text{s}$)
g_T	Specific membrane conductance (S/m^2)
g_{AS}	ChR2 specific membrane conductance (S/m^2)
g_{Ca-K}	Axon and soma connecting specific conductance (S/m^2)
g_{Ca2+}	Ion channel specific membrane conductance (S/m^2)
g_{Ca}	Calcium type channel specific membrane conductance (S/m^2)
g_{Ca}	Ion channel specific membrane conductance (S/m^2)
$g_{ChR2,SFO}$	Ion channel specific membrane conductance (S/m^2)
g_{ChR2}	Ion channel specific membrane conductance (S/m^2)
G_{d1}	ChR2 deactivation transition rates ($1/\text{s}$)
G_{d2}	ChR2 deactivation transition rates ($1/\text{s}$)
G_{ion}	Ion conductance (S)
g_{K+}	Ion channel specific membrane conductance (S/m^2)
g_K	Ion channel specific membrane conductance (S/m^2)
$g_{l,A}$	Leakage channel specific membrane conductance (S/m^2)
$g_{l,S}$	Leakage channel specific membrane conductance (S/m^2)
g_{Na+}	Ion channel specific membrane conductance (S/m^2)
g_{Na}	Ion channel specific membrane conductance (S/m^2)
g_{SA}	Leakage channel specific membrane conductance (S/m^2)
hc	Product of Planck's constant and the speed of light ($\text{kg m}^3/\text{s}^2$)
I	Light intensity (W/m^2)
i_A	Potassium type channel specific current (A/m^2)
i_h	Calcium type channel specific current (A/m^2)

i_L	Leakage channel specific current (A/m ²)
i_l	Leakage channel specific current (A/m ²)
i_m	Specific transmembrane current (A/m ²)
I_p	Peak current (pA/pF)
i_T	Specific transmembrane current (A/m ²)
i_{AS}	ChR2 specific current (A/m ²)
i_{Ca-K}	Axon and soma connecting specific current (A/m ²)
i_{Ca2+}	Ion channel specific current (A/m ²)
i_{Ca}	Calcium type channel specific current (A/m ²)
i_{Ca}	Ion channel specific current (A/m ²)
$i_{ChR2,SFO}$	Ion channel specific current (A/m ²)
i_{ChR2}	ChR2 specific current (A/m ²)
i_{K+}	Ion channel specific current (A/m ²)
i_K	Ion channel specific current (A/m ²)
$i_{l,A}$	Leakage channel specific current (A/m ²)
$i_{l,S}$	Leakage channel specific current (A/m ²)
i_{Na+}	Ion channel specific current (A/m ²)
i_{Na}	Ion channel specific current (A/m ²)
I_{p1}	Steady-state current (pA/pF)
I_{p2}	Threshold average stimulating current
i_{SA}	Leakage channel specific current (A/m ²)
I_{SS}	Steady-state current (pA/pF)
$I_{th,avg}$	Threshold average stimulating current
k_1	ChR2 light dependent activation, transition rates (1/s)

k_2 ChR2 light dependent activation, transition rates (1/s)

M Concentration anion (μM)

P_- Permeability of ion

P_{Mj} Permeability of ion

P_X Permeability of ion

R The universal gas constant (J/(K mol))

R_m Membrane resistance (Ω)

R_{axial} Axial resistance (Ω)

S_{Rheo} Rheobase strength

S_{th} Threshold strength

T Temperature (K)

V, V_m, V_A, V_S Membrane potential (mV)

V_{m0} Resting membrane potential (mV)

w_∞ Gate variable steady-state function

w_{loss} Scaling factor for losses of photons due to scattering or absorption

z, z_X Valence of ion

Chapter 1

Introduction

Optogenetics holds considerable promise for treating neurological and psychiatric disorders, yet several significant challenges persist. These include optimizing light delivery to target neurons, ensuring the safety and effectiveness of optogenetic treatments, and translating preclinical results into clinically applicable therapies. Despite these hurdles, ongoing research in optogenetics is enhancing our comprehension of brain function and provides hope for developing innovative therapeutic approaches for various neurological and psychiatric conditions.

The primary focus of this master's thesis is the widely studied opsin channelrhodopsin-2 (ChR2), which originates from the algae species *Chlamydomonas reinhardtii*[123]. The dissertation also looks at computational models for optogenetic stimulation. The study starts with an extensive analysis of the literature to identify the best modeling strategies for encapsulating the kinetics of ChR2. Next, MATLAB R2023b is used to implement the precise four-state ChR2(H134R) model, which was created by Williams[176]. This model forms the basis for *in silico* comparative studies of electrical and optical stimulation within the subthalamic nucleus. Moreover, preliminary steps are being taken to develop a precise computational model for the locus caeruleus.

In the initial chapter of this dissertation, an in-depth exploration of the core components comprising the optogenetic toolbox is conducted. Presently, a diverse array of opsins is available, offering a wide range of functionalities. These include natural microbial and vertebrate opsins, as well as bioengineered variants designed to enhance specific characteristics. Notable examples include red-shifted opsins for improved tissue penetration, step-function opsins for precise temporal control, ultrafast opsins for rapid neuronal activation, and opsins with enhanced ion selectivity for more targeted modulation of cellular activity.

Furthermore, various delivery methods and illumination techniques have been developed and are continually evolving to optimize optogenetic experiments. These methods encompass viral-mediated gene delivery, transgenic animal models, and synthetic biology approaches, among others. Additionally, advancements in light delivery technologies, such as fiber optics and miniaturized implantable devices, have facilitated precise spatial and temporal control of optogenetic stimulation.

The chapter concludes by discussing the burgeoning clinical applications of optogenetics and the challenges that must be addressed to realize its full potential in clinical settings. While optogenetics holds promise for treating neurological and psychiatric disorders, several hurdles need to be overcome, including optimizing opsin expression and targeting, ensuring safety and efficacy in human subjects, and addressing ethical considerations surrounding the genetic manipulation of neural circuits. By addressing these challenges, optogenetics may offer novel therapeutic strategies for a variety of medical conditions. Before delving into the modeling of ChR2, a thorough examination of cellular electrophysiology is undertaken. Cells are enveloped by a phospholipid bilayer, rendering them impermeable to ions. Ion channels and transporters facilitate the movement of ions across the membrane, leading to transmembrane currents. Consequently, a cell can be modeled as an electrical equivalent circuit. Voltage-gated ion channels are essential for initiating action potentials. These channels are commonly characterized using a particle gating scheme, initially introduced by Hodgkin and Huxley. Chapter 2 of this thesis encapsulates these fundamental principles of cell modeling, laying the groundwork for the sophisticated models utilized throughout the research.

Chapter 3 delves into a meticulous exploration of ChR2 dynamics, particularly focusing on computational modeling techniques tailored for optogenetic stimulation. The segment presents a comprehensive comparative analysis of various models designed to capture the complex behavior of ChR2 under continuous stimulation. One of the key observations highlighted in this chapter is the biphasic trajectory of the photocurrent generated by ChR2. An early transient peak and a stable steady-state current follow each other on this track. Such complex dynamics need the use of advanced modeling techniques. A minimum of three states are needed in the model to sufficiently represent ChR2's behavior. The chapter does, however, address how two different models, the four-state model having two open and two closed states and a three-transitional state's model featuring an additional light-dependent step—have proven effective in accurately simulating the dynamics of ChR2. This chapter's discussion extends beyond a simple description to examine these models' application, validation, and critical analysis. The

state-of-the-art four-state model described by Williams[176], which has been implemented with Python and MATLAB R2023b, is particularly noteworthy. Furthermore, the chapter explores additional modeling approaches beyond the three-state and four-state models, including six-state and two-state models. Each of these approaches has its own merits and limitations, and the chapter critically evaluates their applicability to accurately represent ChR2 ion channel behavior.

In Chapter 4, we delved into the intricate modeling of Channelrhodopsin-2 (ChR2) ion channels, a pivotal aspect of optogenetic research aimed at understanding neural circuit dynamics. By scrutinizing the biphasic current course exhibited by ChR2 under continuous light stimulation, we encountered the challenge of accurately capturing its behavior within a computational framework. Using the knowledge from earlier research, we implemented a Williams et al. (2013) four-state model to capture the voltage and irradiance dependencies that are present during ChR2 activation. This model, although sophisticated, necessitated empirical adjustments to reconcile discrepancies and enhance its fidelity to experimental observations. By incorporating empirically derived rectification functions and other refinements, we refined the model's predictive power and applicability to our experimental context.

Transitioning from theoretical modeling to practical application, Chapter 5 ventured into the realm of neurodegenerative brain dysfunctioning, particularly Alzheimer's disease (AD), and explored the therapeutic potential of ChR2-based optogenetic interventions. Drawing inspiration from the growing body of evidence implicating aberrant neuronal activity in AD pathology, we sought to mitigate the detrimental effects of Alzheimer's related axonal damage through targeted optogenetic modulation. By activating ChR2 ion channels in affected neuronal populations, we aimed to restore neural communication and ameliorate cognitive deficits associated with AD progression.

Through a series of experiments and computational simulations, we demonstrated the efficacy of ChR2-based interventions in counteracting the effects of axonal damage and enhancing signal propagation along neural circuits. Our results highlighted the potential of optogenetic methods to restore neuronal function and possibly reduce cognitive decline in neurodegenerative diseases such as Alzheimer's. Additionally, by clarifying the mechanisms behind ChR2-mediated neural modulation, we added to the expanding understanding of optogenetic techniques and their use in treating neurological disorders.

By integrating theoretical modeling with experimental validation, our study bridged the gap between basic research and clinical application, paving the way for future

advancements in optogenetic therapy for neurodegenerative diseases. Moving forward, further investigations into the molecular mechanisms of ChR2 activation, as well as the optimization of optogenetic protocols for clinical translation, hold the promise of revolutionizing the treatment landscape for Alzheimer's disease and other neurological disorders.

Conclusion is that chapter 5 of this thesis has illuminated the multifaceted landscape of neuroscientific research, from theoretical modeling of ion channels to practical applications in neurodegenerative disease therapy. Through meticulous examination of Channelrhodopsin-2 (ChR2) ion channels and their role in optogenetic modulation, we have advanced our understanding of neural circuit dynamics and explored novel avenues for therapeutic intervention. By leveraging computational tools such as NEURON simulator and Python environments tailored for computational neuroscience, we have equipped ourselves with powerful tools to probe the complexities of the brain and develop innovative treatments for neurological disorders.

In the appendices, we have provided detailed insights into the NEURON simulator and Python environment, indispensable resources for neuroscientists seeking to unravel the mysteries of the brain through computational modeling and analysis. These appendices serve as practical guides for researchers embarking on similar endeavors, offering valuable tips and techniques for leveraging these tools effectively in their own studies.

As we look to the future, the findings presented in this thesis pave the way for further exploration and innovation in the field of neuroscience. By continuing to refine our understanding of neural circuitry and develop sophisticated tools for neural modulation, we hold the promise of revolutionizing the diagnosis and treatment of neurological disorders. Through interdisciplinary collaboration and a relentless pursuit of knowledge, we can unlock the full potential of the human brain and alleviate the burden of neurological disease for generations to come.

Finally, the references provided at the end of this thesis serve as a comprehensive repository of the literature that has informed and inspired our research. By acknowledging the contributions of our predecessors and contemporaries, we honor the collective effort of the scientific community in advancing our understanding of the brain and striving towards a future where neurological disorders are a thing of the past.

Chapter 2

Optogenetic Toolbox

Evolution, Components, and Applications

In recent decades, the field of neuroscience has undergone a remarkable transformation, fueled by advancements in classical biochemistry, neural circuitry, and electrophysiology. These developments have not only deepened our understanding of the intricate workings of the nervous system but have also opened up new avenues for the diagnosis and treatment of neurological disorders. Classical biochemistry techniques have enabled researchers to unravel the molecular pathways underlying neural function and dysfunction. Through biochemical assays and molecular profiling, scientists have gained insights into the signaling cascades, neurotransmitter systems, and protein interactions that govern neuronal activity. These insights have proven invaluable in elucidating the pathophysiology of various neurological conditions, laying the groundwork for targeted therapeutic interventions. Similarly, advances in neural circuitry have shed light on the complex networks of neurons that underlie cognitive processes, sensory perception, and motor control. Techniques such as neural tracing, electrophysiological recording, and functional imaging have allowed researchers to map out the intricate connections between different brain regions and decipher the dynamics of information processing within neural circuits. This comprehensive comprehension of neural circuitry has yielded essential insights into the mechanisms that underlie neurological disorders and has facilitated the advancement of innovative therapeutic approaches. One of the most significant breakthroughs in the field of neuroengineering has been the development of neural prostheses and brain-computer interfaces (BCIs). These devices leverage advances in bioengineering, materials science, and signal processing to restore lost sensory or motor function in individuals with neurological impairments. For instance, cochlear implants bypass damaged hair cells

in the inner ear and directly stimulate the auditory nerve, allowing individuals with hearing loss to perceive sound. Similarly, visual prostheses deliver electrical stimulation to the retina or visual cortex, bypassing damaged photoreceptor cells to restore vision in individuals with retinal degenerative diseases. Deep brain stimulation (DBS) is another revolutionary neurotechnological advancement that has transformed the treatment of disorders like Alzheimer's disease. DBS delivers electrical impulses to targeted brain regions, which can modulate abnormal neural activity and alleviate symptoms such as tremors, rigidity, and bradykinesia. In addition to Alzheimer's disease, DBS has shown promise in the management of epilepsy, obsessive-compulsive disorder (OCD), and treatment-resistant depression, highlighting its versatility as a therapeutic tool. Despite these remarkable achievements, several challenges remain in the field of neuroscience. The temporal resolution of biochemical techniques often limits our ability to capture rapid changes in neural activity, while electrophysiological methods lack the spatial specificity required to target specific cell types within complex neural circuits. Optogenetics offers a promising solution to these challenges by enabling precise control over neural activity with millisecond precision and cellular specificity. Optogenetics harnesses the power of light-sensitive proteins called opsins, which are genetically encoded into neurons. By selectively expressing opsins in specific cell types using viral vectors or transgenic animal models, researchers can precisely control neuronal activity using pulses of light. This precise spatiotemporal control over neural activity has revolutionized our ability to probe the neural circuits underlying behavior, cognition, and disease. In the upcoming chapter, we will explore the foundational principles of optogenetics, including the mechanisms of opsin function, the strategies for opsin expression, and the methods for optical stimulation. We will also delve into the diverse applications of optogenetics in basic neuroscience research, disease modeling, and therapeutic intervention. Additionally, we will discuss the current challenges and future directions of optogenetics, with a focus on its potential for clinical translation and its role in advancing our understanding of the brain.

2.1 Intricacies of Neurons

Neurons, the fundamental components of the nervous system, are incredibly complex and diverse cells that play essential roles in transmitting electrical and chemical signals throughout the body. Furthermore, we delve into the multifaceted nature of neurons, exploring their structure, function, and the mechanisms underlying their remarkable capabilities. Through a comprehensive examination of neuronal anatomy, physiology,

and connectivity, this topic aims to provide a deeper understanding of these intricate cells and their pivotal role in orchestrating diverse physiological processes. Neurons, often referred to as the fundamental components of the nervous system, are specialized cells that enable the transmission of information through electrical and chemical signals. These cells exhibit remarkable diversity in structure and function, allowing them to perform a wide array of tasks ranging from sensory perception to motor control and cognitive processing. Grasping the intricacies of neurons is crucial for deciphering the complexities of brain function and behavior, as well as for progressing treatments for neurological disorders. This assay aims to explore the various aspects of neurons, including their structure, classification, signaling mechanisms, and contributions to neural networks.

Optogenetics hailed as a revolutionary technique in neuroscience, embodies the optical control of genetically modified cells, particularly neurons, by harnessing the expression of light-sensitive ion channels or pumps known as opsins[119]. Among these opsins, channelrhodopsin-2 (ChR2) is particularly notable, first discovered for its significant role in phototaxis and photophobic behaviors in the green algae *Chlamydomonas reinhardtii*[123]. The inception of using light as a tool for neuromodulation dates back to 1979, with Francis Crick's pioneering proposal, which laid the conceptual groundwork for subsequent breakthroughs in optogenetics. The evolutionary trajectory of optogenetics was shaped by landmark discoveries of various opsins, including bacteriorhodopsin, a proton pump identified by Oesterhelt and Stoeckenius in 1971[127] as well as halorhodopsin, an inhibitory chloride pump that was characterized by Matsuno-Yagi and Mukohata in 1977[115]. However, it wasn't until 2002 that the advent of channelrhodopsin, the first light-gated ion channel, catalyzed a paradigm shift in neuroscience research, opening up unprecedented avenues for investigating neural circuit dynamics and behavior[122, 179, 182, 131].

The optogenetic toolbox, essential for harnessing the power of light to manipulate neural activity, comprises three fundamental components. Firstly, the selection of an appropriate opsin is paramount, with considerations including ion selectivity, kinetics, spectral band, and conductance. This meticulous choice ensures optimal compatibility with the experimental objectives and biological context. Subsequently, a robust delivery method is indispensable for introducing opsin into target cells, often accomplished through viral vectors such as adeno-associated or lentiviruses. These vectors serve as vehicles for genetic manipulation, facilitating precise targeting of specific neuronal populations. Finally, a reliable light source, typically a light-emitting diode (LED) or laser, serves as the catalyst for activating the genetically modified cells, enabling

precise temporal and spatial control over neural activity[131]. This comprehensive approach enables researchers to explore the complexities of neural circuits and behavior while also offering significant potential for uncovering the mechanisms underlying neurological disorders and developing novel therapeutic strategies. The fusion of genetics, optics, and neuroscience in optogenetics heralds a new era of exploration, offering unprecedented insights into the brain's inner workings and paving the way for transformative advancements in neuroscience and medicine.

2.1.1 Structure of Neurons

Understanding the intricacies of neuronal structure is fundamental to deciphering their functional properties and contributions to neural circuits. This assay delves into the multifaceted aspects of neuronal architecture, encompassing the soma, dendrites, axons, synapses, and specialized adaptations.

2.1.1.1 The Soma

The soma, or cell body, serves as the command center of the neuron, housing the nucleus and essential organelles. It is the metabolic hub responsible for protein synthesis, energy production, and cellular maintenance. The size and shape of the soma vary across different neuronal types, reflecting their functional specialization and metabolic demands.

2.1.1.2 Dendrites

Dendrites are elaborately branched extensions emanating from the soma, tasked with receiving and integrating synaptic inputs from other neurons. Dotted with dendritic spines, these formations serve as hubs for synaptic connections and play a pivotal role in synaptic integration as well as plasticity. Dendritic morphology, including branching patterns and spine density, contributes to the computational capabilities of neurons and influences information processing within neural networks.

2.1.1.3 The Axon

The axon is a slender, elongated projection that transmits electrical impulses away from the soma to other neurons or effector cells. Structurally specialized for rapid signal propagation, the axon features distinct regions such as the axon hillock, initial segment, and axon terminals. Some neurons exhibit myelinated axons, where segments

are ensheathed in myelin produced by glial cells, facilitating saltatory conduction and enhancing signal transmission efficiency.

2.1.1.4 Synapses

Synapses represent the functional junctions between neurons, where communication occurs through the release and reception of neurotransmitters. Presynaptic terminals, located at axon terminals, house synaptic vesicles containing neurotransmitters. Postsynaptic membranes, typically situated on dendrites or the soma of the receiving neuron, harbor neurotransmitter receptors that initiate postsynaptic potentials upon neurotransmitter binding. Synaptic plasticity, mediated by alterations in synaptic strength and connectivity, underlies learning, memory, and neural adaptation.

2.1.1.5 Specialized Adaptations

Neurons exhibit specialized adaptations to meet the demands of their functional roles and environmental challenges. These adaptations encompass a myriad of structural modifications, including changes in dendritic arborization, axonal branching, and synaptic connectivity. Moreover, neurons display remarkable plasticity, allowing for structural remodeling in response to developmental cues, sensory experiences, and pathological insults.

The structure of neurons embodies a remarkable convergence of form and function, finely tuned to support their diverse roles in neural communication and information processing. Through an in-depth exploration of neuronal architecture, this assay has unveiled the intricate structural adaptations that underpin the remarkable functional capabilities of neurons. Further elucidating the structural complexities of neurons holds immense promise for unraveling the mysteries of brain function and advancing therapeutic interventions for neurological disorders.

2.1.2 Types of Neurons

Neurons can be classified based on various criteria, including their structural and functional properties. The three primary types of neurons are sensory neurons, motor neurons, and interneurons. Sensory neurons transmit signals from sensory receptors to the central nervous system (CNS), allowing for the perception of sensory stimuli. Motor neurons convey signals from the CNS to muscles and glands, enabling voluntary and involuntary movements. Interneurons form connections within the CNS and play crucial roles in processing and integrating information.

2.1.2.1 Sensory Neurons

Sensory neurons, also termed afferent neurons, are uniquely equipped to detect external stimuli or internal states and transmit sensory information to the central nervous system. These neurons play a crucial role in sensory perception, allowing organisms to sense touch, temperature, pain, vision, hearing, taste, and smell. Sensory neurons exhibit diverse morphological and functional adaptations depending on the modality they detect and the receptors they innervate.

2.1.2.2 Motor Neurons

Motor neurons, or efferent neurons, transmit signals from the CNS to muscles or glands, enabling voluntary and involuntary movements as well as the regulation of glandular secretion. Somatic motor neurons innervate skeletal muscles, while autonomic motor neurons control smooth muscle, cardiac muscle, and glandular activity. Motor neurons exhibit specialized structural features to facilitate rapid and precise transmission of signals to effector organs, contributing to motor coordination and homeostatic regulation.

2.1.2.3 Interneurons

Interneurons, also known as association neurons, form connections within the CNS and mediate communication between sensory and motor neurons. These neurons integrate and process signals received from sensory neurons before transmitting them to motor neurons, thereby contributing to information processing and coordination of complex behaviors. Interneurons play a pivotal role in shaping neural circuits, modulating synaptic transmission, and regulating neuronal excitability.

2.1.2.4 Specialized Neuronal Variants

Beyond the classical classification of sensory, motor, and interneurons, the nervous system encompasses specialized neuronal variants adapted to specific functions and anatomical locations. Pseudounipolar neurons, found in the dorsal root ganglia, serve as primary sensory neurons conveying information from peripheral receptors to the CNS. Multipolar neurons, the most common type in the CNS, exhibit diverse functions depending on their location and connectivity within neural circuits.

The diversity of neuronal types reflects the complexity of neural circuits and their remarkable adaptability to diverse physiological and environmental demands. By elucidating the distinct characteristics and roles of sensory neurons, motor neurons,

interneurons, and specialized variants, this essay provides a deeper understanding of the intricate organization of the nervous system. Continued investigation into the diversity of neurons holds the potential to reveal fresh understandings of brain function and behavior, leading to the development of novel approaches in neurological research and therapeutic interventions.

2.2 Ion Channels in Neurons

The functionality of the nervous system, with its intricate network of neurons communicating via electrical signals, fundamentally depends on the dynamic interaction of ion channels. These remarkable molecular entities, embedded within the neuronal membrane, act as regulators of neuronal excitability by controlling the flow of ions. This process is essential for generating and transmitting electrical impulses critical for brain function. Exploring the basics of ion channels in neurons unveils a fascinating realm of molecular machinery, providing insights into the mechanisms governing neuronal communication and paving the way for groundbreaking discoveries in neuroscience.

At its essence, the concept of ion channels revolves around the permeability of cellular membranes to ion-charged particles crucial for electrical signaling. Ion channels are transmembrane proteins that form channels or pores across the lipid bilayer of the neuronal membrane. These channels selectively allow ions to pass through based on their electrochemical gradients. This selective permeability enables ion channels to regulate the membrane potential—the voltage difference across the neuronal membrane—by adjusting the balance of ions inside and outside the cell.

The diversity of ion channels in neurons encompasses a wide range of types, each characterized by distinct structural features, functional traits, and regulatory mechanisms. Among the most prominent are voltage-gated ion channels, which respond to changes in membrane potential and play pivotal roles in initiating and propagating action potentials. Action potentials are rapid electrical impulses that facilitate quick communication between neurons. Sodium Na^+ , potassium K^+ , and calcium Ca^{2+} channels are notable examples of voltage-gated channels, each contributing to specific phases of the action potential and influencing neuronal excitability. Here, we present a concise overview of the primary types of ion channels present in neurons:

2.2.1 Voltage-Gated Ion Channels

These channels react to variations in membrane potential and are essential for the initiation and propagation of action potentials, which are quick electrical impulses that allow neurons to communicate with one another. Classic examples of voltage-gated channels are sodium (Na^+), potassium (K^+), and calcium (Ca^{2+}) channels. These channels influence neuronal excitability and contribute to different phases of the action potential.

2.2.2 Ligand-Gated Ion Channels

Also known as ionotropic receptors, these channels respond to the binding of specific neurotransmitters or ligands. Ligand-gated channels mediate fast synaptic transmission at chemical synapses, converting chemical signals into electrical signals by facilitating ion flux across the neuronal membrane. Excitatory neurotransmitters such as glutamate activate channels like the AMPA and NMDA receptors, promoting depolarization and excitatory synaptic transmission.

2.2.3 Mechanosensitive Ion Channels

These channels are responsive to mechanical stimuli and are essential for sensory transduction. Mechanosensitive channels react to mechanical forces like touch, stretch, and pressure, converting mechanical energy into electrical signals that can be relayed to the central nervous system. They are involved in multiple sensory functions, including tactile perception, proprioception, and auditory sensation.

2.2.4 Transient Receptor Potential (TRP) Channels

TRP channels constitute a diverse family of ion channels that respond to a wide range of stimuli, including temperature, pH, and chemical compounds. Within the nervous system, TRP channels contribute to sensory transduction, pain perception, and thermoregulation. Examples include TRPV1 channels, activated by capsaicin, and TRPM8 channels, activated by menthol and cool temperatures.

2.2.5 Light-Gated Ion Channels

Light-gated ion channels are engineered proteins derived from microbial opsins, light-sensitive proteins originally found in microorganisms such as algae and bacteria. These

proteins possess the unique ability to respond to light stimulation by undergoing conformational changes that alter their ion permeability, thereby modulating neuronal activity. By introducing light-gated ion channels into neurons via genetic or viral methods, researchers can effectively control neuronal excitability with millisecond precision using pulses of light.

2.3 Light-Sensitive Proteins in Optogenetics

In the field of optogenetics, naturally occurring light-sensitive proteins sourced from plants, fungi, bacteria, and algae have revolutionized the precise control and observation of neural activity in both cultured tissue and living organisms, utilizing light of different wavelengths[138, 38]. Among the most extensively studied proteins in optogenetics are microbial rhodopsin channels and pumps[57]. These opsins are subject to thorough investigation and categorization based on their kinetics, light sensitivity, ion selectivity, conductance, and suitability for various experimental applications[72, 44]. In neurons expressing opsins, the process of photoisomerization of the embedded retinal molecule induces conformational changes in the opsin molecule, leading to the transient opening of an ionic pore across the membrane[140, 141]. This opening occurs for a limited duration, allowing ions to flow through the pore due to the potential gradient and ion-concentration gradient across the neuron membrane. Consequently, this ion flow alters the membrane potential of the neuron. The probability of optogenetic excitation or inhibition of neurons hinges on the total light-evoked current, also known as the photocurrent, generated by light-sensitive opsin molecules. A thorough examination of the molecular properties of these opsins is pivotal, as it not only aids in comprehending the mechanism underlying ion flow but also facilitates the identification of strategies to modify conductance, absorption spectrum, expression density, kinetics, and ion-selectivity[90, 112, 133]. Extensive endeavors have been dedicated to the discovery or engineering of new opsins with enhanced properties tailored for various neuroscience applications[110, 108, 44, 64].

There are many types of light-gated ion channels as Rhodopsin (Rho), Channelrhodopsin (ChR)[122, 123, 20], Halorhodopsin (NpHR), Archaelrhodopsin (Arch), Sensory rhodopsin (SRI), Bacteriorhodopsin (BR), Microbial rhodopsin (MR), Anion channelrhodopsin (ACR), Sensory rhodopsin II (SRII), Proton pump rhodopsin (PPR). Some variants of Channelrhodopsin (ChR) along with their commonly used names as Channelrhodopsin-2 (ChR2)[20, 121], Chlamydomonas channelrhodopsin-1 (ChlamyChR1), Volvox channelrhodopsin-1 (VChR1), Enhanced Channelrhodopsin-2

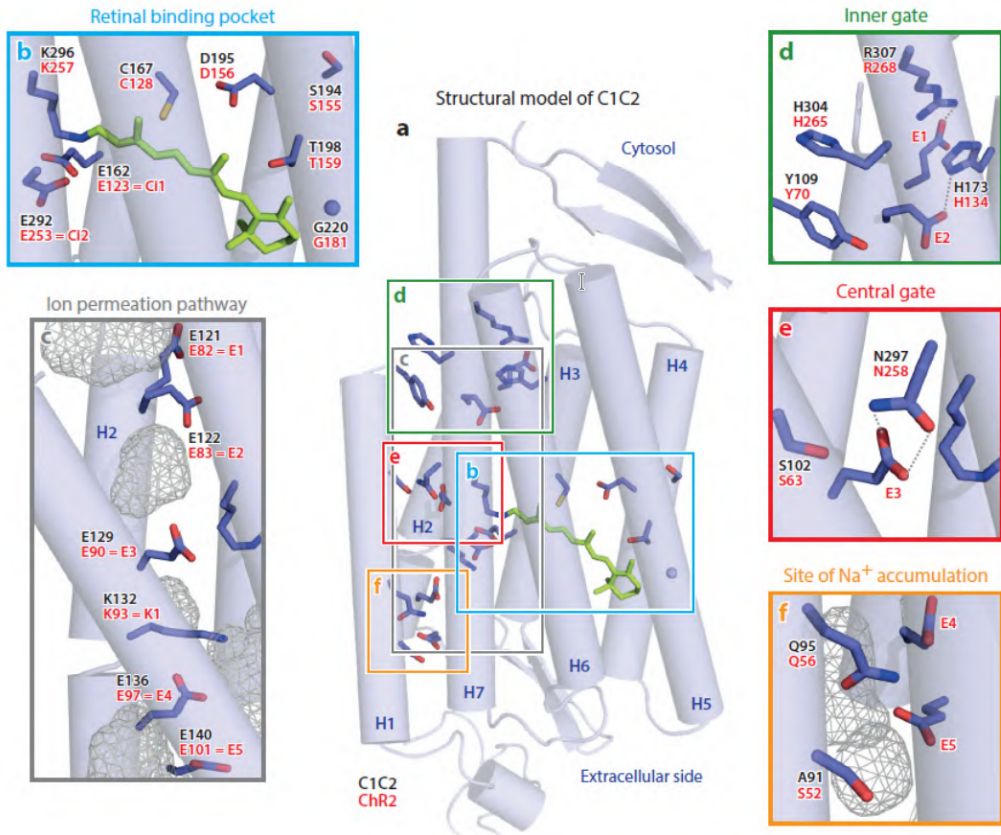


Fig. 2.1 Crystal structure determined by Kato in (2012)[92] provided the basis for the structural model of C1C2. The closed dark adapted conformation is reflected in the model. While helices H6 and H7 come from ChR2, helices H1–H5 come from ChR1. (a) the framed regions of interest within the overall protein structure. The green molecule in (b), which shows the retinal binding pocket, is the retina. (c) the pathway of ion permeation. (d) the inner gate. (f) the location of Na^+ accumulations and (e) the central gate. The protein's cavities, which may contain cations and water molecules, are shown in the grey wireframes. Reproduced from Schneider and colleagues (2015)[146].

(eChR2), Chrimson, Chronos, ReaChR (Red-activatable Channelrhodopsin), CoChR (Conductance-tuned Channelrhodopsin), ChETA (Chimeric Channelrhodopsin-2/E123-T/T159C), CheRiff (Chimeric rhodopsin-expressing firefly).

Further, some variants of Channelrhodopsin-2 (ChR2) are engineered to perform excellent desired results. These variants of ChR2 have been engineered to expand the capabilities of optogenetics, allowing researchers to achieve precise and versatile control over neuronal activity for a wide range of experimental and therapeutic applications.

ChR2(H134R): This variant has an enhanced light sensitivity compared to wild-type ChR2[104, 121].

ChR2(C128S): This variant exhibits improved kinetics, allowing for faster channel closure.

ChR2(E123T/T159C): This variant has been engineered to achieve red-shifted activation, enabling excitation with longer wavelength light.

ChETA (ChR2(E123A/E136A/T159C)): This variant displays faster kinetics and reduced desensitization compared to wild-type ChR2.

ChrimsonR: A red-shifted variant of ChR2 that enables excitation with longer wavelength light, reducing phototoxicity and allowing for deeper tissue penetration.

Chronos: This variant has been engineered for ultrafast kinetics, enabling precise control over neuronal firing with high temporal resolution.

CoChR (ChR2(E123T/T159C/V98A)): A variant with enhanced light sensitivity and improved membrane trafficking compared to wild-type ChR2.

ReaChR: A red-shifted variant of ChR2 that enables excitation with near-infrared light, facilitating deeper tissue penetration and minimizing tissue damage.

ChrimsonR-tdT: A fusion protein combining ChrimsonR with a red fluorescent protein (tdTomato), allowing for simultaneous optogenetic stimulation and visualization of targeted neurons.

Chronos-EYFP: A fusion protein combining Chronos with enhanced yellow fluorescent protein (EYFP), enabling simultaneous optogenetic control and visualization of neuronal activity.

In the realm of neuroscience, where the intricate dance of neuronal signaling shapes the landscape of brain function, Channelrhodopsin-2 (ChR2) and its variants stand as beacons of innovation and promise. Within the vast spectrum of ion channels, ChR2 emerges as a radiant protagonist, harnessing the power of light to unravel the mysteries of neuronal circuitry with unparalleled precision and elegance. At the heart

of ChR2 lies a mesmerizing interplay of molecular architecture and photonic sensitivity. Derived from microbial opsins found in algae, ChR2 is a cation-selective ion channel that responds with exquisite sensitivity to blue light. Its elegant design allows for the precise manipulation of neuronal excitability, enabling researchers to illuminate specific populations of neurons with a mere flicker of light. Yet, the story of ChR2 is not one of static brilliance, but rather of dynamic evolution and adaptation. Through ingenious engineering and relentless innovation, researchers have crafted an array of ChR2 variants, each endowed with unique properties and capabilities. From enhanced light sensitivity to optimized kinetics, these variants expand the palette of optogenetic tools, opening new avenues for exploration and discovery in the realm of neuronal control. In this thesis, our gaze is fixated upon ChR2 and its illustrious variants, as we embark on a journey to unlock the secrets of optogenetic manipulation. With ChR2 as our guiding light, we traverse the intricate terrain of neuronal circuits, probing the depths of brain function and unraveling the mysteries of behavior. Through meticulous experimentation and insightful inquiry, we seek to illuminate the path to optogenetic discovery, casting light upon the enigmatic realm of neural dynamics and paving the way for transformative insights into the workings of the mind.

As we embark on this odyssey of scientific inquiry, let us harness the radiant potential of ChR2 and its variants to illuminate the darkest corners of the brain, shedding light upon the complexities of neural circuitry and charting a course towards a deeper understanding of the human experience. With ChR2 as our beacon and curiosity as our compass, we embark on a voyage of discovery, guided by the radiance of scientific inquiry and the promise of illumination that lies beyond the horizon. Based on their applications, these opsins have been categorized.

2.3.1 Excitatory opsins

The inaugural showcase of optogenetic excitation of neurons was achieved through the utilization of Channelrhodopsin-2 (ChR2), a light-gated cation channel devoid of ion specificity[122, 123],[20]]. Upon exposure to light, ChR2 permits the influx of cations into the cell, resulting in depolarization. Notably, brief blue light pulses lasting only milliseconds have been shown to elicit temporally precise spiking of up to approximately 30 Hz in ChR2-expressing hippocampal neurons[20]. After this pioneering demonstration, various research teams have corroborated the functionality of ChR2 and leveraged its capabilities to tackle challenges encountered in neuroscience experiments[101, 121, 148, 61]. A single point mutation in ChR2 at position H134R has given rise to a mutant variant known as ChR2(H134R). ChR2(H134R) exhibits

an augmented photocurrent and demonstrates heightened light sensitivity compared to wild-type ChR2 [121]. Subsequently, efforts were made to engineer ChR2 to allow the permeation of calcium ions across the membrane. This Ca²⁺-permeable variant, named CatCh, showcases enhanced sensitivity and a larger photocurrent. However, it has been observed to exhibit inherent toxicity in certain experimental contexts[29].

Moreover, a more blue-shifted opsin with heightened photosensitivity, termed CheRiff, was developed by incorporating a trafficking sequence and introducing a mutation at position E154A in Scherffelia dubia channelrhodopsin (sdChR). CheRiff, characterized by its excitation peak at approximately 460 nm, mitigates optical crosstalk with fluorescent reporters in all-optical experiments[79].

Furthermore, a myriad of other opsins have been unearthed for diverse applications in optogenetics. Some of these potential opsins are categorized below.

2.3.1.1 Red-shifted Opsins for Deep Excitation

Light at red-shifted wavelengths possesses the advantageous ability to penetrate deep into tissue, thereby minimizing invasiveness in optogenetic applications. VChR1, the first red-shifted mutant of ChR2, features an absorption peak at approximately 535 nm. However, despite its red-shifted properties, VChR1 exhibits a smaller photocurrent compared to ChR2[187]. Another red-shifted variant, C1V1, generates a larger photocurrent but demonstrates slower kinetics than ChR2[182]. Additionally, a further red-shifted variant, ReaChR, with a peak response at 590-630 nm, has been discovered. ReaChR produces higher photocurrents due to enhanced membrane trafficking and expression in mammalian cells[103]. Furthermore, a faster version of ReaChR, known as bReaChES, was engineered by introducing a Glu123Ser mutation and replacing the first 51 amino-terminal residues with the first 11 amino-terminal residues of ChR2 in the ReaChR construct[95]. bReaChES enables simultaneous optogenetic excitation and activity readout in conjunction with calcium indicators[95].

Recently, there has been a surge in the discovery of potent, red-shifted opsins, including Chrimson and its mutants[110, 114, 96, 95]. One notable variant, the faster Chrimson kinetic mutant known as ChrimsonR, shares a similar activation wavelength with Chrimson and enables temporally precise excitation at frequencies exceeding 20 Hz [96]. Additionally, CsChrimson, another mutant of Chrimson, possesses nearly identical spectral and kinetic properties. It was engineered by replacing the Chrimson N-terminus with that of CsChR [96]. More recently, guided by crystal structure-derived insights into residues forming the ionic pore, a screening process identified approximately 1000 new ChR variants. Optimization of these sequences for improved

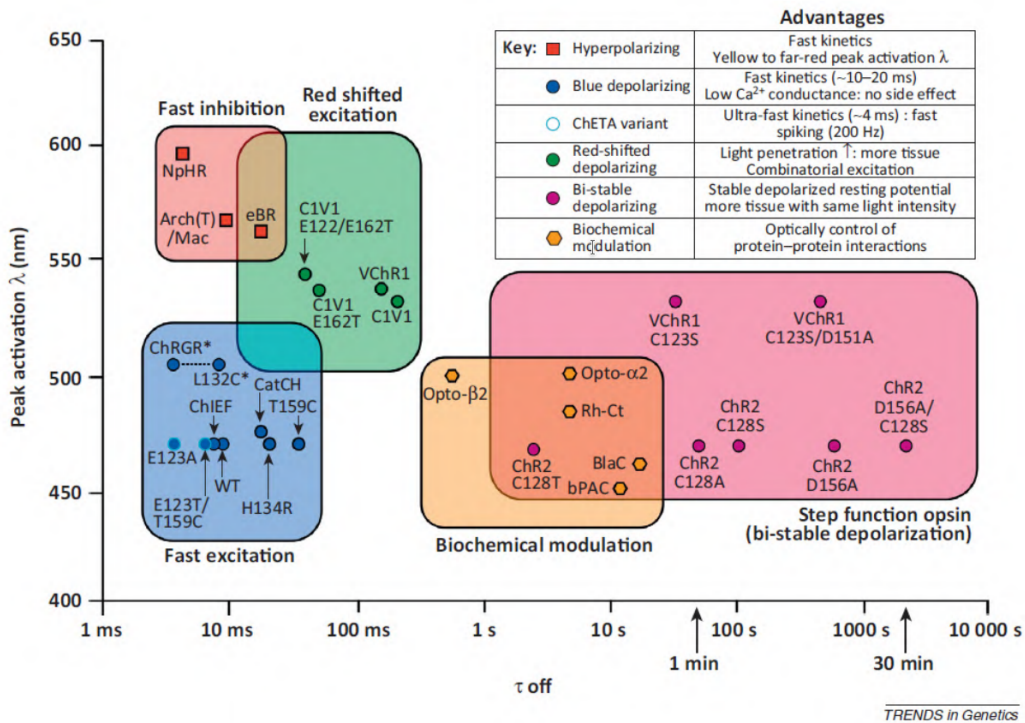


Fig. 2.2 Summary of various opsins including their activation peak wavelength, decay kinetics, and associated benefits, taken from Gerits and Vanduffel (2013).[49]

expression in mammalian cells led to the discovery of a promising marine opsin gene called ChRmine. Derived from Tiarina fusus, ChRmine exhibits exceptionally high sensitivity and generates a large photocurrent of approximately 4 nA, along with millisecond temporal kinetics[114].

2.3.1.2 Opsins for Ultrafast Optogenetic Excitation

ChR2 and other slow mutants with turn-off times exceeding 10 ms struggle to maintain single spike resolution at high gamma frequencies and beyond (50 Hz – 200 Hz), leading to undesirable signal confounds such as extra spikes and plateau potentials[69]. A single point mutation at position E123T in ChR2 resulted in the creation of a mutant variant with accelerated channel kinetics, approximately 5.2 ms. This engineered mutant, named ChETA, enables high-fidelity spiking of up to 200 Hz in fast-spiking interneurons[69]. However, ChETA exhibits poor light sensitivity and a small photocurrent amplitude, consequently failing to generate later spikes in response to a stimulus train[116, 10].

Furthermore, the de novo sequencing of opsins from over 100 algal species has led to the discovery of a new opsin called Chronos. Chronos, which exhibits sensitivity to both blue and green light, boasts very fast turn-on (2.3 ± 0.3 ms) and turn-off (3.6 ± 0.2 ms) kinetics of its photocurrent, alongside high sensitivity[96]. Recently, high-frequency spikes of up to 100 Hz with sub-ms precision were elicited in Chronos-expressing pyramidal cells and interneurons under two-photon excitation. Notably, Chronos does not exhibit plateau potentials or extra spikes at higher frequencies, making it well suited for low-power ultrafast optogenetic excitation[144, 139].

Very recently, fast variants of Chrimson have been developed through site-directed mutagenesis. Two such variants, namely fast (f-) Chrimson and very fast (vf-) Chrimson, exhibit improved expression levels and are particularly intriguing for achieving deep low-power and high-frequency optogenetic excitation of neurons[110]. vf-Chrimson has enabled precise firing in interneurons of up to 300 Hz[110].

2.3.1.3 Opsins for Bistable Optogenetic Control

In certain experimental contexts, there is a preference for inducing more naturalistic spiking patterns or sensitizing neurons to native synaptic signals rather than promoting synchronized spiking with stimulation[182]. Research has demonstrated that by slowing down the turn-off kinetics of opsins through protein residue modification, a brief light pulse can be transformed into a prolonged depolarization[17]. These genetically engineered slow mutants, termed bistable or step-function opsins, maintain activity for an extended duration beyond the duration of the stimulating light pulse[17]. Unlike fast ChRs, where the conducting photo-intermediate in the photocycle is short-lived, bistable opsins offer an opportunity to accelerate turn-off kinetics using light of different colors. Two notable bistable opsins, ChR2(C128A) and ChR2(C128S), exhibit turn-off times of approximately 52 ± 2 s and 106 ± 9 s, respectively. They can be activated with a brief blue light pulse and deactivated with a green light pulse[17]. The controlled and prolonged depolarization induced by bistable opsins is instrumental in elucidating the roles of different cell types in homeostatic and adaptive processes within the adult brain, chronic disease models, and neuroplasticity during development[17].

An imbalance between excitation and inhibition within neural microcircuits is implicated in the manifestation of severe behavioral deficits observed in psychiatric disorders such as schizophrenia and autism[113, 165, 93, 142, 54]. Investigating this hypothesis necessitates the selective excitation of one neural population over another for extended durations. However, the prolonged depolarization induced by ChR2(C128A) and ChR2(C128S) is not sufficiently stable for complex behavioral testing. Therefore,

more stable step-function opsins (SSFO) were developed, exhibiting a turn-off time of approximately 30 minutes[182]. More recently, a variant of SSFO with enhanced photosensitivity, termed step-function opsin with ultra-light sensitivity (SOUL), has enabled minimally invasive and reversible modulation of neural spiking in the macaque cortex through optical stimulation from outside the dura[55]. Additionally, the recent integration of SFOs with ChETA has facilitated low-power sustained excitation of neurons[9].

2.3.2 Inhibitory opsins

Instead of stimulating neurons, reversible suppression of neural activity patterns in both space and time presents a promising approach to assess the contributions of specific brain structures, neuronal populations, and projection pathways across a wide range of brain functions and behaviors[171]. Optogenetics utilizes light-driven ion pumps and light-gated anion channels to achieve inhibition of neural activity[171]. Optogenetic seizure suppression has demonstrated effective outcomes in the treatment of epilepsy[159, 72]. While light-driven pumps are advantageous for precisely inhibiting spikes within a high-frequency spike train, light-gated anion channels offer advantages over pumps, particularly when large-volume and sustained inhibition is required.

2.3.2.1 Light-driven Ion-pumps

The initial application of optogenetic inhibition of neurons involved the use of halorhodopsin from *Natronomonas pharaonis* (NpHR). Functioning as a light-sensitive ion pump in neurons, NpHR, when illuminated, transports chloride ions into the neuron, thereby inducing hyperpolarization or suppression of ongoing electrical activity[189]. Sensitive to orange light (590 nm), NpHR generates a small photocurrent (50 pA) with a turn-off time of approximately 6.9 ± 2.2 ms[74, 189]. Subsequent engineering efforts led to the discovery of eNpHR2.0 and eNpHR3.0, which were designed to enhance surface membrane localization[60, 62, 187]. Notably, eNpHR3.0, with its larger photocurrent and faster kinetics, effectively suppresses spiking with green, yellow, or red light, thus enabling the utilization of less expensive laser systems in optogenetic neuronal inhibition.

More recently, Jaws, an optimized cruxhalorhodopsin derived from *Haloarcula salinarum*, has been identified. Jaws, also functioning as a chloride-selective ion pump, generates a photocurrent three times larger than other chloride pumps at red-shifted wavelengths, with a rapid turn-off time of approximately 6 ms. Due to its heightened

sensitivity and larger photocurrent, Jaws and similar molecular tools are particularly advantageous for non-invasive neuronal inhibition in deep brain structures or more effective inhibition in larger primate brains[34].

In addition to chloride pumps, proton pumps such as Mac (from the fungus *Leptosphaeria maculans*), ArchT (an archaerhodopsin from *Halorubrum* strain TP009), and Arch (archaerhodopsin-3 from *Halorubrum sodomense*) are also employed for optogenetic inhibition[62, 33, 75]. Upon illumination, these opsins pump protons out of the cell body, leading to robust suppression of ongoing electrical activity or hyperpolarization in resting neurons. Proton pumps offer several advantages over chloride pumps, including high photocurrents and fast recovery kinetics[72].

2.3.2.2 Light-gated Anion Channels

To address the limitations associated with light-driven pumps, efforts have been made to engineer ion channels to modify their selectivity to anions. Unlike ion pumps, light-gated anion channelrhodopsins (ACRs) enable the flow of multiple anions per photon, with their photocurrent regulated by the potential difference and concentration gradient of specific anions across the membrane[171]. Engineered ACRs such as C1C2, iC++, and iChloC exhibit minimal photocurrent and are selective to chloride ions[92, 173, 172, 14, 15]. Neurons expressing these chloride-selective ACRs exhibit membrane potential shunting towards the reversal potential of chloride channels upon light stimulation[171].

Recently, natural ACRs have been discovered by screening various cryptophyte species. These natural ACRs produce several-fold larger photocurrents and demonstrate near-perfect anion selectivity compared to engineered ACRs[56]. GtACR1 and GtACR2, the first natural ACR derived from *Gaillardia theta*, have exhibited complete inhibition of the electrical activity of cardiomyocytes, a task where Arch was ineffective[56]. Consequently, natural ACRs have been utilized to rapidly suppress neural systems associated with locomotion, wing expansion, memory retrieval, and gustation in *Drosophila*[118]. A rapid variant of natural ACR, named ZipACR, with a photocurrent half-decay time of approximately 2 - 4 ms, has enabled precise inhibition of spikes up to 50 Hz in hippocampal neurons of mice[57]. More recently, RubyACRs have been identified, exhibiting spectral sensitivities with maxima at 590 to 610 nm, making them the most red-shifted ACRs discovered to date[58].

2.3.3 Step-function opsins

Due to their ability to provide bistable step-like control, step-function opsins (SFOs) have a special benefit that makes them ideal for varying spontaneous firing rates. They aren't, however, designed with single action potential (AP) regulation in mind. The ChR2(C128S) mutant is the most widely selected SFO among the others. The C128 residue and D156 make up the DC-gate mechanism, which is essential to channel operation (see Figure 2.1). Changes made at this location significantly lengthen the open state of the channel and slow down kinetics. For example, the C128S mutation leads to a considerable reduction in kinetics and an increase in the open-state lifespan. Furthermore, a stabilized SFO with an unusually extended deactivation duration of almost thirty minutes is obtained by altering the complete DC-gate (C128S/D156A)[72].

This enhanced stability and prolonged activity make SFOs like ChR2(C128S) valuable tools for experimental setups requiring sustained modulation of neural activity over extended periods, offering researchers greater flexibility and control in their optogenetic experiments.

2.3.4 Ion selectivity

Another significant aspect that researchers have targeted for modification is ion selectivity in opsins. While natural opsins typically exhibit a strong selectivity for protons over other ions, such as sodium, modifications have been made to enhance selectivity for specific ions.

For example, investigations by Schneider et al. (2015) show that the mutant ChR2(L132C-T159C) exhibits extended magnesium conductance, enhanced sodium conductance, and calcium selectivity. As shown by Pan et al. (2014)[132], this mutation not only modifies ion selectivity but also increases light sensitivity by 1.5 to 2 log units, albeit at the cost of decreased temporal kinetics.

A sodium-carrying current can also be produced by mutations that target certain residues, such as H134, which are essential components of the gating mechanism and sodium interaction site. A prominent instance that is commonly employed in optogenetic experiments is ChR2(H134R), as studies by Yizhar et al. (2011) and Schneider et al. (2015)[182, 146] have demonstrated.

These advancements in modifying ion selectivity broaden the capabilities of opsins in optogenetic research, enabling researchers to fine-tune neural modulation with increased precision and control.

2.3.5 Opsin Pairs for Bidirectional Optogenetic Control

Precise modulation of neural populations is crucial for demonstrating their sufficiency and necessity in various cognitive functions, specific behavioral activities, or pathological conditions[46, 167]. Optogenetics offers bidirectional control of neurons using two-color light when these neurons co-express spectrally separated excitatory and inhibitory opsins. The pioneering study of bidirectional optogenetic control employed ChR2 and NpHR. ChR2, with its peak activation wavelength around 460 nm, is well-separated from the absorption spectrum of NpHR, which peaks at 590 nm. Consequently, the ChR2-NpHR opsin construct enables bidirectional control of locomotion activity in *Caenorhabditis elegans* in response to blue (470 nm) and orange (590 nm) light pulses[189]. Precise bidirectional control up to 5 Hz has been demonstrated with the ChR2-NpHR system[189].

Additionally, a novel opsin pair, ChR2(H134R)-eNpHR3.0, utilizing potential mutants of ChR2 and NpHR, has facilitated bidirectional control up to 20 Hz at enhanced light irradiances[189, 74, 62]. Bidirectional modulation of basolateral amygdala terminals, implicated in anxiety, and modulation of prefrontal-hippocampal connectivity in pain-related working memory deficits, have been demonstrated with ChR2(H134R)-eNpHR3.0[162, 42, 27]. In the context of Parkinson's disease, bidirectional optogenetic control of neural populations using the ChETA-NpHR opsin pair has shown superior outcomes compared to electrical excitation methods[137]. Furthermore, a study has showcased bidirectional modulation of neural circuits in the Mongolian Gerbil, a model organism for the human auditory system, employing the CatCh-eNpHR3.0 opsin pair[94]. However, CatCh failed to achieve the necessary high-frequency and temporal precision required to stimulate auditory neurons effectively.

More recently, advancements in optogenetics have led to the development of bidirectional opsin pairs by replacing light-driven pumps with anion channelrhodopsins (ACRs)[167]. The study demonstrates that co-expression of GtACR2 with Chrimson enables bidirectional control at significantly lower power compared to earlier opsin pairs utilizing light-driven pumps[167]. However, it should be noted that Chrimson and GtACR2 exhibit similar light sensitivity, potentially increasing the risk of optical cross-talk under high-intensity blue light conditions. To mitigate this issue, it would be advisable to either opt for a more sensitive blue-light-activated ACR or choose less sensitive red-shifted cation channelrhodopsins (CCR) when designing new opsin pairs. As of now, GtACR2 stands as the sole ACR with an absorption peak at the blue wavelength and high light sensitivity. Therefore, the preferable approach would be to select a less sensitive red-shifted excitatory opsin to minimize optical crosstalk.

Numerous new mutants of Chrimson, exhibiting varying light sensitivity and kinetics, have been engineered. For example, the vf-Chrimson, characterized by its rapid kinetics but reduced sensitivity compared to Chrimson, holds the potential for mitigating optical crosstalk concerns.

2.4 Gene expression

The next step involves delivering the genetic material of the opsin into the target cells, typically accomplished using viral vectors. These vectors consist of several essential components, as illustrated in Figure (2.1).

First, the basic building block is the viral expression system itself. Adeno-associated viruses (AAV) and lentivirus are two of the most often used systems. Compared to AAV, which has a packaging capacity of 4 kb, lentivirus has a capability of up to 8 kb. Lentivirions, on the other hand, incorporate their genetic information into the host genome, increasing the risk of cancer while also causing permanent expression. Additionally, this integration reduces the variety of cell types that can be specifically targeted by limiting the promoter alternatives that are available. Conversely, AAV shows benefits such as decreased immunogenicity, wider dissemination because of its smaller size and greater titers, and less sensitivity to temperature changes. These differences make AAV a more desirable choice in some situations on optogenetics.[49, 119, 182].

In optogenetics, cell type specificity is achieved using a number of methods, including as the vector's intrinsic tropism, spatial targeting techniques, and the choice of particular promoters. As the second part of the vector build, the promoter selection presents a variety of options, as Figure (2.1) shows. As mentioned in section 2.3, the third component consists of the genetic information of the opsin itself. Lastly, a reporter gene expressing fluorescent proteins usually makes up the fourth block, which makes it easier to quantify opsin expression[49]. To overcome packaging capacity limitations, alternative techniques are employed. Transgenic or knock-in animals are one such approach, offering high specificity but limited to preclinical studies due to their impracticality for human use. Generating transgenic lines requires substantial time and effort, and introducing new opsins necessitates the creation of new mouse lines. However, this method sacrifices specificity due to spatial localization. Combining transgenic mice, particularly those utilizing cre recombinase-based mouse lines, with viral vector systems enhances specificity[72].

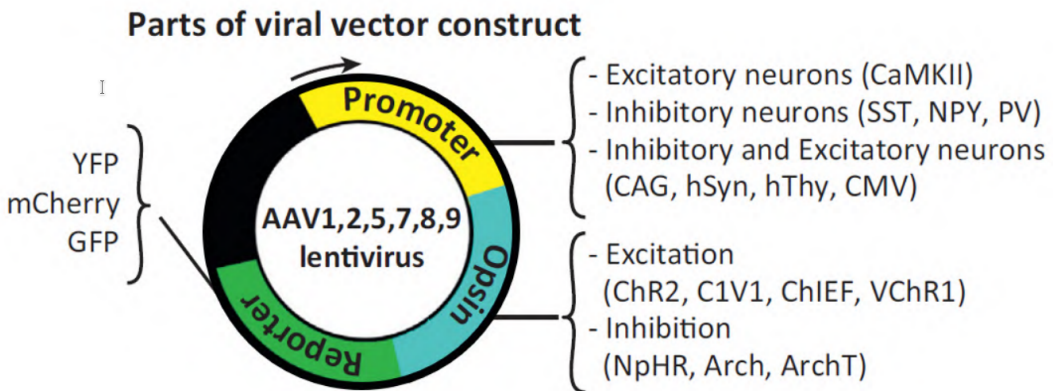


Fig. 2.3 An illustration of a viral vector. Reproduced from Gerits and Vanduffel (2013)[49]

Other methods include lipofection, optoporation, cell-to-myocyte electrical coupling with donor cells[21], electroporation, and gene gun delivery [190]. In particular, optoporation shows potential for improving site-specificity and lessening tissue injury. This method combines micro-injection of opsin genes with an ultrafast near-infrared laser beam to generate highly localised cell poration[119].

2.5 Illumination

The final step in optogenetics involves illuminating the genetically modified cells. Several options exist, each with its drawbacks and advancements. Light sources include mercury or xenon bulbs, light-emitting diodes (LEDs), continuous-wave lasers, or ultrafast pulsed lasers. Bulbs emit a broad spectrum of light, necessitating filtering, and are rarely used due to heat generation and rapid degeneration[129]. Optimal optogenetic experiments recommend using light wavelengths close to the opsin's peak wavelength to minimize phototoxicity, photobleaching, or spontaneous cell activation. Additionally, this approach allows for multicolored simultaneous activation and requires high temporal control, making LEDs and lasers preferable. Laser advantages include coherent light production, higher coupling efficiency, and superior temporal resolution, particularly in ultrafast lasers capable of emitting femtosecond-long pulses. However, lasers are associated with increased complexity and cost[119, 129, 190].

Figure 2.4 showcases diverse methodologies for refining spatial resolution within optogenetics. Enhanced focus of the light beam emerges as a pivotal technique, signifi-

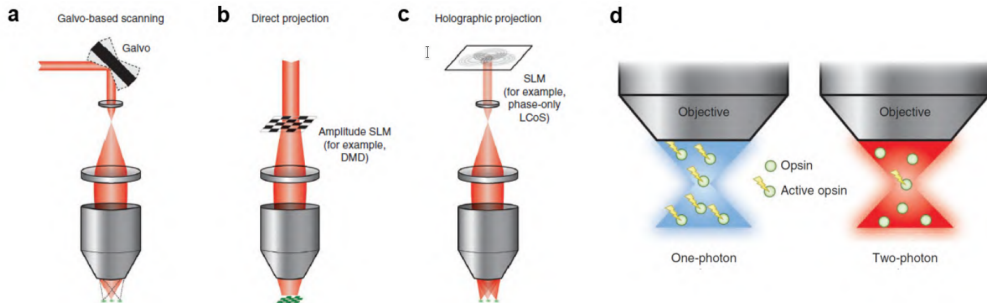


Fig. 2.4 strategies for lighting that improve spatial specificity. (A) scanning using galvos. (b) using a digital micromirror for direct projection. (c) the projection of holography. (d) Activation by one or two photons. Reproduced from (Packer et al., 2013)[129].

cantly refining resolution in the transverse plane. However, there persists a challenge regarding axial stimulation of neighboring cells. To counteract this, modulating the light source intensity ensures that only the focal point surpasses the activation threshold. Galvanometer mirrors are then employed to precisely direct light towards the intended region, as depicted in Figure 1.4 (a).

An alternative approach involves refining temporal control through spatial light modulators or digital micromirror devices, as illustrated in Figure 1.4 (b). Despite its complexity, holographic projection offers improved axial resolution (refer to Figure 1.4 (c)).

While visible light-based one-photon excitation holds promise, it grapples with subpar axial resolution and scattering, particularly in primate models. Two-photon activation presents a remedy by leveraging an ultrafast pulsed near-infrared (NIR) laser. Through the synchronized delivery of two NIR photons within femtoseconds, opsins are selectively activated solely at the focal point. This nonlinear process augments spatial resolution in both transverse and axial planes, enabling minimally invasive *in vivo* stimulation due to reduced scattering (Mohanty et al., 2015; Packer et al., 2013; Petersen et al., 2016).[119, 129, 135].

2.6 Neuronal Signaling

Neuronal signaling is the fundamental process through which information is transmitted and processed within the nervous system, enabling complex behaviors, cognition, and perception. At its core, neuronal signaling involves the generation, propagation, and

modulation of electrical and chemical signals among neurons and their interconnected networks. Understanding the intricacies of neuronal signaling is essential for unraveling the mechanisms underlying brain function and dysfunction, with profound implications for neuroscience, medicine, and beyond. At the cellular level, neuronal signaling begins with the generation of electrical impulses, known as action potentials, which propagate along the length of nerve fibers, or axons, to transmit information over long distances. At synapses, specialized junctions between neurons, electrical signals are converted into chemical signals in the form of neurotransmitters. These neurotransmitters are released from the presynaptic neuron in response to an action potential and bind to receptors on the postsynaptic neuron, leading to changes in its membrane potential and, ultimately, signal propagation.

2.6.1 Types of Neuronal Signaling

Neuronal signaling encompasses diverse mechanisms that allow for precise control and modulation of information flow within neural circuits. Excitatory signaling, mediated primarily by neurotransmitters such as glutamate, promotes neuronal depolarization and the generation of action potentials, facilitating the transmission of excitatory signals between neurons. In contrast, inhibitory signaling, mediated by neurotransmitters like GABA (gamma-aminobutyric acid), hyperpolarizes the postsynaptic neuron, reducing its excitability and dampening signal transmission. Beyond traditional chemical signaling, neurons also employ a variety of neuromodulatory mechanisms to regulate synaptic transmission and network activity. Neuromodulators, such as dopamine, serotonin, and acetylcholine, exert widespread effects on neuronal excitability and synaptic plasticity, shaping complex behaviors and cognitive processes.

2.6.2 Signaling Pathways and Cellular Mechanisms

At the molecular level, neuronal signaling involves intricate signaling pathways and cellular mechanisms that underlie synaptic transmission, plasticity, and integration of neuronal inputs. Key players in these processes include neurotransmitter receptors, ion channels, and intracellular signaling molecules, which govern the strength and dynamics of synaptic communication. Long-term changes in synaptic strength, known as synaptic plasticity, are fundamental for learning and memory formation. Synaptic plasticity mechanisms, such as long-term potentiation (LTP) and long-term depression (LTD), involve alterations in the efficacy of synaptic transmission through modifications in neurotransmitter release, receptor trafficking, and changes in synaptic structure.

2.6.3 Integration of Signals and Network Dynamics

Neuronal signaling does not occur in isolation but within the context of complex neural networks, where individual neurons integrate and process incoming signals to generate coordinated patterns of activity. The emergent properties of neural networks, including synchronization, oscillations, and population coding, play crucial roles in information processing and computation within the brain.

Furthermore, neuronal signaling is dynamic and adaptive, allowing for the flexible modulation of neural circuits in response to changing environmental demands, experiences, and internal states. Homeostatic mechanisms ensure the stability and robustness of neuronal signaling networks, preventing runaway excitation or inhibition and maintaining the overall balance of neural activity.

2.6.4 Implications for Neuroscience and Medicine

The study of neuronal signaling holds immense promise for advancing our understanding of brain function and dysfunction, with far-reaching implications for neuroscience and medicine. Dysregulation of neuronal signaling underlies a wide range of neurological and psychiatric disorders, including epilepsy, schizophrenia, and Alzheimer's disease, highlighting the importance of unraveling the molecular and cellular mechanisms involved. Moreover, insights into neuronal signaling mechanisms have inspired the development of novel therapeutic approaches aimed at restoring normal brain function in disease states. Targeted modulation of synaptic transmission, neuromodulatory systems, and synaptic plasticity pathways offers potential avenues for the development of precision therapies for neurological and psychiatric disorders.

2.7 The clinical translation

The advent of optogenetics stands as a monumental milestone in neuroscience, heralding a paradigm shift in our understanding of the brain. Its exquisite temporal precision, cellular specificity, and bi-directional manipulation capabilities have rendered it a veritable Swiss army knife for researchers. With the power to selectively activate or silence neuronal populations, optogenetics has unraveled the intricate tapestry of neural circuits underlying behavior with unprecedented clarity. Its utility extends beyond the laboratory, offering profound insights into the pathophysiology of neurological disorders. While hurdles remain on the journey toward clinical translation, a burgeoning body of

research attests to its transformative potential in reshaping the landscape of therapeutic interventions.

2.7.1 Application

Optogenetics has indeed emerged as a groundbreaking technique in neuroscience over the past decade. By enabling precise control of cellular activity through the genetic expression of light-sensitive proteins (opsins) and optical stimulation, optogenetics offers unparalleled spatial and temporal resolution. This capability has revolutionized our ability to study neural circuits and behavior, allowing researchers to manipulate neuronal activity with unprecedented precision.

Moreover, the versatility of optogenetics extends beyond basic research applications. It holds immense potential as a therapeutic tool for a wide range of medical disorders, including neurological conditions like epilepsy and Parkinson's disease. By selectively modulating neural activity in targeted brain regions, optogenetics could offer novel approaches for treating neurological disorders that are currently challenging to manage with conventional therapies.

Overall, the combination of genetic manipulation and optical control provided by optogenetics represents a transformative advancement in neuroscience and holds promise for both advancing our understanding of brain function and developing innovative therapeutic interventions for neurological and psychiatric disorders. While the field is still in its early stages of development, researchers have been exploring the application of optogenetics in preclinical models of various disorders, with promising results. Some of the disorders and diseases that could potentially benefit from optogenetic interventions include:

2.7.1.1 Epilepsy

Epilepsy poses a significant therapeutic challenge, with pharmacological interventions (effective in only 50% of cases treated with AEDs) and electrophysiological approaches offering limited success [159]. A substantial portion of patients, over 20%, continue to experience refractory epilepsy despite treatment efforts [180]. In cases of partial epilepsies, seizures originate from focal areas, rendering them susceptible to optogenetic neuromodulation. Research has demonstrated the efficacy of optogenetic interventions in managing epileptic seizures in animal models, employing two primary strategies.

First, optogenetic inhibition has demonstrated promise in controlling seizures. Proof of principle was demonstrated by Tønnesen[160], who was able to effectively attenuate

bursts in pyramidal neurons using NpHR activation. Later in vivo investigations by Paz[134] and Krook-Magnuson[100] showed thalamic inhibition or the cessation of seizures in cases of temporal lobe epilepsy with a hippocampal focus[159, 190].

As an alternative, activating inhibitory interneurons can be used to control seizures. Research conducted in vivo and in vitro has demonstrated the promise of optogenetics in this context. The efficacy of ChR2 activation in PV-cre and SST-cre mouse brain slices, as well as in PV-cre animals, was shown by Kokaia et al. (2013), Krook-Magnuson et al. (2013), and Wykes et al. (2016)[13, 159, 180, 97].

2.7.1.2 Parkinson's Disease

Parkinson's disease stands as a prevalent neurodegenerative disorder, marked by the degeneration of dopaminergic neurons in the substantia nigra pars compacta (SNc), leading to debilitating symptoms like bradykinesia, tremor, walking difficulties, and rigidity. The principal treatment is still L-DOPA, but long-term use of it frequently results in serious adverse effects such as dyskinesia and motor fluctuations[32, 135, 184]. High-frequency deep brain stimulation (DBS) has been shown to be an effective treatment for these symptoms, although its processes are still not fully understood and lack cell specificity[184].

Optogenetics is a promising field with a variety of intervention options. One strategy is to directly activate medium-sized spiny neurons that express the D1 receptor. This effectively engages the basal ganglia circuitry's direct pathway and subsequently reduces symptoms. This was demonstrated in vivo by Kravitz[98], who also observed exacerbation of symptoms upon activation of the indirect pathway using ChR2. Alternatively, modulation of the subthalamic nucleus via optogenetic inhibition has shown promise in alleviating symptoms of akinesia and L-DOPA-induced dyskinesia[185, 184, 156].

2.7.1.3 Depression and Anxiety Disorders

Optogenetics has been used to investigate the neural circuits underlying mood disorders such as depression and anxiety. By targeting specific brain regions implicated in emotional regulation, researchers aim to modulate neuronal activity and restore normal mood states. Optogenetic manipulation of neuronal circuits involved in reward processing, stress response, and emotional regulation could offer novel therapeutic approaches for treating depression and anxiety disorders[161].

2.7.1.4 Chronic Pain

Chronic pain conditions, such as neuropathic pain and fibromyalgia, are often challenging to manage with existing therapies. Optogenetics offers the potential to selectively modulate pain processing pathways in the nervous system, providing targeted relief from chronic pain while minimizing side effects associated with traditional analgesic drugs[181].

2.7.1.5 Addiction

Optogenetic studies have shed light on the neural circuits underlying addiction and substance abuse disorders. By targeting specific brain regions involved in reward processing and addiction-related behaviors, researchers aim to modulate neuronal activity to reduce drug-seeking behavior and prevent relapse in individuals with substance use disorders[22].

2.7.1.6 Neurodegenerative Diseases

Optogenetics holds promise for studying and potentially treating neurodegenerative diseases such as Alzheimer's disease, Huntington's disease, and amyotrophic lateral sclerosis (ALS). By targeting specific neuronal populations affected by these disorders, researchers aim to mitigate disease progression and improve cognitive function or motor control[164].

2.7.2 Apart from the brain

Optogenetics extends beyond the central nervous system, offering potential applications in the peripheral nervous system, cardiac tissues, and muscular cells. Noteworthy advancements have been achieved in cardiovascular research. Optical defibrillation, for example, holds promise for pain relief without stimulating surrounding skeletal muscles, as demonstrated by Boyle et al. (2015)[146]. Moreover, optogenetic techniques allow prolonged stimulation without the electrochemical reactions associated with electrical stimulation, as shown in the work of Bruegmann et al. (2010)[25]. Researchers have also explored optogenetic approaches in human embryonic stem cells, successfully expressing ChR2 and differentiating them into cardiomyocytes, as demonstrated by Abilez et al. (2011)[3]. Nevertheless, applying optogenetics to the spinal cord and peripheral nervous systems poses challenges due to their intricate and diverse characteristics, mobility, and vigorous immune responses. Despite these challenges, optogenetics offers diverse

illumination techniques, ranging from cuff implants to minimally invasive methods like transdermal illumination. Although *in vitro* and *ex vivo* studies have demonstrated promise in somatosensation and pain modulation, the advancement of transdermal illumination is necessary for its effective *in vivo* application. According to Alilain[4], optogenetics also has the capacity to regulate motor circuits and can therapeutically repair damaged spinal circuits. Llewellyn[106] and Montgomery[120] have proposed that it may also have benefits over electrical stimulation in terms of regulating lower motor neurons, supplying physiological recruitment order, and lowering muscle fatigue.

2.8 Hurdles and Challenges

Optogenetics emerged as a groundbreaking tool aimed at unraveling the mysteries of the brain's inner workings and seeking solutions for a spectrum of neurological disorders. While initial strides were made through experiments conducted on small animal models, the ultimate frontier lies in conducting human trials. Notably, a recent milestone in the field was the successful execution of human trials utilizing optogenetic-based retinal prostheses[143]. However, the dream of achieving precise optogenetic control over human brain neurons with the desired spatiotemporal resolution remains elusive.

A formidable obstacle in the realm of optogenetics is the quest for achieving temporally precise, high-frequency control over activity patterns within targeted neural circuits, at the desired spatiotemporal resolution[151, 110, 6, 11]. This pursuit is underpinned by the recognition that precisely timed neural events and high-frequency spiking are integral to a myriad of neural phenomena spanning behavior, learning, and pathology[139, 71, 144, 12, 11]. Of particular significance is the role of high-frequency spiking in modulating the propagation of spikes throughout dendrites and influencing localized cellular processes.

Many neurons, including fast-spiking interneurons in cortical areas and spiral ganglion neurons in the auditory system, exhibit firing frequencies reaching several hundred Hertz[110]. Dysfunction in fast-spiking parvalbumin-positive interneurons has been implicated in cerebral aging and a spectrum of acute and chronic brain diseases, such as epilepsy, stroke, Alzheimer's disease, vascular cognitive impairment, and schizophrenia[144, 139]. Furthermore, it may contribute to the impairment of fast oscillations in neural networks and higher brain functions. Consequently, the development of a method capable of precisely eliciting spiking at higher frequencies is imperative for probing these phenomena and deciphering how the brain encodes information within such high-frequency spiking patterns.

Heating poses a significant challenge in the context of long-term optical stimulation required for sustaining spiking activity. Temperature fluctuations during *in vivo* optogenetic experiments can have notable electrophysiological and behavioral ramifications[128]. Studies indicate that even a modest increase in tissue temperature, ranging from 0.2 to 2 degrees Celsius, can lead to spike suppression across multiple brain regions[149, 128]. Consequently, there is a pressing need for opsins with heightened light sensitivity and larger photocurrents. However, achieving this desirable trait is complicated by the inverse relationship between light sensitivity and opsin kinetics, posing a challenge to achieving both low-power and high-frequency control[116].

Furthermore, noninvasively stimulating deeply situated neurons presents another hurdle in optogenetics. Conventional methods involve surgically implanting optical fibers or μ LEDs to activate neurons embedded deep within brain tissue, which is inherently invasive and can result in brain lesions, significant neuronal loss, and acute inflammatory responses[178]. Moreover, such interventions disrupt plasticity and homeostasis by activating microglia and astrocytes[55]. Opsins with red-shifted activation wavelengths offer a promising solution for deep excitation, as longer wavelengths experience smaller absorption and scattering coefficients within brain tissue[44, 163]. Alternatively, increasing light intensity at the source-tissue interface can activate larger volumes and deeper areas, although this approach must adhere to safety thresholds to mitigate the risk of photothermal damage and undesirable changes in tissue temperature[128].

Currently, the optogenetic toolbox boasts an extensive array of hundreds of opsins and their mutants, each offering a diverse spectrum of kinetics, spectral sensitivity, photosensitivity, conductances, and ion-selectivity. However, the process of meticulously selecting the most suitable opsin for a specific application demands considerable effort and often entails repetitive experiments. The complexity escalates further when attempting to optimize photostimulation parameters and physiological conditions to achieve desired control with each opsin. In this landscape, computational optogenetics emerges as a potent ally in guiding experimental endeavors. Nevertheless, the field is relatively nascent, with only a scant number of theoretical models and studies reported to date.

In table 2.1 the numbers refers to the citation and "all" refers to all the written below:
1: Azimihashemi et al. (2014)[5], 2: Boyle et al. (2015)[21], 3: Diester et al. (2011)[39],
4: Entcheva and Williams (2014)[40], 5: Gerits and Vanduffel (2013)[49], 6: Guru
et al. (2015)[72], 7: Häusser (2014)[76], 8: Lin et al. (2009)[104], 9: Mohanty et

al. (2015)[119], 10: Packer et al. (2013)[129], 11: Paz et al. (2013)[134], 12: Tao et al. (2018)[158] 13: Tønnesen and Kokaia (2017)[159], 14: Williams and Denison (2013)[174], 15: Williams and Entcheva (2015)[175], 16: Wykes et al. (2016)[180], and 17: Yizhar et al. (2011)[183].

Table 2.1 Benefits and obstacles for conversion to clinical use, along with potential solutions

Advantages	Obstacles	Possible Solutions
Cell specificity ^{all}	Toxicity of expression ^{2,3,6,16}	opsin Alter promoter combination ³
High temporal resolution (ms) ^{all}	Heterogeneous light delivery and attenuation ^{2,3,6,7,14,16}	Branched fiber illumination ¹³ , red-shifted opsins ^{2,5,6,13} or synthetic retinal analogues ¹
Rapid reversibility ^{5,6}	Heterogeneous expression ^{2,3,6,7,14,16}	opsin Multi site injection ¹⁰
Co-expression and bidirectional control ^{3,5,6,15} No electrochemical reactions ^{2,15}	Small capacity of viral vectors limits co-expression ^{5,17} No subset specificity ^{6,7}	INTERSECT ⁶ , optoporation ⁹
True electrical and fMRI recordings ¹⁴	Reliable high frequency spiking ^{8,17}	ChETAs, ChEFs ^{5,6,8}
No extra need for cofactors (retinal) in mammals ¹⁷ Control studies are easy ¹⁷	Non physiological behavior ^{6,7,16} Antidromic activation ^{6,7}	
Silent in the dark (no effect on cell properties) ¹³	Phototoxicity and bleaching ¹⁷	High light-sensitive opsins ¹⁷
Applicable in Thalamus ¹¹	Invasiveness of optrodes ^{3,16,17}	Two photon stimulation ^{9,10} , Nanoparticle upconversion ¹²
Minimally invasive beyond the brain ^{2,14,15}	Synchronization of cells ^{6,7}	SFOs ^{6,7}
	Heating ¹⁷	High light-sensitive opsins ¹⁷ , red-shifted opsins ^{2,5,6,13}
	Rapid evolution and discoveries delay clinical trials ¹⁴	

Chapter 3

Neuronal Modeling

The human brain, a marvel of biological architecture, harbors within its intricate folds and convolutions two fundamental classes of cells: neurons and glial cells. Neurons, the quintessential communicators of the nervous system, reign supreme in numbers, with estimates soaring above a staggering 100 billion. Each neuron, akin to a miniature universe, intricately weaves a web of connections, establishing a vast network of synaptic pathways crucial for information processing and transmission. Remarkably, a single neuron may boast thousands of synaptic connections, forming a labyrinth of intricate circuitry that orchestrates the symphony of neural activity within the brain.

In concert with the neurons, the glial cells, often overshadowed yet indispensable, serve as the unsung heroes of brain function. With their supportive, protective, and homeostatic roles, glial cells outnumber their neuronal counterparts by an astonishing tenfold, underscoring their profound influence on brain physiology. These cellular allies, encompassing various subtypes such as astrocytes, oligodendrocytes, and microglia, form an intricate tapestry that interweaves with the neurons, collectively sculpting the dynamic landscape of the brain. Despite their numerical disparity, the harmonious coexistence of neurons and glial cells underscores the brain's remarkable complexity. Each cell type, with its unique morphology, molecular profile, and functional repertoire, contributes to the kaleidoscopic diversity that defines the brain's cellular mosaic. This exquisite diversity, coupled with the intricate interplay between neurons and glial cells, engenders a dynamic and adaptive organ capable of unparalleled feats of cognition, perception, and behavior.

Indeed, it is through the ceaseless ballet of neuronal firings, synaptic transmissions, and glial interactions that the brain orchestrates the symphony of human experience. From the acquisition of knowledge to the modulation of emotions, from the perception

of sensations to the execution of motor actions, the intricacies of brain function permeate every aspect of our existence. Thus, to unravel the enigma of brain function, to decipher the mysteries of cognition and consciousness, we must embark on a journey to understand its fundamental components. At the heart of this quest lies the neuron, the elemental unit of neuronal communication and the cornerstone of neuroscientific inquiry. As we peel back the layers of complexity, delving deeper into the neural circuits and cellular mechanisms that underpin brain function, we inch closer to unlocking the secrets of the mind.

In the forthcoming chapter, an exploration into the electrophysiology of cellular activity will be undertaken, alongside an in-depth examination of the Hodgkin-Huxley model[80]. This model serves as the cornerstone of numerous neural models elucidated throughout this thesis. Drawing from a wealth of scholarly insights, this chapter synthesizes findings from five pivotal sources: Petersen and Foustoukos (2016)[135], part one of Neural dynamic by Wulfram Gerstner, Werner M. Kistler, Richard Naud[? 53, 51, 50, 52], An Introductory Course in Computational Neuroscience by Paul Miller[117], Computational and Mathematical Modeling for Neural Systems by Peter Dayan, L. F. Abbott[1] and Izhikevitch [87], unless expressly noted otherwise. Citations for specific details will be meticulously provided within the text, ensuring transparency and academic rigor.

3.1 Cell electrophysiology

Neurons, like all cells, are surrounded by a cell membrane composed of phospholipids that form a bilayer around 5 nanometers in thickness. This membrane is impermeable to ions and other charged molecules, somewhat permeable to water, and allows lipophilic compounds to pass through due to its lipid bilayer structure. Consequently, this creates a distinct internal ion concentration compared to the external environment, imparting capacitor-like properties to the cell membrane.

Scattered throughout this membrane are an array of transmembrane proteins, as depicted in Figure 3.1. These proteins play pivotal roles in facilitating the movement of ions across the membrane, thus regulating the signaling abilities of neurons and, consequently, brain function. Two primary classes of transmembrane proteins include ion channels and transporters/pumps. Transporters utilize energy to actively transport ions against their electrochemical gradient, maintaining concentration gradients. On the other hand, as ions follow their electrochemical gradient, ion channels create aqueous pores that allow large ion fluxes to pass through the membrane. Many ion channels have

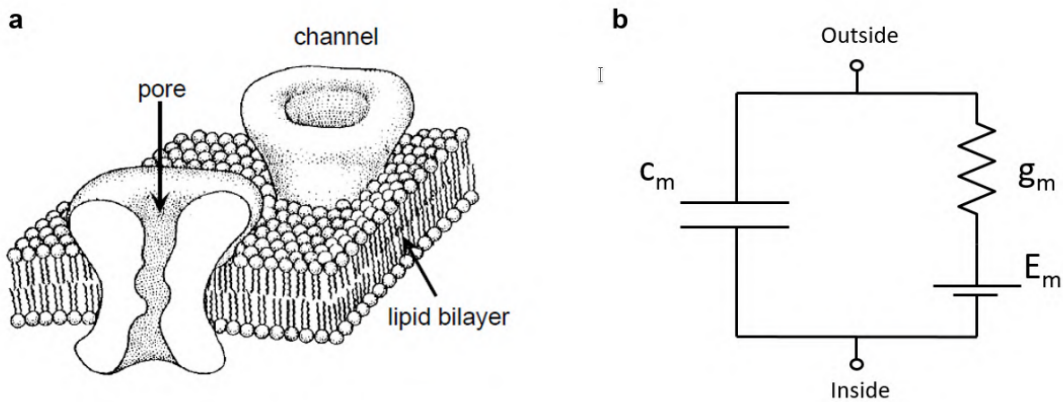


Fig. 3.1 Taken from Abbott and Dayan[2], this schematic illustration shows a portion of the cell membrane with two ion channels.

great selectivity for a particular ion; these channels are often characterized by a size filter in conjunction with a charged filter that imparts cation or anion channel features. Neurons precisely control the flow of ions across their membranes by orchestrating these transmembrane proteins, an essential mechanism for the complex signaling events that underpin brain information processing and neural function.

Globally, the composition within a cell predominantly consists of potassium ions (K^+) and anions, while extracellularly, the environment resembles seawater, characterized by the presence of sodium ions (Na^+) and chloride ions (Cl^-), alongside a higher concentration of calcium ions (Ca^{2+}) (approximated values provided in Table 3.1). When the membrane is at rest, the outside is often described as zero and there is a negative potential across it.

Table 3.1 Ion Concentrations and Equilibrium Potentials.

Numbers adapted from An Introductory course in computational neuroscience book[117].

Ion	Intracellular	Extracellular	Equilibrium Potential
Potassium (K^+)	150 mM	6 mM	-86.1 mV
Sodium (Na^+)	15 mM	120 mM	61.6 mV
Chlorine(Cl^-)	10 mM	120 mM	-66.4 mV
Calcium (Ca^{2+})	50 nM	2 mM	141.7 mV

As a result, an ion is subject to two opposing forces: the concentration gradient and the electrical potential difference. These forces cancel one another out at the equilibrium potential, creating a situation in which there is no net current flow. The Nernst

equation can be used to determine the equilibrium potential for ion channels that only conduct one ion selectively:

$$E_X = \frac{RT}{zF} \ln \left(\frac{[X]_{\text{out}}}{[X]_{\text{in}}} \right) \quad (3.1)$$

The equilibrium potential, denoted as E_X , is determined by several factors: the universal gas constant (R), the temperature (T), the ion's valence (z), Faraday's constant (F), and the concentrations of the ion inside ($[X]_{\text{in}}$) and outside ($[X]_{\text{out}}$) the cell. Although ion channels are typically specific to certain ions, they also allow passage to other ions to a lesser extent. This selectivity and permeability to multiple ions can be described using the Goldman-Hodgkin-Katz (GHK) equation. The GHK equation calculates the reversal potential for monovalent ions considering their permeability and concentrations inside and outside the cell.

Here is the GHK equation for monovalent ions:

$$E_m = \frac{RT}{F} \ln \left(\frac{\sum_i^n P_{m_i^+} [M_i^+]_{\text{out}} + \sum_j^m P_{A_j^-} [A_j^-]_{\text{in}}}{\sum_i^n P_{m_i^+} [M_i^+]_{\text{in}} + \sum_j^m P_{A_j^-} [A_j^-]_{\text{out}}} \right) \quad (3.2)$$

In this context, $[M_i^+]$ and $[A_j^-]$ represent the concentrations of the i -th cation and the j -th anion, respectively. The term P_{ion} indicates the permeability of the membrane to a specific ion. For ions with multiple valence states, the Goldman-Hodgkin-Katz equation has been extended to accommodate these cases, with such generalizations being developed in 1976 (Pickard, 1976)[136].

3.1.1 The trans-membrane current

The Hodgkin-Huxley (HH) model stands as a seminal framework in computational neuroscience, providing a comprehensive understanding of the electrical activity within neurons. The model's foundation lies in its meticulous representation of the neuronal membrane dynamics through a series of interconnected components. At its core, the HH model encapsulates the behavior of the neuronal membrane as a dynamic interplay between ion channels, ion concentrations, and membrane capacitance. Each of these elements plays a pivotal role in shaping the electrical properties of the neuron.

Firstly, the membrane capacitance represents the ability of the neuronal membrane to store charge, akin to a capacitor in an electronic circuit. This capacitance arises from the lipid bilayer structure of the membrane, which acts as a dielectric separating the intracellular and extracellular environments, Figure 3.1 (a). As ions flow across

the membrane during neuronal activity, the membrane capacitance undergoes charging and discharging processes, contributing to the generation and propagation of electrical signals.

Secondly, the HH model incorporates the presence of ion channels embedded within the neuronal membrane. These ion channels serve as selective gates that regulate the flow of ions across the membrane in response to changes in the membrane potential. The HH model distinguishes between different types of ion channels, such as voltage-gated sodium (Na^+) channels, voltage-gated potassium (K^+) channels, and leak channels. Each type of channel exhibits distinct kinetics and conductances, influencing the membrane's excitability and the generation of action potentials. Furthermore, the HH model accounts for the role of ion concentrations in shaping neuronal dynamics. Changes in the concentrations of ions, particularly sodium (Na^+) and potassium (K^+), influence the driving forces for ion movement across the membrane, thereby impacting neuronal excitability and firing patterns. In addition to these components, the HH model also incorporates the concept of equilibrium potentials, which represent the membrane potentials at which the net flow of ions across the membrane ceases due to opposing electrochemical gradients. These equilibrium potentials, determined by the Nernst equation, play a crucial role in establishing the resting membrane potential and shaping the dynamics of action potential generation.

Overall, the Hodgkin-Huxley model offers a comprehensive framework for understanding the biophysical mechanisms underlying neuronal excitability and action potential generation. By integrating multiple components such as membrane capacitance, ion channels, ion concentrations, and equilibrium potentials, the HH model provides a sophisticated depiction of the electrical properties of neurons, paving the way for advances in computational neuroscience and our understanding of neural function.

In the Hodgkin-Huxley model, the intricate dynamics of a neuron's membrane are elegantly captured through a three-component conceptualization. Visualized in Figure 2.1 (b), this model portrays the cell as comprising a capacitor, symbolizing the cell membrane's ability to store charge; a conductance or resistor, representing the ion channels that regulate the flow of ions across the membrane; and a voltage source, indicative of the equilibrium potential that governs ion movement. For each ion channel, a pair of this resistance and voltage source is added parallelly. This holistic representation offers a nuanced understanding of the complex interplay between electrical and chemical processes within neurons. Figure 2.2 provides a more detailed illustration of these components, underscoring the model's granularity in capturing the intricacies of neuronal membrane dynamics. As per Kirchhoff's law, the total

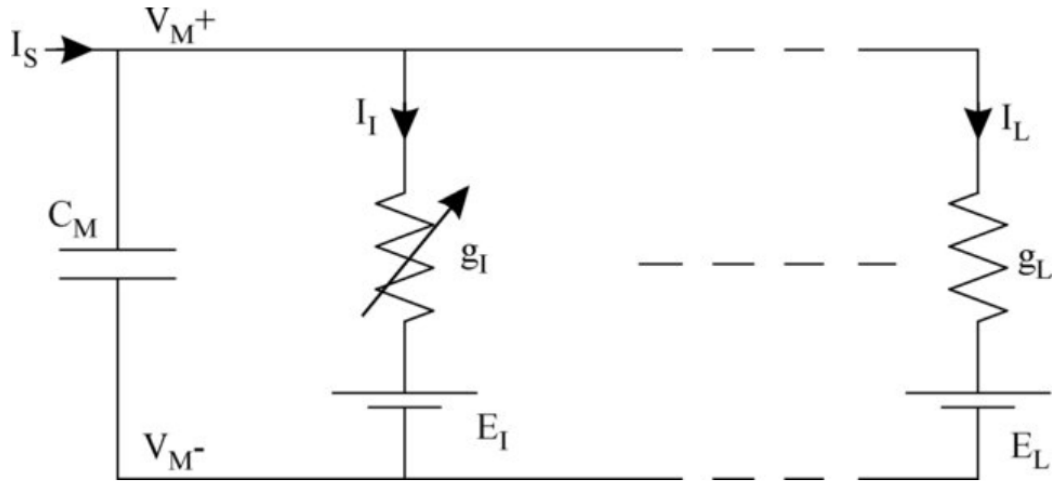


Fig. 3.2 An electrotonically compact cell's electric equivalent. Arrows are used to show different conductance levels.[145]

current flowing through the membrane is determined by combining the capacitive current, which accounts for membrane charging and discharging, with the ionic current, reflecting ion movement through channels, and any additional current sources that impact membrane dynamics.

The electrical representation of a compact electrotonic cell. Varying conductances are illustrated with arrows[145].

This comprehensive method provides a solid foundation for comprehending brain signaling and information processing systems in addition to clarifying the basic ideas guiding neuronal function. The total current across the membrane with K, Na, Cl, Ca, and a leak ion channel is computed as follows, per Figure 3.2:

$$i_m = C_m \frac{dV_m}{dt} + g_{K^+}(V_m - E_{K^+}) + g_{Na^+}(V_m - E_{Na^+}) + g_{Cl^-}(V_m - E_{Cl^-}) + g_{Ca^{2+}}(V_m - E_{Ca^{2+}}) + (V_m - E_{\text{leak}}) \quad (3.3)$$

In this equation:

- i_m represents the total membrane current,
- C_m is the membrane capacitance,
- g_{K^+} , g_{Na^+} , g_{Cl^-} , $g_{Ca^{2+}}$, and g_{leak} are the conductances of potassium, sodium, chloride, calcium, and leak ions, respectively,

- V_m is the membrane potential,
- E_{K^+} for potassium, E_{Na^+} for sodium, E_{Cl^-} for chloride, $E_{Ca^{2+}}$ for calcium, and E_{leak} for leak ions.

The equilibrium potential for ions (E_{ion}) and their respective conductances (g_{ion}) are denoted as such. These values, calculated via the Nernst equation, represent the equilibrium potential and the specific conductance of the ion channel. The symbol C_m denotes the specific membrane capacitance, defined as the total membrane capacitance divided by the cell's surface area. The total membrane current per unit area is represented by i_m [81].

Table 2.1 provides estimated values for the reversal potentials. The driving force for any given current (X) is given by $(V_m - E_X)$. When the membrane potential (V_m) exceeds the reversal potential, an outward current is generated; conversely, when V_m is below the reversal potential, an inward current is generated. These currents act to return V_m towards the Equilibrium potential. At equilibrium, the membrane voltage is predominantly shaped by the reversal potentials, favoring the one linked to the greatest conductance. In steady-state conditions, Equation 3.3 undergoes simplification.

$$V_m = \frac{g_K E_K + g_{Na} E_{Na} + g_{Cl} E_{Cl} + g_{Ca} E_{Ca} + g_{\text{leak}} E_{\text{leak}}}{g_{\text{total}}} \quad (3.4)$$

In this equation:

$$g_{\text{total}} = g_{K^+} + g_{Na^+} + g_{Cl^-} + g_{Ca^{2+}} + g_{\text{leak}}$$

and g_K , g_{Na} , g_{Cl} , g_{Ca} , g_{leak} are the conductances of potassium, sodium, chloride, calcium, and leak ions, respectively.

While Figure 3.2 provides a more intricate depiction of a cell compared to Figure 3.1 (b), it still presents a basic representation. As the thesis progresses, it will become evident that there are additional and varied types of currents that must be taken into account. Moreover, Equation 2.3 may not always suffice, necessitating a more elaborate expression. This is particularly relevant to calcium ion-regulated channels, where the link between membrane current, conductance, and potential is found using the Goldman-Hodgkin-Katz equation.

$$i_X = P_x \cdot z_X^2 \cdot \left(\frac{V_m F^2}{RT} \right) \cdot \frac{([X]_{\text{in}} - [X]_{\text{out}} \cdot \exp\left(-\frac{z_X V_m F}{RT}\right))}{1 - \exp\left(-\frac{z_X V_m F}{RT}\right)} \quad (3.5)$$

above equation represents This equation represents the membrane current i_X for a specific ion X and is expressed in terms of the ion's permeability P_x , valence z_X ,

membrane potential V_m , universal gas constant R , temperature T , and Faraday's constant F , as well as the ion concentrations inside $[X]_{\text{in}}$ and outside $[X]_{\text{out}}$ the cell.

3.1.2 The axial current

In the previous section, we assumed the cell to be electrically homogeneous, implying a consistent membrane potential across its entire surface. This simplification is suitable for modeling a cell as a single, small, spherical compartment. However, in reality, cells consist of various structures such as dendrites, soma, and axons (refer to Figure 3.3). This complexity introduces significant axial resistance (R_{Axial}), resulting in spatial variations in membrane potential when the cell is disturbed. This spatial diversity is effectively described by the cable equation.

The cable equation is a partial differential equation commonly used in neuroscience to describe the propagation of electrical signals along neuronal structures such as dendrites and axons. It takes into account the effects of both passive electrical properties (such as membrane capacitance and resistance) and the spatial distribution of ion channels and conductances along the neuronal membrane. By considering the axial resistance and the spatial variation in membrane potential, the cable equation provides a more accurate representation of the electrical behavior of neurons with complex morphology. So the equation can be modeled as:

$$\frac{R_m}{R_{\text{Axial}}} \frac{\partial^2 V_m(x, t)}{\partial x^2} - R_m C_m \frac{\partial V_m(x, t)}{\partial t} - V(x, t) = 0 \quad (3.6)$$

In this equation:

- R_m : Membrane resistance.
- R_{Axial} : Axial resistance.
- C_m : Membrane capacitance.
- $V_m(x, t)$: Membrane potential as a function of position x and time t .
- $V(x, t)$: Voltage input.

Axial current, for the most part, the cellular models in this thesis assume electrotonic compactness. The bicomponent LC model, which is introduced in Chapter 5 and uses the Rall model[43] to implement the equation mentioned above, is an exception to this rule.

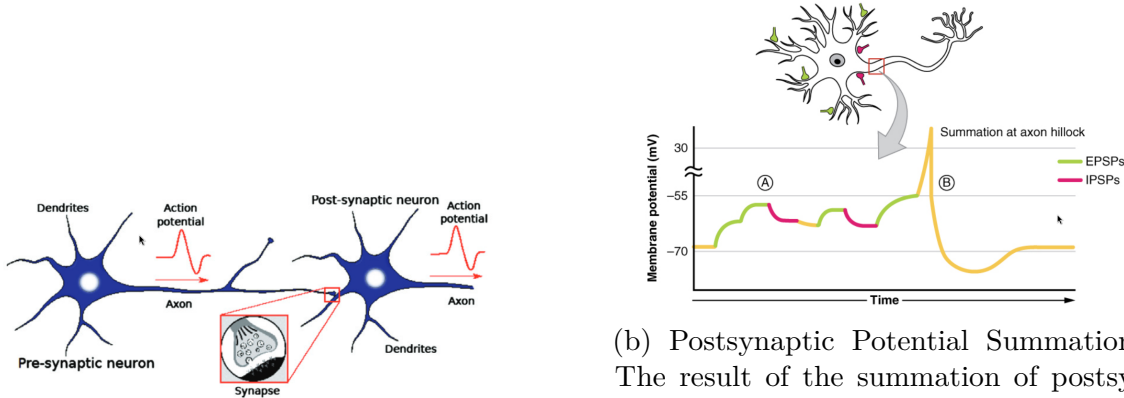
3.2 The Dynamics of Neuronal Action Potentials

Neurons, the fundamental units of the nervous system, play a pivotal role in processing and transmitting information throughout the brain and nervous system. While the concept of neurons as integrators may not universally apply to all neuron types, it serves as a foundational principle in understanding their function within neural circuits. Integral to neuronal function is their capacity to receive and integrate inputs from other neurons. These inputs, received through specialized structures called dendrites, manifest as post-synaptic potentials. As these signals propagate along the dendritic tree toward the soma, the central region housing the cell's nucleus and essential organelles they undergo spatial and temporal integration.

At the axon hillock, a critical juncture located at the junction between the soma and the axon, these diverse inputs are consolidated. Here, synaptic inputs are integrated both spatially and temporally, determining whether the neuron will generate an action potential, a rapid and transient change in membrane potential that serves as the basis for neuronal communication. Integrated signals surpass a certain threshold, typically through the summation of excitatory and inhibitory inputs, an action potential is triggered (as illustrated in Figure 3.5). This electrochemical signal subsequently propagates down the axon, facilitating communication between neurons at synapses. A schematic depicting two interconnected neurons can be observed in Figure 3.3 (a) and how signals get sum and generate an action potential after reaching a specific membrane potential in Figure 3.3 (b).

In the earlier section, our focus was on simulating the passive characteristics of neurons, where capacitance and conductances remained stable over time. Following a disruption to the neuron's equilibrium potential, the membrane potential gradually reverts to its resting state, unfolding over both temporal and spatial dimensions. This phenomenon is quantified by parameters like $\lambda = \sqrt{\frac{R_m}{R_{\text{Axial}}}}$ and $\tau = R_m C_m$, representing the length and time constants, respectively.

However, the initiation of an action potential (AP) is a binary event, necessitating the incorporation of the cell's active behavior into our model. To achieve this, we must consider the dynamic conductance of ion channels, which varies based on factors like membrane potential, ion concentrations, and neurotransmitter activity. This dynamic conductance is visualized in Figure 3.2, where fluctuations are illustrated using arrows. By integrating this active behavior into our model, we can more accurately simulate the initiation and propagation of action potentials in neurons.



(a) In biology, excitatory and inhibitory postsynaptic potentials are delivered from one neuron to the next through chemical and electrical messaging at synapses, driving the generation of new ‘action potentials’. The picture is adapted from an article "Neuromorphic computing using non-volatile memory"[48].

(b) Postsynaptic Potential Summation: The result of the summation of postsynaptic potentials is the overall change in the membrane potential. At point A, several different excitatory postsynaptic potentials add up to a large depolarization. At point B, a mix of excitatory and inhibitory postsynaptic potentials results in a different result for the membrane potential. The picture is adapted from Anatomy & Physiology by OpenStax[19].

Fig. 3.3 Neuronal Action Potential

3.2.1 Voltage gated ion channels

The structure of voltage-gated ion channels typically consists of several transmembrane segments, forming a pore through which ions can selectively pass. Importantly, these channels possess a voltage-sensing domain that is sensitive to changes in the membrane potential. When the membrane potential reaches a certain threshold, the conformation of the voltage-sensing domain undergoes a conformational change, leading to the opening of the ion channel pore. This allows ions, such as sodium Na^+ , potassium K^+ , calcium Ca^{2+} , or chloride Cl^- , to flow down their electrochemical gradients across the membrane. The opening of voltage-gated ion channels results in changes in membrane conductance, leading to alterations in the membrane potential. This phenomenon is crucial for generating electrical signals, such as action potentials in neurons and muscle cells. Once the membrane potential returns to its resting state, voltage-gated ion channels undergo a conformational change that closes the pore, thereby terminating ion flow. Voltage-gated ion channels exhibit remarkable specificity and selectivity for particular ions, allowing for precise control of ion movement across the cell membrane. Moreover, these channels can display various gating kinetics, including fast activation

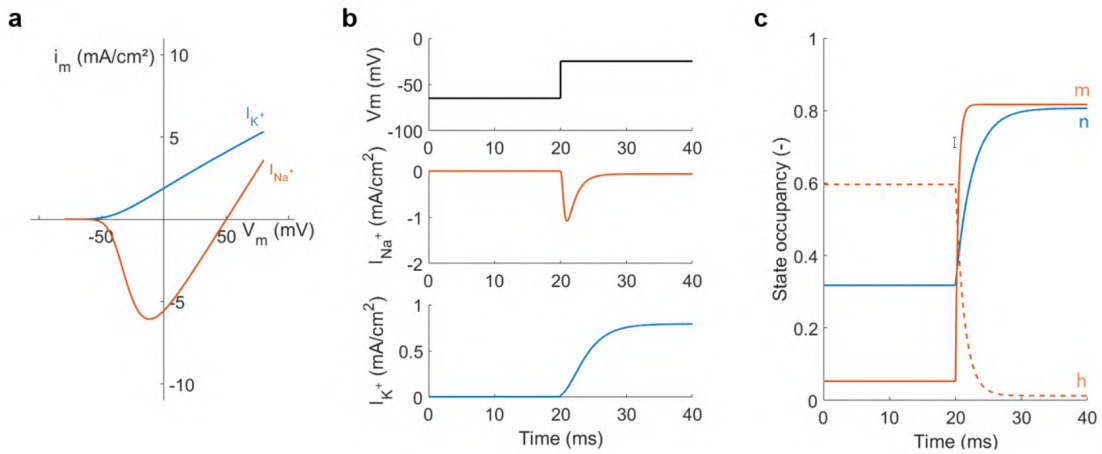


Fig. 3.4 Ion channels that are voltage-dependent are crucial for the operation of neurons. (a) The current-voltage ($I - V$) relationship for potassium (K^+) and sodium (Na^+) currents in these channels is non-linear. (a) They also show how transient and persistent current properties differ from one another. (c) Gate probabilities for K^+ and Na^+ currents provide additional insight into the behavior of these channels. The Hodgkin-Huxley model in MATLAB R2032b was used to construct these visualisations[2].

and inactivation processes, enabling rapid and finely tuned responses to changes in membrane potential.

During an action potential (AP), the membrane potential undergoes sequential changes, starting with depolarization, characterized by an increase relative to the equilibrium potential. Subsequently, repolarization occurs, leading the membrane potential back towards its equilibrium potential. In some cases, hyperpolarization may also occur, resulting in a decrease below the equilibrium potential. Action potentials are generated through the operation of voltage-gated ion channels, essential for regulating ion flux across the cell membrane. These channels display a non-linear current-voltage (I-V) relationship, depicted in Figure 3.4 (a).

3.3 The Hodgkin and Huxley model

Hodgkin and Huxley conducted pioneering experiments in the 1950s, where they measured action potentials (APs) in the giant axon of the squid. Their groundbreaking work, published in 1952[80], revealed crucial insights into the underlying mechanisms of neuronal excitability. As shown in Figure 3.4 (b), Hodgkin and Huxley's tests revealed two different currents connected to the AP: a fast transient sodium current and a sluggish persistent potassium current. The sodium current is responsible for

the rapid depolarization phase of the AP, while the potassium current contributes to the subsequent repolarization and hyperpolarization phases. Building upon their experimental findings, Hodgkin and Huxley developed a mathematical model to describe the behavior of voltage-gated ion channels underlying the generation of the AP. This model, known as the Hodgkin-Huxley (HH) model, revolutionized our understanding of neuronal excitability and laid the foundation for computational neuroscience.

The HH model describes the dynamics of ion currents across the neuronal membrane using a set of differential equations based on the principles of electrical circuit theory. By incorporating the properties of voltage-gated ion channels, including their activation and inactivation kinetics, the HH model accurately captures the temporal dynamics of the AP. Hodgkin and Huxley's HH model provided a comprehensive framework for understanding the complex interplay of ion channels in generating and propagating electrical signals in neurons. Their work remains a cornerstone of neuroscience and continues to influence research in the fields of computational neuroscience, neural modeling, and ion channel physiology.

Equation 3.3 illustrates how the currents are defined in the Hodgkin-Huxley model. Where i_X represents the current for ion X , g_X is the conductance of ion X , V_m is the membrane potential, and E_X is the reversal potential for ion X .

$$i_X = g_X(V_m - E_X) \quad (3.7)$$

The conductance, however, is variable and depends on the open probability of the channel. Therefore, this can be written as:

$$g_X = g_{X,\max} \cdot P_X \quad (3.8)$$

When the open probability, P_X , equals 1, the conductance is represented by the maximal conductance, $g_{X,\max}$. A particle gating technique models this voltage-dependent open probability. Activation and inactivation are the two gating mechanisms identified by Hodgkin and Huxley. As a result, the open probability may be determined using the formula below:

$$P_X = m^a h^b \quad (3.9)$$

where the activation and inactivation probabilities are represented by m and h , respectively, and the number of activation and inactivation gates is represented by a and b .

There is no inactivation in the slow persistent potassium current, also known as the delayed rectifier K^+ . Consequently, it is possible to reduce the gating variable h to unity and ignore it. Furthermore, a is set to four in accordance with the tetrameric shape of the channel and the observations of Hodgkin and Huxley. Thus, the open probability can be expressed as follows:

$$P_{K^+} = n^4 \quad (3.10)$$

According to Hodgkin and Huxley's theory, the activation probability is represented by the symbol n . The open probability's rate of change can be represented as follows:

$$\frac{dn}{dt} = \alpha_n(V) \cdot (1 - n) - \beta_n(V) \cdot n \quad (3.11)$$

The transition rate from the closed state $(1 - n)$ to the open state (n) is represented by the symbol α_n , whereas the reverse transition rate is represented by β_n . Below is an illustration of this:

$$(1 - n) \xrightleftharpoons[\beta_n]{\alpha_n} n$$

The rate equation is frequently represented in another way, as follows:

$$\tau_n(V) \frac{dn}{dt} = n_\infty(V) - n \quad (3.12)$$

where:

$$\tau_n(V) = \frac{1}{\alpha_n(V) + \beta_n(V)} \quad (3.13)$$

and

$$n_\infty(V) = \frac{\alpha_n(V)}{\alpha_n(V) + \beta_n(V)} \quad (3.14)$$

One benefit of this formulation is that, with a time constant $\tau_n(V)$, the value of n converges exponentially to its asymptotic value $n_\infty(V)$.

$$P_{Na^+} = m^3 h \quad (3.15)$$

with the rate equations:

$$\frac{dm}{dt} = \alpha_m(V) \cdot (1 - m) - \beta_m(V) \cdot m \quad (3.16)$$

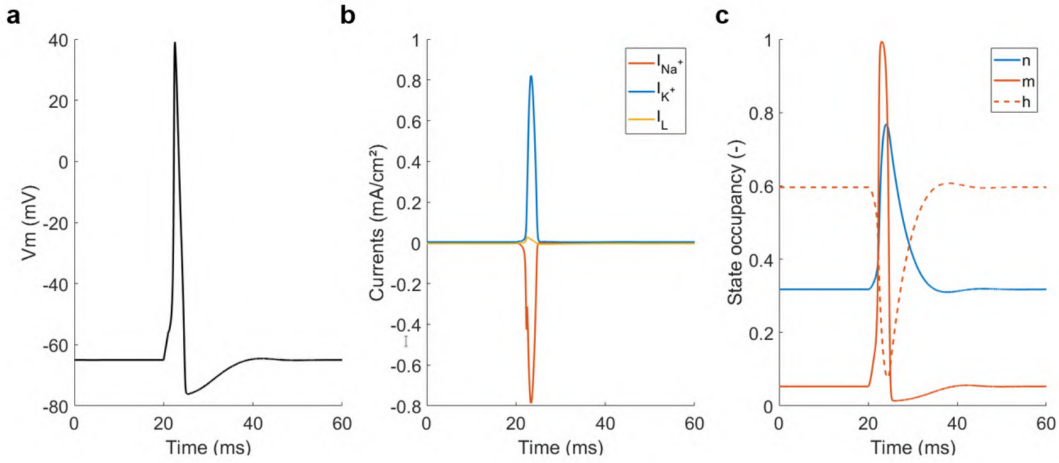


Fig. 3.5 Action potential in accordance with the giant squid axon Hodgkin and Huxley model[82]. (A) APD. (b) single currents. (c) gate probabilities of matching currents, produced by MatlabR2023b and color-coded.

$$\frac{dh}{dt} = \alpha_h(V) \cdot (1 - h) - \beta_h(V) \cdot h \quad (3.17)$$

Figure 3.4 (b) shows both the potassium and sodium currents. The sodium channel's activation probability (m) first rises with cell depolarization, and then h falls, resulting in inactivation. At the same time, potassium channel activation probability rises. These potassium channels stay open until repolarization of the cell occurs (Figure 3.4(c)). Notably, the refractory duration is influenced by the sodium current's delayed deactivation, which happens only after repolarization. Due to this delayed deactivation phenomenon, the refractory period can be divided into two distinct categories: the absolute refractory period, which is defined as the time when firing another action potential is not possible, and the relative refractory period, which is defined as the time when firing an action potential has an increased threshold.

Three different currents were included by Hodgkin and Huxley in their action potential generation model:

$$I_m = C_m \frac{\partial V}{\partial t} + I_{Na^+} + I_{K^+} + I_l \quad (3.18)$$

I is the leakage current, with I_{Na^+} standing for the quick transient sodium current that was previously addressed and I_{K^+} for the persistent potassium current. These currents are represented per unit area and together they comprise the time-independent currents. Equations 3.7, 3.8, 3.10, 3.15, and 3.18 are combined to produce the following:

$$I_m = C_m \frac{\partial V}{\partial t} + g_{Na^+} m^3 h (V_m - E_{Na^+}) + g_{K^+} n^4 (V_m - E_{K^+}) + g_l (V_m - E_l) \quad (3.19)$$

The Hodgkin-Huxley equations constitute a set of interconnected nonlinear differential equations involving variables V , n , m , and h . These equations are derived from the combination of Equations 3.11, 3.16, and 3.17. Figure 3.5 illustrates an action potential, offset by 65 mV, generated using these equations and parameters detailed by Hodgkin and Huxley (1990) [81]. The equations were numerically solved in Matlab R2023b and Python using an `ode113` solver with a maximum step size of 10 microseconds. All variables, except for membrane voltage expressed in millivolts (mV), were implemented in SI units.

Chapter 4

Modeling of Channelrhodopsin-2

Channelrhodopsin-2 (ChR2) stands as a pivotal protein in the realm of optogenetics, an interdisciplinary field bridging neuroscience, optics, and genetics.

First identified in the green algae *Chlamydomonas reinhardtii*, ChR2 is a light-responsive ion channel that has attracted considerable interest due to its precise modulation of neuronal activity [123]. ChR2's significance stems from its unique properties as a blue light-sensitive opsin, capable of inducing neuronal excitation upon illumination with blue light (470 nm). This excitation arises from the rapid influx of cations, including H⁺, Na⁺, K⁺, and Ca²⁺, through the opened ChR2 channel pore[169]. The discovery of ChR2 has revolutionized neuroscience research by providing researchers with a powerful tool to manipulate neuronal activity with high spatiotemporal resolution[20].

The conductivity of ChR2, estimated to be approximately 50 fS[41], is relatively low compared to endogenous ion channels such as the sodium channel, which typically exhibits a conductivity of around 10 pS. However, the expression of ChR2 in neuronal cells at sufficient levels can evoke action potentials upon light stimulation, allowing for precise control over neural firing[125]. Understanding the intricate dynamics of ChR2 activation is crucial for optimizing its use in optogenetic experiments. Upon exposure to blue light, ChR2 undergoes a series of conformational changes, leading to the formation of intermediate states and eventually leading to the activation of the channel pore[7]. This process, often described in terms of the photocycle of ChR2, involves the isomerization of the retinal chromophore and the deprotonation of the Schiff base[109].

Moreover, the advent of multimodal optogenetics has further expanded the utility of ChR2. By co-expressing ChR2 with other opsins such as halorhodopsin (NpHR),

researchers can achieve bidirectional control over neuronal activity, enabling both excitation and inhibition of specific neuronal populations[188].

In this chapter, we embark on an exploration of the properties and applications of ChR2 in optogenetics. Drawing upon insights from experimental studies and computational modeling, we aim to provide a comprehensive understanding of ChR2-mediated neuronal excitation and its implications for neuroscience research.

4.1 Photocycle Dynamics of Channelrhodopsin-2 (ChR2)

Channelrhodopsin-2 (ChR2) has emerged as a transformative tool in optogenetics, offering precise control over neuronal activity through light stimulation[126]. Central to its functionality is the intricate process of the ChR2 photocycle, which governs its response to light and underpins its applications in neuroscience research. The ChR2 photocycle encompasses a series of molecular events, including the kinetics of photocurrents, characterized by distinct features such as an initial peak, steady-state plateau, and post-illumination decay[85]. To elucidate these dynamics, various models have been proposed, ranging from three-state to four-state models[23]. These models offer insights into the molecular mechanisms driving ChR2 activation and deactivation, shedding light on factors like light intensity and duration that influence its behavior.

Channelrhodopsin-2 (ChR2) is composed of seven transmembrane helices coupled with a retinal chromophore, forming a protonated Schiff base (RSBH+), as indicated previously[126]. The retina receives photons from light and changes into an excited state. Within 150 femtoseconds (fs), this transition happens quickly. Within 2.7 picoseconds (ps), the retinal trans-cis isomerization is initiated, resulting in the development of the first intermediate state, P500 (or K).

Studies have revealed the influence of light stimulation parameters on the distribution of ChR2 molecules between open states, highlighting a built-in light adaptation mechanism[89]. The ratio of conductances between high and low conducting states (O1 and O2) dynamically shifts during illumination, impacting ChR2 behavior in response to light. Moreover, the kinetics of ChR2 recovery processes, including spontaneous recovery in the dark and light-assisted recovery from inactivation, underscore the complexity of the ChR2 photocycle[153]. Light intensity modulates the recovery time constants, emphasizing the role of light in regulating ChR2 activity and recovery processes. Channelrhodopsin-2 (ChR2) is composed of seven transmembrane helices coupled with a retinal chromophore, forming a protonated Schiff base (RSBH+), as

indicated previously[126]. The retina absorbs photons when exposed to light, which causes it to change into an excited state. Rapidly occurring within 150 femtoseconds (fs), this transition starts the retinal trans-cis isomerization within 2.7 picoseconds (ps), resulting in the development of the first intermediate state, P500 (or K).

This description provides insight into the early events of the ChR2 photocycle, highlighting the rapidity of the light-induced transitions and the formation of key intermediate states. By unraveling these complexities, researchers can advance the field of optogenetics and harness the full potential of light-sensitive ion channels for controlling neuronal activity. Here's a detailed breakdown of its photocycle dynamics:

4.1.1 Initial Light Absorption

During the initial light absorption phase in the channelrhodopsin-2 (ChR2) photocycle, the retinal chromophore undergoes photoisomerization from the all-trans to the 13-cis configuration upon absorption of a photon. This process initiates the activation cascade, leading to subsequent conformational changes in ChR2 and the opening of the ion channel pore.

4.1.1.1 Ground State (D470)

In the context of channelrhodopsin-2 (ChR2), the ground state, often denoted as D470, represents the initial state of the protein before light stimulation. At this stage, ChR2 is in its resting state, with the retinal chromophore adopting an all-trans configuration. The term "D470" originates from the characteristic absorption spectrum of ChR2, which peaks around 470 nanometers, corresponding to the blue light spectrum[123].

In the D470 state, the retinal chromophore is bound within the protein's transmembrane domain, embedded in the lipid bilayer of the cell membrane. This configuration positions the retinal in proximity to key residues within the protein structure, setting the stage for subsequent conformational changes upon photon absorption. The ground state serves as the starting point for the ChR2 photocycle, wherein photon absorption triggers a cascade of events leading to channel activation. In this state, the protein is primed to undergo photoisomerization upon interaction with light of appropriate wavelength. The absorption of a blue light photon by the retinal chromophore initiates the transition of ChR2 from the ground state to an excited state, marking the onset of the photocycle[123].

Understanding the characteristics and dynamics of the ground state is essential for elucidating the mechanisms underlying ChR2 function and its utility in optogenetics.

By characterizing the ground state properties, researchers can gain insights into the initial steps of ChR2 activation and tailor experimental conditions to manipulate neural activity with precision.

4.1.1.2 Photoisomerization

Photoisomerization is a fundamental process in the photocycle of channelrhodopsin-2 (ChR2) that occurs upon absorption of a photon by the retinal chromophore. This process involves a rapid and reversible change in the configuration of the retinal molecule, transitioning it from an all-trans to a 13-cis configuration[123]. At the outset, ChR2 exists in its ground state (often denoted as D470), with the retinal chromophore in the all-trans configuration. Upon absorption of a blue light photon, typically with a peak wavelength around 470 nanometers, the retinal undergoes a structural rearrangement, facilitated by the energy from the absorbed photon. This rearrangement triggers the conversion of the retinal molecule from its linear all-trans conformation to a bent 13-cis configuration[7].

The process of photoisomerization is rapid, occurring within femtoseconds to picoseconds after photon absorption. This rapidity is crucial for ChR2's function as a light-gated ion channel, as it ensures a swift response to changes in light stimuli. The newly formed 13-cis retinal configuration serves as an intermediate state in the ChR2 photocycle, setting the stage for subsequent conformational changes within the protein structure. Photoisomerization is a reversible process, meaning that the 13-cis retinal can spontaneously revert to the all-trans configuration under specific conditions, such as thermal energy. This reversibility is essential for the recycling of ChR2 back to its ground state after the cessation of light stimulation, allowing the protein to respond to subsequent light stimuli[59].

Understanding the intricacies of photoisomerization in ChR2 is critical for deciphering its mechanism of action and optimizing its use in optogenetics. By elucidating the kinetics and energetics of this process, researchers can gain insights into the dynamics of ChR2 activation and tailor experimental parameters to modulate neuronal activity with precision.

4.1.2 Intermediate States and Ion Channel Gating

Intermediate states and ion channel gating are critical aspects of the channelrhodopsin-2 (ChR2) photocycle, governing its function as a light-gated ion channel. These intermediate states, such as P500 and P390, represent transient structural configurations

that facilitate the opening and closing of the ion channel pore in response to light stimulation. Ion channel gating, mediated by conformational changes within ChR2, regulates the influx of cations, such as sodium and potassium, across the cell membrane, thereby modulating neuronal activity. Understanding the dynamics of intermediate states and ion channel gating is essential for unraveling the mechanisms underlying ChR2 activation and optimizing its use in optogenetic experiments.

4.1.2.1 Early P States (P500)

The early P states (P500) represent an essential phase in the photocycle of channelrhodopsin-2 (ChR2) following photoisomerization of the retinal chromophore. Upon absorption of a photon and subsequent photoisomerization, ChR2 transitions to an excited state characterized by the formation of an intermediate species known as P500. The designation "P500" stems from the peak absorption wavelength of this intermediate state, typically around 500 nanometers[123].

During the early P states, several molecular events occur rapidly, within picoseconds of photon absorption. One prominent event is the transfer of a proton from the protonated Schiff base (RPSH^+) of the retinal to a nearby counterion, often a glutamate residue (E123) within the protein structure[7]. This proton transfer event is facilitated by the energy from the absorbed photon and contributes to the stabilization of the P500 state.

The formation of the P500 state marks the initial steps towards channel activation in ChR2. While the exact structural and functional changes occurring during this phase are still under investigation, it is believed that the transition to the P500 state primes ChR2 for subsequent conformational changes that lead to channel opening and ion conductance. The lifetime of the P500 state is relatively short, lasting only for a few picoseconds before transitioning to subsequent intermediate states in the ChR2 photocycle. Despite its transient nature, the formation and dynamics of the P500 state play a crucial role in the overall function of ChR2 as a light-gated ion channel.

Understanding the characteristics and dynamics of the early P states (P500) is vital for unraveling the mechanisms underlying ChR2 activation and its modulation of neuronal activity in optogenetics. By elucidating the molecular events occurring during this phase, researchers can gain insights into the kinetics and energetics of ChR2 activation and optimize its use in neurobiological studies.

4.1.2.2 Late P States (P390)

The late P states (P390) constitute a pivotal phase in the photocycle of channelrhodopsin-2 (ChR2), occurring subsequent to the early P states (P500). Following the rapid formation of the P500 intermediate state, ChR2 transitions to the more stable P390 state, representing a critical juncture in the activation process. The designation "P390" derives from the peak absorption wavelength of this intermediate state, typically around 390 nanometers[123].

During the late P states, ChR2 undergoes further structural rearrangements and molecular events that facilitate the opening of the ion channel pore, enabling the influx of cations such as sodium and potassium. While the precise molecular mechanisms underlying this transition are still under investigation, it is believed that the P390 state comprises multiple sub-states, including P390 early and P390 late, each characterized by distinct structural conformations and dynamics[7].

One significant event during the late P states is the continued transfer of protons within the protein structure, potentially involving additional residues and water molecules. These proton transfers contribute to the stabilization of the P390 state and facilitate the conformational changes necessary for channel gating and ion conductance. The duration of the late P states is longer compared to the early P states, spanning milliseconds, which allows for sustained ion flux through the channel pore. The transition from the P390 state to subsequent states marks the completion of the channel opening process, culminating in the activation of ChR2 and the modulation of neuronal activity.

Understanding the characteristics and dynamics of the late P states (P390) is crucial for elucidating the mechanisms underlying ChR2 activation and its role in optogenetic applications. By dissecting the molecular events occurring during this phase, researchers can gain insights into the kinetics and energetics of ChR2 channel gating and optimize its use as a tool for manipulating neuronal activity.

4.1.2.3 Channel Closure and Reprotonation (P520)

The phase of channel closure and reprotonation, designated as P520, represents a critical step in the photocycle of channelrhodopsin-2 (ChR2). Following the activation of the ion channel pore during the late P states (P390), ChR2 transitions to the P520 state, signaling the closure of the channel pore and the initiation of the reprotonation process. The designation "P520" derives from the peak absorption wavelength of this intermediate state, typically around 520 nanometers[123].

During the P520 phase, several molecular events occur within the ChR2 protein structure, leading to the restoration of the initial ground state configuration. One key event is the reprotonation of the retinal chromophore, wherein a proton is transferred back to the protonated Schiff base (RPSH^+), resulting in the stabilization of the retinal molecule in the 13-cis configuration. This reprotonation event signifies the closure of the ion channel pore, preventing further ion flux through the channel.

The closure of the channel pore and the return to the ground state configuration mark the completion of the channel activation-deactivation cycle in ChR2. The protein structure undergoes conformational changes to revert to a state similar to the initial dark-adapted state (D470), albeit with the retinal in the 13-cis configuration. This transition prepares ChR2 for subsequent rounds of activation upon exposure to light stimuli. The duration of the P520 state is relatively short, spanning milliseconds, as ChR2 rapidly transitions back to the ground state to await further light stimulation. The reprotonation process is essential for resetting the protein for subsequent activation cycles and maintaining the functionality of ChR2 as a light-gated ion channel.

Understanding the characteristics and dynamics of the channel closure and reprotonation phase (P520) is crucial for deciphering the mechanisms underlying ChR2 deactivation and its role in modulating neuronal activity in optogenetic applications. By elucidating the molecular events occurring during this phase, researchers can gain insights into the kinetics and energetics of ChR2 deactivation and optimize its use as a tool for manipulating neuronal activity.

4.1.3 Thermal Relaxation

The process of thermal relaxation in the channelrhodopsin-2 (ChR2) photocycle, where the retinal chromophore transitions from the activated 13-cis configuration back to the ground-state all-trans configuration in the absence of light stimuli, is crucial[104]. This spontaneous process allows ChR2 to reset to its dark-adapted state (D470), preparing the protein for subsequent light-induced activations. The kinetics of thermal relaxation, influenced by factors such as temperature and protein environment, significantly impact the overall dynamics of the ChR2 photocycle and are essential for optimizing ChR2's temporal properties for effective use in optogenetic applications.

4.1.3.1 Thermal Isomerization

Thermal isomerization is a crucial process in the photocycle of channelrhodopsin-2 (ChR2) that occurs following the completion of light-induced activation and deactivation

events. After the closure of the ion channel pore and the return to the ground state configuration (P520), ChR2 undergoes thermal isomerization, wherein the retinal chromophore transitions from the 13-cis to the all-trans configuration. This process occurs spontaneously in the absence of light stimuli and is driven by thermal energy present in the surrounding environment[123].

The thermal isomerization of the retinal chromophore represents a fundamental step in resetting ChR2 for subsequent rounds of activation and deactivation. By transitioning back to the all-trans configuration, ChR2 restores its initial dark-adapted state (D470), preparing the protein for light-induced activation upon exposure to new light stimuli. This spontaneous relaxation process allows ChR2 to respond to changes in the light environment with high temporal resolution and sensitivity[7].

The kinetics of thermal isomerization in ChR2 can vary depending on factors such as temperature and protein environment. At physiological temperatures, thermal relaxation from the 13-cis to the all-trans configuration occurs over timescales ranging from tens to hundreds of milliseconds. However, alterations in temperature or mutations in the ChR2 protein can modulate the rate of thermal isomerization, affecting the overall dynamics of the photocycle[104].

Despite occurring in the absence of light, thermal isomerization plays a crucial role in maintaining the functionality of ChR2 as a light-gated ion channel. By resetting the protein to its dark-adapted state, thermal isomerization ensures the readiness of ChR2 for subsequent light-induced activations and enables the precise control of neuronal activity in optogenetic experiments.

Understanding the characteristics and dynamics of thermal isomerization in ChR2 is essential for optimizing its use in optogenetic applications. By elucidating the kinetics and energetics of this process, researchers can gain insights into the mechanisms underlying ChR2 deactivation and develop strategies to modulate its temporal properties for specific experimental requirements.

4.1.4 Additional Points

- The specific timing and details of each intermediate state can vary depending on factors like temperature, surrounding environment, and ChR2 mutations[104, 84].
- Recent research suggests the involvement of additional protein interactions and conformational changes during the photocycle that contribute to efficient ion channel gating[104, 16, 170].

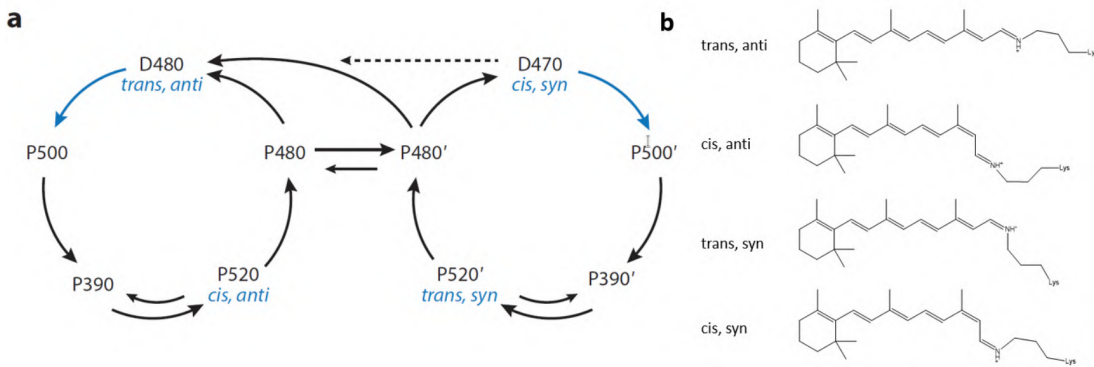


Fig. 4.1 Figure 4.1(a) shows a model of the ChR2 photocycle, suggesting the photoactivation of two separate dark states (D480 and D470) with differing retinal geometries. This model includes five states each cycle and is based on results from differential infrared and UV/Vis spectroscopy. To allow for electrical measurements, an additional cycle is incorporated, and the transition between the two cycles takes place when late P480 photointermediates are present. Blue arrows indicate when the light is on. Figure 4.1(b), which was taken from Biophysics of Channelrhodopsin (Annual Review of Biophysics), 2015[146], depicts the retinal isomers.

Based on data from UV/Vis and difference infrared spectroscopy, the anticipated photocycle is shown in Figure 4.1. The structural alterations seen in electrophysiological measurements and research findings covered in section 3.2 are explained by a single cycle. [77, 146, 155].

Channelrhodopsin (ChR) is made up of seven transmembrane helices and a retinal chromophore, which together produce a protonated Schiff base (RSBH⁺), as was previously mentioned in section 4.1. When exposed to light, photons are absorbed by the retina, which then becomes stimulated. The first intermediate state, P500 (or K), is formed when the retina deactivates within 150 femtoseconds (fs). This deactivation sets off a trans-cis isomerization within 2.7 picoseconds (ps).

The blue-shifted P390 (or L) state is then formed as a result of the RSBH⁺ being deprotonated on a nanosecond period. This state is in balance with the P520 (or M) state, which is the channel's conducting state and is identified by a reprotonated RSB. Before returning to the dark-adapted state, D480, the channel transitions to a non-conducting state, P480. This transition occurs on a millisecond timescale, while complete recovery to the dark-adapted state takes several seconds.

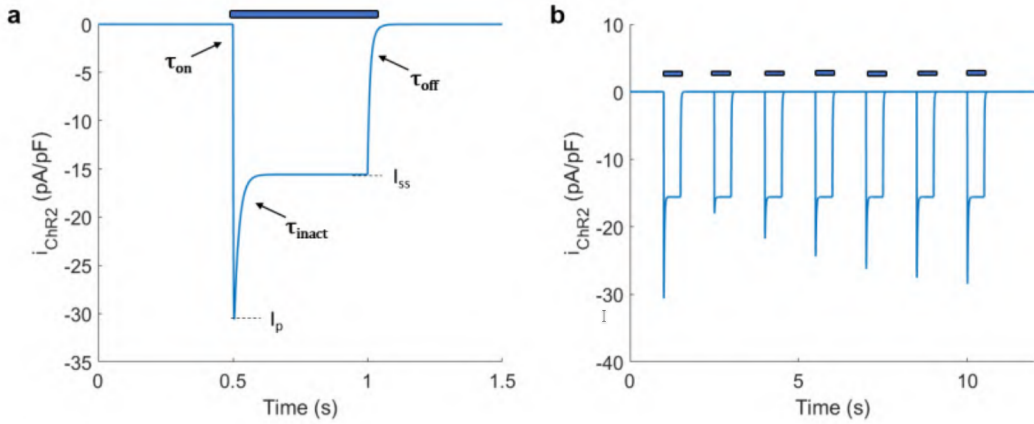


Fig. 4.2 The channelrhodopsin-2 photocurrent is depicted in Figure 4.2. (a), illustrating the response to a single 0.5-second light pulse. In Figure 4.2. (b), the peak recovery kinetics are shown, with light pulses represented by blue bars. These figures were generated using MatlabR2023b, with the model described in section 4.3.

4.2 Photocycle models

Prior to exploring the details of the photocycle model, it is important to comprehend the experimental results concerning Channelrhodopsin-2 (ChR2) voltage clamp readings. In the presence of voltage clamp, ChR2 displays a distinctive photocurrent pattern. There is a sudden surge at the beginning, usually occurring 1-2 milliseconds after stimulation. After reaching its peak, the channel desensitises, causing a sharp decline that ends in a steady-state plateau. Following illumination, a bi-exponential decline is seen, which ultimately brings the current back to baseline values (see Figure 4.2(a)). The ChR2 4-state model yielded the results shown in Figure 4.2, which are covered in depth in Section 4.4.

Moreover, upon repeated stimulation within a short time interval (typically less than 10 seconds), the transient response diminishes, while a sustained steady-state current is maintained (refer to Figure 4.1 (b)). These observations highlight the dynamic nature of ChR2 activation and its ability to adapt to repetitive light stimuli, which are crucial aspects to consider in understanding its functionality and optimizing optogenetic applications.

At the moment, there are two main approaches used to estimate the photocurrent in channelrhodopsin-2 (ChR2): the three-state and four-state models. Figure 4.3 provides a summary of these suggested models. Unlike the multi-state photocycle, which involves

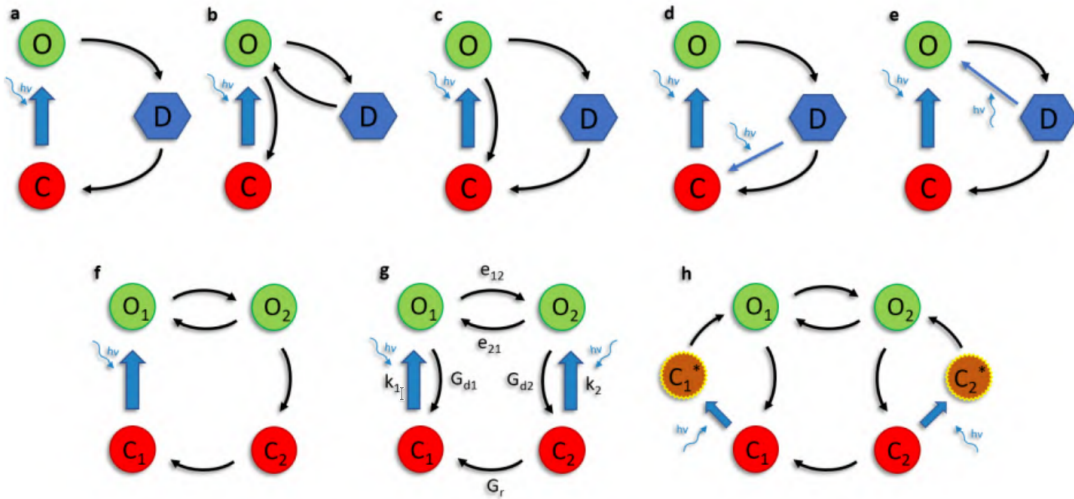


Fig. 4.3 The proposed models of the Channelrhodopsin-2 (ChR2) photocycle are depicted in Figure 4.3, each offering unique insights into the dynamics of ChR2 activation and deactivation. (a) A simplified three-state cycle model illustrates the transition from closed to open state, capturing the essential kinetics of ChR2 activation[77]. (b) An alternative model illustrates the desensitised state as an incidental response, elucidating the intricate relationship between desensitisation and channel opening[?]. (c) A cycle incorporating partial recovery through the desensitized state (*D*) offers a nuanced understanding of the transient and steady-state behaviors observed in ChR2 photocurrents[77]. (d, e) Additional models introduce a second light-dependent step, providing alternative mechanisms for ChR2 photoactivation with reduced efficiency[154]. (f, g) Four-state models, depicted as circular and branching structures, respectively, offer comprehensive representations of ChR2 dynamics, accounting for multiple intermediate states and transitions[125]. (h) A six-state model introduces two additional activation intermediates, providing further granularity to the ChR2 photocycle[67, 125].

several stages before channel opening, the modelling reduces the process to a single state transition ($C \rightarrow O$) from closed to open. The quick timelines of transitions like ($D480 \rightarrow P500$) and ($P500 \rightarrow P390$) are responsible for this simplification. The simplest model, which captures the transient to steady-state behaviour, shows the transition from an open state O to a closed, desensitised state D in Figure 4.3(a). Nevertheless, comparable rates are needed to provide a steady-state current for transitions from open to desensitised ($O \rightarrow D$) and from desensitised and from desensitized to closed ($D \rightarrow C$).

An other method, similar to the cycle for halorhodopsin, views the desensitised state as a side reaction (Figure 4.3(b)). However, because of the discrepancy between the requirement for quick transient kinetics and sluggish recovery kinetics lasting

seconds, many models find it difficult to adequately capture both the transition and recovery kinetics. The models are unable to account for the main characteristics seen in photocurrents, even when an additional transition is included, as shown in Figure 4.3 (c)[?].

A fresh method to overcome this constraint was presented by Nagel et al. (2003)[123], who suggested a secondary photon absorption mechanism. This process involves two phases when illumination occurs: a gradual shift from the desensitised to closed state ($D \rightarrow C$) and a quick photochemical transition from the desensitised to closed state $D \rightarrow C$ (Figure 4.3 (d)). A different approach that uses less efficient light-induced photoactivation is illustrated in Figure 4.3(e) and has been covered by Schneider et al. (2015) and Stehfest and Hegemann (2010)[146, 155]. These two three-state models describe transient behaviour, steady-state plateaus, the quick fall that occurs after illumination, and the gradual recovery of transient current with a reasonable degree of accuracy.

Although the two-cycle model's molecular identity is yet unknown[155], there is strong evidence for it to exist, as Figure 4.2 illustrates. Using flash experiments, [7] found four kinetic intermediates (P1, P2, P3, and P4). P1 has a short lifespan among them, but P4 has a lengthy lifespan. Furthermore, P2 and P3, two intermediates, are regarded as open states. Early and late photocurrents have different selectivities, with steady-state currents showing a larger selectivity for protons[146, 155]. Additional insights from Raman studies and retinal extraction point to a simultaneous combination of retinal isoforms, as shown in Figure 4.2 (b). Some of these isoforms, including 13-cis,15-syn retinal and all-trans,15-anti, promote closed channel conformations by maintaining a salt bridge between the counterion complex and the retinal Schiff base (RSB). On the other hand, according to Schneider et al. (2015), all-trans,15-syn and 13-cis,15-anti could make it easier for conducting states to develop. These facts notwithstanding, the bi-exponential post-illumination current decline is difficult for three-state models to reproduce. Furthermore, Bamann et al. (2008) showed that the current briefly closed but ultimately continued to follow inactivation when green light bursts were delivered on top of blue light stimulation. A single photocycle model is insufficient to describe this phenomenon[155].

Two open and two closed states are implied by the discovery. We can simplify the photocycle to a four-state model by ignoring the rapid intermediate phases. Figure 4.3 (f) depicts the circular four-state model, which is the most fundamental model. However, like with three-state models, a second photon absorption is needed to

adequately predict both the sluggish recovery after illumination and the fast closure during illumination[125, 146].

All of the channel dynamics and dark recovery can be accurately modelled in the four-state branching model (Figure 4.3(g)). The completely dark-adapted condition is denoted by ($C1$) in this case. When illuminated, there is a high quantum efficiency transition to the initial conducting state ($O1$). An equilibrium is reached between ($O1$) and ($O2$) in milliseconds. Following illumination, the conductance states $C1$ and $C2$ transition to their corresponding closed states, and then ($C2$) slowly changes to ($C1$). The quantum efficiency of the ($C2 \rightarrow O2$) transition is less than that of its analogue. Moreover, Nikolic et al. (2009)[125] have demonstrated that ($O1$) and ($O2$) equilibrium depends on light.

The four-state model in Figure 4.3 (g) is extended to a six-state model, as shown in Figure 4.3 (h). In order to avoid explicit time-dependent rates and to correctly account for the activation time after retinal isomerizations, two extra intermediates are introduced[67].

There is still disagreement on the precise location of the transition between the dark and light-adapted cycles, which are symbolised by the left and right cycles, or ($C1 - O1$) and ($C2 - O2$) in Figure 4.2 (a). The nonconducting phases P480 and P480' are most likely where the change takes place, but [155, 146, 154]. In support of this hypothesis is the green flash experiment. Furthermore, as Figure 4.2 (a) illustrates, the recovery process is a little more complicated and may involve a pH-dependent equilibrium (which is not explicitly depicted).

4.3 The 3-State ChR2 Model

The photocycle model proposed for ChR-2, as outlined in [123], is primarily based on experimental observations of photocurrent dynamics[124]. Upon absorption of photons, ChR-2 molecules existing in the closed, sensitized state (C) rapidly transition to an excited state (C^*). This transition occurs swiftly, leading to the opening of ion channels (O) within a timescale of less than 1 millisecond[124]. Following the open channel state, there is a spontaneous transition to a closed, desensitized state (D), wherein the ion channel is closed, but the molecule is not primed for further photoswitching. Subsequently, after a certain recovery period, the molecule reverts to the closed but sensitized state (C)[124].

The process of channel opening ($C \rightarrow C^* \rightarrow O$) is remarkably fast, occurring in less than 1 millisecond. However, the closure of ion channels ($O \rightarrow D$) exhibits a

more variable timescale, dependent significantly on the pH of the extracellular solution, with durations spanning from 10 to 400 milliseconds[124]. Due to the rapidity of the opening process, the model simplifies to a three-state representation ($C \rightarrow O \rightarrow D \rightarrow C$), effectively capturing the essential transitions involved in the ChR-2 photocycle. This simplified model provides valuable insights into the fundamental dynamics of ChR-2 activation and deactivation processes.

The mechanism underlying the recovery from desensitization ($D \rightarrow C$) in ChR-2 remains incompletely understood. While this process typically spans from 2 to 10 seconds in the absence of light, experimental observations suggest that under illumination, this recovery should occur within a much shorter timeframe of approximately 60 milliseconds [123, 91, 20, 86, 124]. Several hypotheses have been proposed to explain this phenomenon. One possibility is that the rate of recovery is influenced by the intensity of light exposure. Alternatively, it has been suggested that the recovery process may bypass the desensitized state (D) altogether, with some molecules transitioning directly from the open state to the closed/sensitized state. To investigate these hypotheses, various experimental approaches have been employed[124].

After thorough experimentation and analysis, it was concluded that the hypothesis suggesting light-dependent recovery rates more accurately aligns with the experimental observations[124]. Consequently, a three-state model, as illustrated in Figure 4.4, was adopted to represent the ChR-2 photocycle dynamics[124]. This model provides a simplified yet insightful framework for understanding the complex processes involved in ChR-2 activation, desensitization, and recovery.

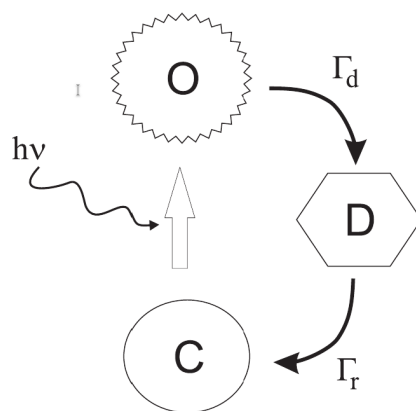


Fig. 4.4 Three-state model of ChR-2 photocycle.[124]

Mathematical representation as shown in Figure 4.4, can be done accordingly:

$$\frac{dX^*}{dt} = \epsilon\phi X - \Gamma_d X^* \quad (4.1)$$

$$\frac{dX_{ds}}{dt} = \Gamma_d X^* - \Gamma_r X_{ds} \quad (4.2)$$

In a cell, X^* , X_{ds} , and X represent the quantities of open/excited (state O), closed/desensitized (state D), and closed/photosensitive (state C) molecules, respectively. $\Gamma_{d,r}$ denote the rates of channel closure and recovery of photosensitivity, ϵ represents the quantum efficiency of the ChR-2 system, and ϕ stands for the number of photons striking the cell per second[124]. If the total number of ChR-2 molecules in a cell is X_0 (where $X_0 = X^* + X_{ds} + X$), then the system of differential equations (4.4) and (4.5) is described as follows:

$$\frac{dx^*}{dt} = p - (p + gd)x^* - px_{ds} \quad (4.3)$$

$$\frac{dx_{ds}}{dt} = gd x^* - gr x_{ds} \quad (4.4)$$

where $x = \frac{X}{X_0}$, representing the fraction of molecules in a specific state relative to the total number of ChR-2 molecules X_0 in the cell; $\Gamma_{d,r} = \frac{\Gamma_{d,r}}{P_{\max}}$, denoting the rates of channel closure and recovery of photosensitivity normalized by the maximum light intensity P_{\max} ; $p = \frac{P}{P_{\max}}$, indicating the light intensity relative to its maximum; and $P = \epsilon\phi$. Under voltage-clamp conditions, the current i is directly proportional to the number of open channels x^* . Simulation results, as illustrated in Figure 4.5, corroborate these findings.

The light illumination rapidly induces a current response, a phenomenon extensively measured via whole-cell patch clamp experiments conducted by various research groups[123, 86, 124]. Specifically, a blue LED with a peak wavelength of 470 nm and energy of 2.6 eV was utilized as the light source[86, 124], with light intensities ranging from 0 to 5 mW mm⁻². The simulation outcomes, illustrated in Figure 4.5, depict the characteristic light-evoked reaction of ChR-2 expressing cells, showcasing a swift rise to the peak current followed by a gradual decline towards the plateau value. The model employed provides an analytical solution for the time-dependent currents, delineating the values for x^* .

$$x^*(t) = A^* + A^*e^{-\alpha t} \left[\xi \left(\frac{\sinh(\beta t)}{\beta} \right) - \cosh(\beta) \right] \quad (4.5)$$

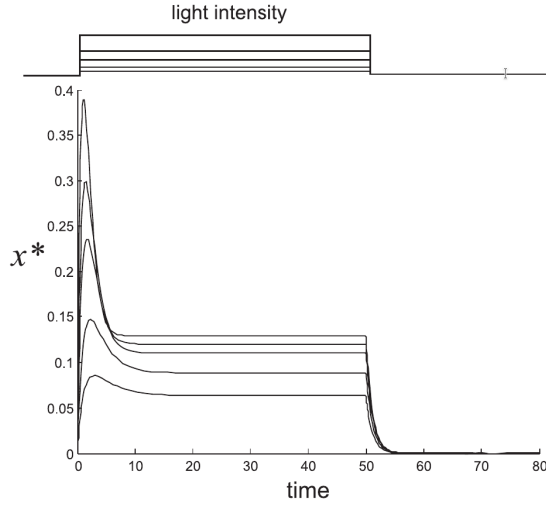


Fig. 4.5 The cell's response to a light pulse is depicted as a time-dependent series, illustrating the number of open ion channels activated by light (i.e., light-activated currents) across various light intensities. The duration of the light pulse is set to 50 time units, equivalent to 1 second when considering a time unit of 20 ms (1/Pmax). Different relative light intensities are examined: 0.1, 0.2, 0.4, 0.6, and 1. Parameters $\Gamma_d = 1$ and $\Gamma_r = 0.15$ are utilized for the simulations[124].

$$A^* = A_{\max}^* \frac{P}{p + K} \quad (4.6)$$

$$A_{\max}^* = \frac{g_r}{g_r + g_d} \quad (4.7)$$

$$K = \frac{g_r g_d}{g_r + g_d} \quad (4.8)$$

$$\alpha = \frac{p + g_r + g_d}{2} \quad (4.9)$$

$$\beta = \sqrt{\left(\frac{g_r + g_d - p}{2}\right)^2 - g_r g_d} \quad (4.10)$$

$$\xi = \frac{p}{A} - \alpha \quad (4.11)$$

The current exponentially turns off When the light is turned off.

$$x^*(t) = A^* e^{-g_d t} \quad (4.12)$$

By determining the dark current, Γ_d can be accurately estimated. Both the peak and plateau currents (A^*) are intricately linked to the light intensity (p). Interestingly, while the plateau value tends to saturate as the light intensity increases (see Equations 4.6-4.8), the peak values demonstrate nearly proportional increments with light intensity, showing slight saturation for the explored illumination levels as depicted in Figure 4.6[124].

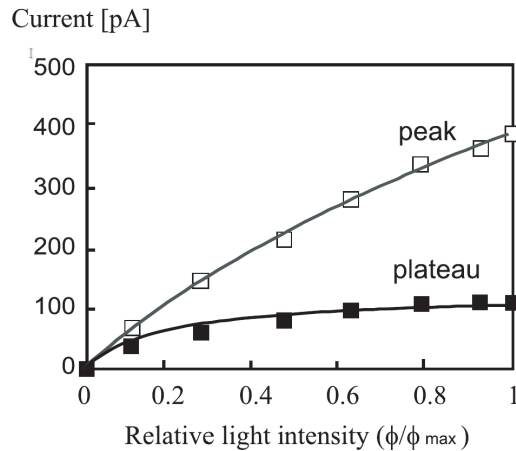


Fig. 4.6 The experimental results from Ishizuka et al.[86] and the theoretical predictions from Nikolic et al. 2006[124] are depicted in Figure 4.6, showcasing both the peak (open squares) and plateau currents (closed squares). The parameters were set to $g_d = 3$ and $g_r = 0.2$ [124].

The observations depicted in Figure 4.6 closely correspond with experimental findings outlined in Ishizuka et al. [86, 124]. For instance, a turning-off time constant of $\tau_{\text{off}} = 11 \text{ ms}$ was recorded for a sample response to a 1 s light pulse at the maximum intensity employed in the experiment. This yielded $\Gamma_d = 1/\tau_{\text{off}} \approx 90 \text{ s}^{-1}$, resulting in $P_{\max} = 30 \text{ s}^{-1}$ and $\Gamma_r = 6 \text{ s}^{-1}$ (given $g_d = 3$ and $g_r = 0.2$). The portion of the response from peak to plateau can be effectively modeled by a single exponential curve of the form $\sim \exp(-t/\tau_i)$, where τ_i represents the inactivation time constant [86, 124]. Approximating τ_i for maximum illumination as $(1/\tau_i) = \alpha - \beta$, the model (Equations 4.6-4.10) estimates τ_i to be approximately 22 ms, closely resembling the experimental value of $23 \pm 2 \text{ ms}$ [124].

4.4 The 4-State ChR2 Model

The computational model employed in this study to dissect the dynamics of ChR2 stands as a testament to the meticulous work of Williams et al. (2013) [176]. Crafted

with precision, this model focuses on unraveling the behavior of the H134R mutant variant of ChR2, a pivotal player in optogenetics. At its core lies a four-state Markov model, adeptly designed to capture the intricate interplay between ChR2's states and transitions. The elegance of this modeling approach lies in its ability to simulate ChR2's response under varying conditions, shedding light on its voltage- and light-sensitive properties with unparalleled accuracy.

Central to understanding the intricacies of the ChR2 model is delving into the meticulously delineated photocycle as expounded by Williams et al. (2013)[176]. Illustrated vividly in their seminal work, the photocycle offers a roadmap of the molecular events governing ChR2's behavior. Through a series of transitions between distinct states, including open and closed configurations, the photocycle encapsulates the essence of ChR2's light-dependent activation and deactivation processes as shown in Figure 4.3(g). By dissecting each step with precision, Williams and colleagues provide a comprehensive framework for understanding ChR2's behavior at a molecular level. Below, we outline the rate equations governing the dynamic behavior of the ChR2 model as in William's model:

$$O1 + O2 + C1 + C2 = 1 \quad (4.13)$$

$$\frac{dC1}{dt} = G_r C2 + G_{d1} O1 - k1 C1 \quad (4.14)$$

$$\frac{dO1}{dt} = k1 C1 - (G_{d1} + e_{12}) O1 + e_{21} O2 \quad (4.15)$$

$$\frac{dO2}{dt} = k2 C2 - (G_{d2} + e_{21}) O2 + e_{12} O1 \quad (4.16)$$

$$\frac{dC2}{dt} = G_{d2} O2 - (k2 + G_r) C2 \quad (4.17)$$

The total occupancy of all states equals one, with C_1 standing for the dark-adapted closed state, C_2 for the light-adapted closed state, and O_1 and O_2 for the strong and weak conducting open states, respectively. The definition of the transition rates is as follows:

$$k_1 = \varphi_1(F, t) = \varepsilon_1 F p \quad (4.18)$$

$$k_2 = \varphi_2(F, t) = \varepsilon_2 F p \quad (4.19)$$

$$F = \frac{\sigma_{\text{ret}} I \lambda}{w_{\text{loss}} \cdot h \cdot c} \quad (4.20)$$

$$\frac{dp}{dt} = \frac{S_0(\theta) - p}{\tau_{\text{ChR2}}} \quad (4.21)$$

$$S_0(\theta) = 0.5 (1 + \tanh(0.120(\theta - 100))) \quad (4.22)$$

$$G_{d1} = 75 + 43 \tanh\left(\frac{V + 20}{-20}\right) \quad (4.23)$$

$$G_{d2} = 50 \quad (4.24)$$

$$G_r = 4.34 \times 10^{-2} \exp(-0.0211539274 \cdot V) \quad (4.25)$$

$$e_{12} = 11 + 5 \ln\left(1 + \frac{I}{24}\right) \quad (4.26)$$

$$e_{21} = 8 + 4 \ln\left(1 + \frac{I}{24}\right) \quad (4.27)$$

All states have a total occupancy of one, where C_1 is the dark-adapted closed state, C_2 is the light-adapted closed state, and O_1 and O_2 are the strong and weak conducting open states, respectively. Here is how the transition rates are defined:

$$\begin{aligned} k_1 &= \varphi_1(F, t) = \varepsilon_1 F p \\ k_2 &= \varphi_2(F, t) = \varepsilon_2 F p \end{aligned} \quad (4.28)$$

$$F = \frac{\sigma_{\text{ret}} I \lambda}{w_{\text{loss}} \cdot h \cdot c} \quad (4.29)$$

$$\frac{dp}{dt} = S_0(\theta) - p \quad (4.30)$$

$$S_0(\theta) = 0.5 (1 + \tanh(0.120(\theta - 100))) \quad (4.31)$$

$$G_{d1} = 75 + 43 \tanh\left(\frac{V + 20}{-20}\right) \quad (4.32)$$

$$G_{d2} = 50 \quad (4.33)$$

$$G_r = 4.34 \times 10^{-2} \exp(-0.0211539274 \cdot V) \quad (4.34)$$

$$e_{12} = 11 + 5 \ln \left(1 + \frac{I}{24} \right) \quad (4.35)$$

$$e_{21} = 8 + 4 \ln \left(1 + \frac{I}{24} \right) \quad (4.36)$$

The light-sensitive and time-dependent rate constants are represented by k_1 and k_2 , where k_1 has a high quantum efficiency and k_2 a low one. The quantity of photons absorbed by ChR2 in a given amount of time is represented by F , where I (W/m^2) is the light intensity and λ (m) is the wavelength. The given rate equations control the activation rate function p . The activation rate under steady-state circumstances is determined by the irradiance-dependent sigmoid function, S_0 . A function of I is the optical stimulation procedure θ . The voltage-dependent transition rates from $O1$ to $C1$ and the constant transition rate from $O2$ to $C2$ are shown by G_{d1} and G_{d2} , respectively. The slow voltage-dependent recovery rate is denoted by G_r . Ultimately, the intensity-dependent transition rates between $O1$ and $O2$ are e_{12} and e_{21} , respectively. Apart for the membrane voltage V , which is measured in mV, all variables and constants are expressed in SI units. See Table 4.1 for other values of the parameters.

Table 4.1 Parameter values for ChR2(H134R) model[176]

Definition	Parameter	Value	Units
Reversal potential ChR2	(E_{ChR2})	0	mV
Ratio of conductances of $O2/O1$	(γ)	0.1	-
Max conductance	(g_{ChR2})	4	S/m^2
Quantum efficiency for photon absorption from $C1$	(ε_1)	0.8535	-
Quantum efficiency for photon absorption from $C2$	(ε_2)	0.14	-
Wavelength of maximal absorption	(λ)	470×10^{-9}	m
Absorption cross-section for retinal	(σ_{ret})	12×10^{-20}	m^2
Scaling factor for losses of photons	(w_{loss})	1.3	-
Time constant of ChR2 activation	(τ_{ChR2})	1.3×10^{-3}	s
Product of Planck's constant and the speed of light	(hc)	1.986446×10^{-25}	$\text{kg m}^3/\text{s}^2$

The distinctive feature of this model lies in its comprehensive incorporation of both light and voltage sensitivities of ChR2, a facet inadequately addressed by previous models [67, 125, 157]. Notably, the model accounts for the voltage dependency of both conductance and kinetics, crucial for an accurate representation of ChR2 behavior. ChR2's current-voltage relationship exhibits significant non-linearity, typified by inward rectification, as noted in prior studies [30, 63, 123]. Williams aptly captured this non-linearity using an empirical equation (4.38) [176]. Additionally, the kinetics of ChR2 exhibit some degree of voltage dependence, evident in the weak voltage dependency of both activation and deactivation time constants (τ_{on} and τ_{off} , respectively, see figure 4.2 (a)), a characteristic adeptly incorporated into the model through G_{d1} (equation 4.32). In addition, as G_r (equation 4.34) explains, the recovery rate also exhibits voltage dependency, with quicker recovery seen at larger negative potentials. Lastly, the process for calculating the photocurrent is outlined below:

$$i_{\text{ChR2}} = g_{\text{ChR2}} G(V)(O1 + \gamma O2)(V - E_{\text{ChR2}}) \quad (4.37)$$

$$G(V) = 10.6408 - \frac{14.6408 \exp\left(\frac{-V}{42.7671}\right)}{V} \quad (4.38)$$

where g_{ChR2} represents the maximal conductance, $G(V)$ denotes the rectification function, γ signifies the ratio of conductance, and E_{ChR2} stands for the reversal potential.

4.5 The 6-State ChR2 Model

The ChR2 model detailed in the document is an advanced six-state representation of the photocycle dynamics of ChR2, encompassing states s1 to s6 and their associated forward and backward transition rates[37].

The ChR2 6-state model serves as a computational framework to elucidate the intricate photocycle dynamics of Channelrhodopsin-2 (ChR2), a pivotal protein in optogenetics. This model meticulously delineates ChR2's behavior through six distinct states, labeled from s1 to s6, each representing different protein configurations during light-induced activation and deactivation. These transitions, governed by forward and backward rates, intricately regulate ChR2's response kinetics to light stimulation [18, 69, 183]. The transitions between these states are crucial determinants of ChR2's functionality, influencing its ability to regulate neuronal activity in response to optical stimuli. By accurately capturing these dynamics, the ChR2 6-state model provides

valuable insights into the underlying mechanisms of optogenetic modulation and facilitates the design of optimized optogenetic tools for precise control of neuronal circuits in various experimental settings. This comprehensive computational approach enhances our understanding of ChR2's behavior and its applications in neurobiological research and therapeutic interventions [18, 69, 183].

One of the notable attributes of the ChR2 6-state model is its capacity to elucidate the intricate interplay between ChR2's structural changes and its functional attributes, including ion permeability and channel gating kinetics. Through a meticulous integration of detailed molecular dynamics simulations and experimental observations, this model offers a comprehensive insight into the molecular mechanisms governing ChR2's response to optical stimulation[63, 123, 65].

The six photo states of ChR2 delineate a sequential cascade of molecular events underlying the protein's activation cycle upon exposure to light. Commencing from the ground state (s_1), ChR2 remains in an inactive state until photon absorption initiates its transition to the initial excited state (s_2). Subsequently, ChR2 traverses through a series of intermediary states (s_3 to s_5), characterized by transient structural alterations that facilitate the opening of the ion channel pore. Ultimately, in the fully activated open state (s_6), ChR2 adopts a conformation conducive to ion flux across the cellular membrane, thereby influencing membrane potential and neuronal excitability[65]. The Grossman's model is represented in Figure 4.7

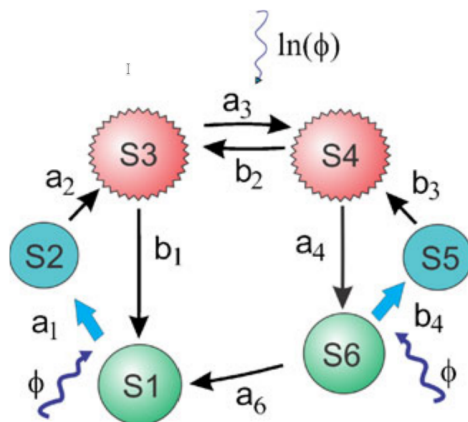


Fig. 4.7 The six-state model of the ChR2 photocycle.[66]

The ChR2 current (I_{ChR}) is succinctly described by the equation:

$$I_{\text{ChR}} = A \cdot g_{\text{ChR}} \cdot (v - E_{\text{rev}}) \quad (4.39)$$

Here, A represents the effective area of the cell or compartment, g_{ChR} denotes the conductance of ChR2 ion channels per unit area, and v signifies the membrane potential, typically expressed in millivolts (mV). The reversal potential for *Chlamydomonas reinhardtii* ChR2 hovers around zero for a pH of 7.35 and extracellular ion concentrations of sodium, potassium, and calcium near their physiological levels. While the exact value can vary within the range of $E_{\text{rev}} \approx 0$ to 8 mV [8, 104, 66].

The conductance of ChR2 is accurately modeled by disentangling its light and voltage dependencies. The mathematical equation can be modeled as:

$$g_{\text{ChR}}(\varphi, v, t) = g_{\text{ChR}} \cdot \psi(\varphi, t) \cdot f(v) \quad (4.40)$$

Where φ represents the photon flux in $[\text{photons} \cdot \text{s}^{-1} \cdot \text{cm}^{-2}]$, v denotes the membrane potential, ψ denotes a normalized light-dependent function (set to 1 when all channels are maximally conductive), f represents the voltage-dependent function, and g_{ChR} stands for the maximum conductance (assuming $f = 1$) measured in $[\text{nS}/\mu\text{m}^2]$. This maximum conductance accounts not only for the conductance of a single ChR2 molecule but also for the level of protein expression within the cell. This separation allows for a more precise representation of ChR2's response to both optical stimulation and changes in membrane potential [8, 104, 66].

The investigation into the voltage sensitivity of Channelrhodopsin-2 (ChR2) involved meticulous experimentation, primarily through photocurrent recordings conducted under controlled light conditions while varying clamped voltages. These experiments, detailed in the works of Bamberg [8] and Feldbauer[41], provided crucial empirical data. Building upon this foundation, Grossman[65] further elucidated the voltage-dependent behavior of ChR2 by proposing a novel equation:

$$f(v) = \frac{1 - \exp(v/v_0)}{v_1} \quad (4.41)$$

This equation encapsulates the intricate interplay between membrane potential and ChR2 conductance, shedding light on the mechanisms underlying ChR2's sensitivity to changes in voltage. By integrating empirical evidence with mathematical modeling, researchers gained deeper insights into the nuanced dynamics of ChR2 activation and its modulation by membrane voltage[66].

The investigation into the conductance properties of Channelrhodopsin-2 (ChR2) delved into both its voltage and light dependencies through meticulous experimentation. Photocurrent recordings conducted under voltage clamp conditions provided crucial insights into the voltage sensitivity of ChR2, with fitting constants v_0 and v_1 in the

above equation (4.41) derived to characterize this relationship. Meanwhile, analyses of photocurrent recordings at varying irradiances under fixed voltage conditions elucidated the light-dependent behavior of ChR2 conductance. Previous studies by Nikolic, Hegemann, and Nagel[124, 125, 77, 123] outlined a four-state kinetic model to describe the dynamics of ChR2 activation, incorporating functional states such as the dark-adapted ground state, high and weak conductance open states, and non-ground closed states[66]. In this study, two additional intermediate states were introduced to accurately capture the kinetics of ChR2 activation following trans-cis and cis-trans retinal transformations. Grossman conducted an analytical assessment of this parameter and introduced time-dependent transition rates between states $s_1 \rightarrow s_3$ and $s_6 \rightarrow s_4$. However, to circumvent the explicit time-dependency of certain rates (which inherently rely on time due to light flux dependency), we introduced intermediate states s_2 and s_5 (as depicted in Fig. 4.7)[66]. The Grossman's model is governed by a set of linear differential equations:

$$\dot{s}_1 = -a_1 s_1 + b_1 s_3 + a_6 s_6 \quad (4.42)$$

$$\dot{s}_2 = a_1 s_1 - a_2 s_2 \quad (4.43)$$

$$\dot{s}_3 = a_2 s_2 - (b_1 + a_3) s_3 + b_2 s_4 \quad (4.44)$$

$$\dot{s}_4 = a_3 s_3 - (b_2 + a_4) s_4 + b_3 s_5 \quad (4.45)$$

$$\dot{s}_5 = -b_3 s_5 + b_4 s_6 \quad (4.46)$$

$$\sum s_i = 1 \quad (4.47)$$

The equation for the normalized light-dependent conductance of ChR2:

$$\psi(\varphi) = (s_3 + \gamma s_4) \quad (4.48)$$

The population of the strong and weak open states denoted as s_3 and s_4 respectively, is represented by their respective population variables. The parameter γ signifies the ratio of single-channel conductance in state s_4 ($G_{1,s4}$) to that in state s_3 ($G_{1,s3}$), typically

denoted as $\gamma = \frac{G_{1,s4}}{G_{1,s3}}$. Since s_4 is generally less conductive than s_3 , γ is expected to be less than 1.

The equations (4.42) to (4.47) can be solved analytically at steady-state, where the time derivative $\dot{s}_i = 0$ for $i = 1, 2, \dots, 6$. The population of state s_i at steady-state (s_i , steady-state) is determined by the ratio of the forward rate r_i to the total transition rate R , expressed as:

$$s_i, \text{steady-state} = \frac{r_i}{R} \quad (4.49)$$

The compound populating rates r_i are defined as follows: $r_1 = b_1 b_2 b_3$, $r_2 = a_1 b_2 b_3$, $r_3 = a_1 a_2 b_3$, and $r_4 = a_1 a_2 a_3$. The total transition rate R is the sum of these compound rates, given by $R = \sum r_i$. At steady state, the ratio between the population of the weak and the strong conducting states is expressed as $\frac{s_4}{s_3} = \frac{a_3}{b_2}$. As a result, the normalized light-dependent conductance in a steady state is given by the expression:

$$\psi_{\text{steady-state}} = \frac{r_3}{R} \left(1 + \gamma \frac{a_3}{b_2} \right) \quad (4.50)$$

At high irradiance, where r_2 and r_3 are much greater than r_1 and r_4 , $\psi_{\text{steady-state}}$ is governed solely by the rates between the open states:

$$\psi_{\text{steady-state}} = \frac{r_2}{(r_2 + r_3)} \left(1 + \gamma \frac{a_3}{b_2} \right) = \frac{b_2 + \gamma a_2}{a_2 + b_2}$$

The Grossman's[66] model's steady-state response is thus easily modulated by parameters such as b_1 and γ . During the transient peak, where $\dot{s}_3 = 0$, and particularly under conditions of high irradiance, the transient peak conductance of ChR2 approximately equals $\psi_{\text{peak}} \approx \frac{a_1}{(a_1 + b_1 + a_2)}$. Given that typically $a_2 < b_1$, the control over the conductance peak primarily rests upon parameters a_2 and b_1 . Consequently, the plateau-to-peak ratio, known as the ChR2 adaptation ratio $\beta = \frac{\psi_{\text{steady-state}}}{\psi_{\text{peak}}}$, finds adjustment through the amalgamation of steady-state and peak parameters. Such analytical insights into model equations (4.42)–(4.47) not only deepen our understanding of ChR2 behavior but also facilitate the exploration of parameter space for optimal alignment with experimental findings.

4.5.1 ChR2 Model Implementation

The light flux-dependent rates are described empirically in Table 4.2 adapted from Grossman's research paper[66], following a similar structure to the previous model as outlined by Nikolic[125]. To streamline calculations, we opted to standardize the

photon flux ϕ to a reference value ϕ_0 , positioned below the threshold illumination. This normalization strategy ensures that transition rates, which display subtle logarithmic dependencies on illumination, maintain values consistent with their spontaneous transition rates in darkness. Specifically, when ϕ is less than or equal to ϕ_0 , we set ϕ equal to ϕ_0 , effectively nullifying the logarithmic term.

Table 4.2 Empirical expressions for the flux-dependent transition rates[66]

Forward rates	Backward rates
$a_1 = a_{10} \left(\frac{\phi}{\phi_0} \right)$	$b_2 = b_{20} + b_{21} \ln \left(\frac{\phi}{\phi_0} \right)$
$a_3 = a_{30} + a_{31} \ln \left(\frac{\phi}{\phi_0} \right)$	$b_4 = b_{40} \left(\frac{\phi}{\phi_0} \right)$

The determination of g_{ChR} emerges from a solitary photocurrent recording, orchestrated under saturated luminance and a voltage clamped at -70 mV. This deduction hinges on the assumption that the parameters in Equation (2) align to yield $f(-70) = 1$. A compendious assortment of values characterizing the model parameters finds elucidation in Table 4.3 adapted from Grossman's research paper[66].

Table 4.3 Fitting parameters[66]

Parameter	Value
a_{10}	5 ms^{-1}
b_{40}	1.1 ms^{-1}
a_2	1 ms^{-1}
b_3	1 ms^{-1}
b_1	0.13 ms^{-1}
a_4	0.025 ms^{-1}
a_{30}	0.022 ms^{-1}
a_{31}	0.0135 ms^{-1}
b_{20}	0.011 ms^{-1}
b_{21}	0.0048 ms^{-1}
a_6	0.00033 ms^{-1}
ϕ_0	$1.016 \times 10^{16} \text{ photons}\cdot\text{s}^{-1}\cdot\text{cm}^{-2}$
γ	0.05
v_0	43 mV
v_1	-4.1

The implementation of the ChR2 model in NEURON introduces a novel mechanism denoted as ChR2.mod. This mechanism operates as a POINT PROCESS module, accompanied by an ELECTRODE CURRENT[66]. Functioning as a localized shunt within a confined region, it is characterized by a net conductance and total current,

where positive currents depolarize the membrane while negative ones hyperpolarize it (Carnevale and Hines, 2006)[28]. Within this framework, the six-state model is delineated in a KINETIC block, where the flow out of one state is balanced by the flow into another[66]. The relative population of individual states, constituting the unknowns of the model, is declared in the STATE block, which is then translated into a set of Ordinary Differential Equations (ODEs) by the NMODL translator (Hines and Carnevale, 2000)[78].

The light-dependent forward and reverse reaction rates are computed in a separate PROCEDURE, invoked by the KINETIC block. Empirical model constants are provided in a PARAMETER block, while the instantaneous light flux is determined within a self-events NET RECEIVE block[66]. The use of the NET RECEIVE block is pivotal for defining the distinct kinetics of ChR2 and is exclusively feasible within a POINT PROCESS, allowing for discontinuous changes in current[66]. Finally, the kinetic model is integrated utilizing the sparse method, which partitions the Jacobian evaluation from the computation of STATE derivatives, generally resulting in improved computational efficiency (Carnevale and Hines, 2006)[28].

Grossman endeavored to validate the six-state model and its NEURON implementation using the identical experimental dataset employed to validate numerous previously documented ChR2 models[66]. The experimental methodologies have been extensively detailed elsewhere[125, 65]. Our findings revealed a favorable concordance between the photokinetics predicted by the six-state ChR2 model and the experimental observations (see Figure 4.8(a)). Notably, the model accurately captured the peak and steady-state ChR2 currents, as well as the action potential latency, across a broad range of irradiance levels spanning two orders of magnitude (power per unit area)[66]. Moreover, the model effectively characterized the recovery rate of the peak ChR2 current, attributable to the slow transition between the s6 and s1 states, particularly for inter-pulse intervals ranging between 1 and 10 seconds. Additionally, the six-state model demonstrated the capability to faithfully reproduce the experimental photocurrent waveforms elicited by both constant and pulsed illumination conditions (refer to Figure 2(b)).

4.6 Double Two-State ChR2 Model

A new mathematical model called the double two-state opsin model is introduced as a novel approach for studying the kinetics of light-gated ion channels. Unlike conventional Markov models, this innovative framework offers a different perspective on analyzing how neurons respond to optogenetic stimulation. The study investigates

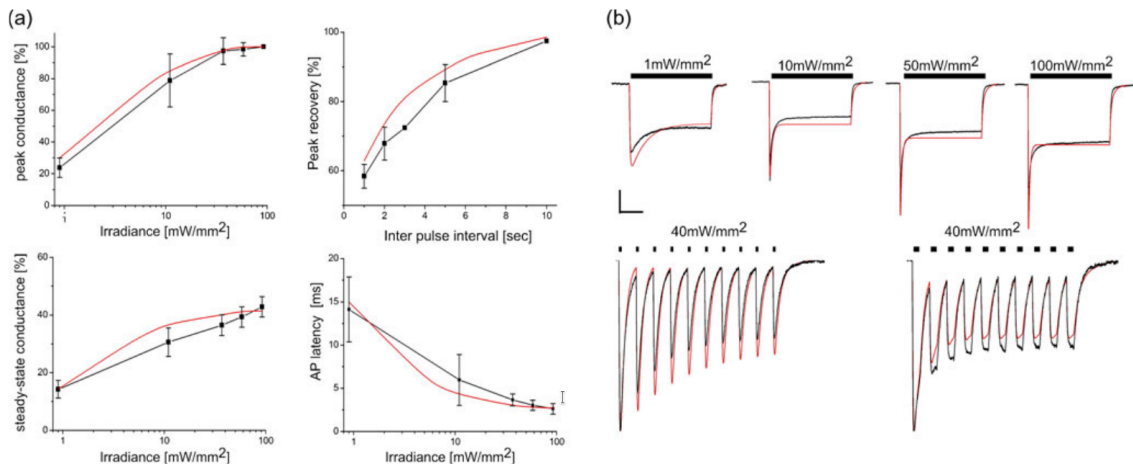


Fig. 4.8 The graph presents the experimental validation of the six-state ChR2 model, implemented within the NEURON simulation environment by Grossman[66]. Experimental data is depicted in black, accompanied by error bars indicating standard deviation, while simulation results are highlighted in red. Panel (a) showcases photokinetic insights of ChR2 conductance, normalized to values acquired at 90 mW/mm². This includes the peak ChR2 current plotted against light intensity (top left), peak current recovery concerning inter-pulse interval (top right), and steady-state (plateau) ChR2 current relative to light intensity (bottom left). Additionally, the correlation between action potential (AP) latency and irradiance is explored in the bottom right panel. Panel (b) illustrates ChR2 photocurrent waveforms under diverse illumination scenarios, encompassing constant and pulsed illuminations across varying intensities. The scale bar denotes a long pulse lasting 50 ms at 0.25 nA and a pulse train lasting 200 ms at 0.5 nA.[66]

the development and practical application of this model, comparing its performance against established models[147].

The proposed model stems from the classical Hodgkin and Huxley voltage-gated sodium model (Hodgkin and Huxley, 1952)[83], yet it ventures into uncharted territory by presenting a dual two-state framework, illustrated in Figure 4.9. Unlike the conventional sodium model, where the second two-state pair traditionally signifies inactivation gating, here it symbolizes the modulation of conductance due to dark-light adaptation. Initially, after an extended period of darkness, all opsin molecules are presumed to inhabit a closed, dark-adapted state. Upon stimulation, channels transition from closed to open ($C \rightarrow O$), albeit slightly slower than the establishment of equilibrium between dark and light-adapted molecules. Remarkably, light-adapted molecules exhibit reduced conductance compared to their dark-adapted counterparts, denoted by the transition from state R to S. The correspondence between these mathematical model states and the physical states of opsin molecules is established through a linear transformation:

$$R = \frac{g_{ChR2} \cdot DA + g_{LA} \cdot LA}{g_{ChR2}}$$

Specifically, R represents the composite conductivity of dark and light-adapted channels. $R(S)$ assumes a value of one (zero) when fully dark-adapted and $\frac{g_{LA}}{g_{ChR2}}$ (respectively, $1 - \frac{g_{LA}}{g_{ChR2}}$) when fully light-adapted, where g_{LA} denotes the conductivity of a light-adapted channel. By incorporating the R state in the model, the need to explicitly determine g_{LA} is circumvented, thereby reducing the number of model parameters. The equilibrium of both state pairs is contingent upon the level of optical excitation. Subsequent to photostimulation, channels revert to a closed state ($O \rightarrow C$) and eventually transition back to a dark-adapted state after a prolonged recovery period, characterized by a considerably slower timescale. Given this slower timescale, the transition from state S to R must also be light-dependent to maintain equilibrium, preventing the dominance of the S state across all levels of optical excitation. Consequently, the ChR2 photocurrent can be succinctly characterized within this innovative framework.

This conceptualization is corroborated by seminal studies in the field (Hodgkin and Huxley, 1952; Nikolic et al., 2009; Grossman et al., 2011)[83, 125, 66].

$$I_{ChR2} = g_{ChR2} \cdot G(V) \cdot (O \cdot R) \cdot (V - E_{ChR2}) \quad (4.51)$$

and

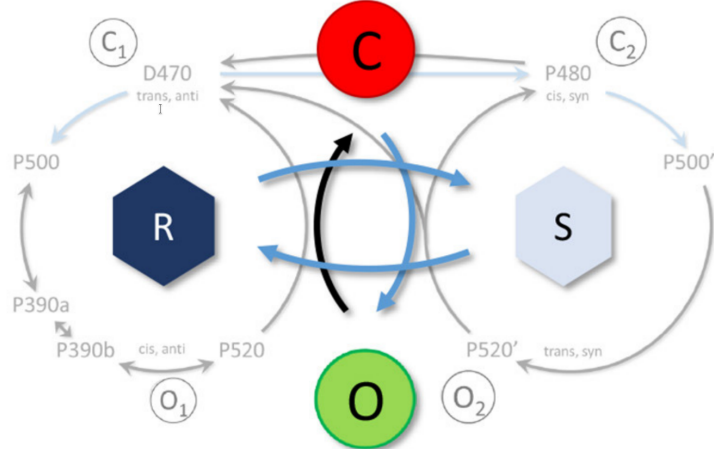


Fig. 4.9 The proposed double two-state opsin model (22OM) with separation of open-closing mechanism and conductance change due to dark-light adaptation. The latter is captured in the mathematical R and S model state pair. DA and LA indicate dark and light adapted molecule states, respectively. O means open, C is closed and D is desensitized. Blue arrows indicate light dependent rates.[147]

$$\frac{dO}{dt} = O_\infty(I, V) - \frac{O(t)}{\tau_O(I, V)} \quad (4.52)$$

$$\frac{dR}{dt} = R_\infty(I, V) - \frac{R(t)}{\tau_R(I, V)} \quad (4.53)$$

In this context, g_{ChR2} represents the maximum specific conductivity of the fully dark-adapted channel, while $G(V)$ denotes a rectification function dependent on the membrane potential V and I symbolizes light intensity. E_{ChR2} signifies the equilibrium potential, and O represents the fraction of molecules in the open state. O_∞ and τ_O correspond to its equilibrium and time constant, respectively. On the other hand, R_∞ and τ_R denote the equilibrium and time constants of the R state.

Under conditions of voltage clamp and when subjected to a rectangular optical pulse with constant light intensity, the photocurrent can be succinctly captured in a closed-form analytical expression as:

$$i_{ChR2} = g_{ChR2} G(V) (O_{on}^{ChR2}(t) + O_{off}^{ChR2}(t)) \cdot (R_{on}^{ChR2}(t) + R_{off}^{ChR2}(t))(V - E_{ChR2}) \quad (4.54)$$

with

$$O(t)_{\text{ChR2}}^{\text{on}}(t) = \left[O_\infty - (O_\infty - O_0) \exp\left(-\frac{t - t_{\text{on}}}{\tau_O(I, V)}\right) \right] \Theta(t - t_{\text{on}}) \Theta(t_{\text{off}} - t) \quad (4.55)$$

$$O(t)_{\text{ChR2}}^{\text{off}}(t) = O(t)_{\text{ChR2}}^{\text{on}}(t_{\text{off}}) \exp\left(-\frac{t - t_{\text{off}}}{\tau_O(O, V)}\right) \Theta(t - t_{\text{off}}) \quad (4.56)$$

$$R(t)_{\text{ChR2}}^{\text{on}}(t) = \left[R_\infty - (R_\infty - R_0) \exp\left(-\frac{t - t_{\text{on}}}{\tau_R(I, V)}\right) \right] \Theta(t - t_{\text{on}}) \Theta(t_{\text{off}} - t) \quad (4.57)$$

$$R(t)_{\text{ChR2}}^{\text{off}}(t) = \left[1 - (1 - R(t)_{\text{ChR2}}^{\text{on}}(t_{\text{off}})) \exp\left(-\frac{t - t_{\text{off}}}{\tau_R(O, V)}\right) \right] \Theta(t - t_{\text{off}}) \quad (4.58)$$

where θ represents the Heaviside function, O_0 and R_0 denote the initial values of O and R at $t = t_{\text{on}}$ (where they respectively equal 0 and 1 when fully dark-adapted), and t_{on} and t_{off} represent the onset and offset of the optical pulse.

This aspect becomes notably advantageous during the parameter fitting phase, where the model undergoes alignment with experimental datasets collected under identical conditions[147]. Notably, discernible correlations emerge between the model's time constants and experimentally derived features, as vividly depicted in Figure 4.2. These correlations serve as invaluable guides for initially approximating the model's parameters[147]. Particularly, when the transition rate time constant τ_O substantially precedes τ_R , it can be promptly inferred from the activation (τ_{on}) and deactivation (τ_{off}) time constants. Likewise, under analogous conditions, τ_R exhibits a robust correlation with the inactivation time constant (τ_{inact}), particularly when $I \neq 0$. For accurate estimation of the dark-light adaptation time constant under dark conditions ($I = 0$), the recovery time constant necessitates a judicious scaling, as prescribed in Equation 4.60. This scaling relation is derived by scrutinizing the recovery time definition using the provided model equations, namely $\tau_{\text{recov}} = t_{\text{on},2} - t_{\text{off},1} \rightarrow I_{\text{p},2}/I_{\text{p},1} = 1 - \exp(-1)$. Here, $t_{\text{on},2}$ denotes the onset time of the second pulse, $t_{\text{off},1}$ signifies the offset of the first pulse, and $I_{\text{p},2}$ and $I_{\text{p},1}$ represent the peak current values of the second and first pulses, respectively.

$$\tau_O(I, V) \approx \tau_{\text{on}}, \quad \tau_O(0, V) \approx \tau_{\text{off}} \quad \text{and} \quad \tau_R(I, V) \approx \tau_{\text{inact}} \quad (4.59)$$

$$\tau_R(0, V) \approx \frac{\tau_{\text{recov}}}{1 - \ln\left(\frac{1}{1-\text{I ratio}}\right)} \quad (4.60)$$

To make the relationship true there are few conditions should be satisfy[147].

$$t_{p,1} - t_{on,1} \approx t_{p,2} - t_{on,2}, t_{p,1} - t_{on,1} > \tau_O, t_{off,1} - t_{on,1} > \tau_R \quad (4.61)$$

The time span from the onset to the peak of each pulse, denoted as $t_{p,i} - t_{on,i}$, should be roughly equivalent for both initial and subsequent pulses, exceeding notably the activation time constant. Additionally, the condition demands that the steady-state value is achieved by the end of the first pulse.

Finally Ruben rectified and fitted the function parameters $G(V)$, R_∞ , O_∞ , $\tau_O(I)$, $\tau_R(I)$, $\tau_X(I, V)$, and $\tau_X(V)$ as:

$$O_\infty(I) = \frac{1}{1 + \exp\left(\frac{p_1}{p_2} \cdot I^{-\frac{1}{p_2} \ln(10)}\right)} \quad (4.62)$$

$$R_\infty(I) = 1 - \frac{p_3}{1 + \exp\left(\frac{p_1}{p_2} \cdot I^{-\frac{1}{p_2} \ln(10)}\right)} \quad (4.63)$$

$$G(V) = \frac{p_1 \cdot (1 - p_2 \exp(-(V - E_{\text{ChR2}})/p_3))}{V - E_{\text{ChR2}}} \quad (4.64)$$

$$\tau_O(I) = \frac{p_3}{1 + \exp\left(\frac{p_1}{p_2} \cdot I^{(1/p_2) \cdot \ln(10)}\right)} \quad (4.65)$$

$$\tau_R(I) = p_1 \left(1 - \frac{p_2}{1 + \exp\left(\frac{p_3}{p_4} \cdot I^{-1/p_4 \cdot \ln(10)}\right)} - \frac{1 - p_2}{1 + \exp\left(\frac{p_5}{p_6} \cdot I^{-1/p_4 \cdot \ln(10)}\right)} \right) \quad (4.66)$$

$$\tau_X(V) = \frac{p_1}{1 + \exp\left(-\frac{(V-p_2)}{p_3}\right)} \quad (4.67)$$

$$\tau_X(I, V) = \tau_X(I) \cdot \tau_X(V) \quad (4.68)$$

or,

$$\tau_X(I, V) = \left[(\tau_X(I))^{-1} + (\tau_X(V))^{-1} \right] \quad (4.69)$$

Ruben's proposed double two-state opsin model presents a compelling departure from standard Markov models, offering a fresh perspective on analyzing neural responses to optogenetic stimuli[147]. Demonstrating superior performance in fitting experimental data for ChR2(H134R) and MerMAID opsins, this model exhibits enhanced computational efficiency and accuracy compared to traditional counterparts. Despite its strengths, limitations such as an instantaneous light response and the absence of pH and ion concentration dependencies warrant further investigation and refinement. Nevertheless, the model underscores the potential of the double two-state opsin model to propel advancements in optogenetic neurostimulation research. In this report I only have taken the parameters for ChR2. The initial conditions are summarized in Table 4.4 and 4.5. for the upper and lower boundaries.

Table 4.4 Parameters[147]

$\tau_O(I)$			$\tau_O(V)$			$\tau_R(I)$						$\tau_R(V)$						
	p_1	p_2	p_3		p_1	p_2	p_3		p_1	p_2	p_3	p_4	p_5	p_6		p_1	p_2	p_3
LB	-10	0	0	0	-100	-1,000	0	0	-10	0	-10	0	0	-100	-1,000	0	-100	-1,000
UB	10	20	1	100	100	1,000	10	1	10	20	10	20	100	100	1,000	100	100	1,000
X0	1	1	0.5	1	-50	10	1	0.5	0	0.125	3	0.5	1	-50	10	1	-50	10

Table 4.5 Parameters[147]

$O_\infty(I)$			$R_\infty(I)$			$G(V)$						
	p_1	p_2		p_1	p_2	p_3		p_1	p_2	p_3	g_{ChR2}	E_{ChR2}
LB	-10	0	-10	0	0 0.8	0 -	1.1 -	0 -	- 0	- 0	- 0	- 0
UB	10	20	10	20	1	100 -	100 -	500 -	- 100	- 100	- 100	- 100
X0	1	1	1	1	0.1 0.9	1	10 -	0.5 -	- 30	- 30	- 30	- 30

Here, lower bounds (LB), upper bounds (UB), and initial values (X0) for the first two steps of the fitting procedure, based on Ruben's research "Double Two-State Opsins Model with Autonomous Parameter Inference (2021)"[147], along with the model fitted for H13R and MerMAID mutants.

Chapter 5

Model Simulation and Results

Researching how neurons respond to different stimulation protocols is crucial for unraveling the fundamental mechanisms of neuronal excitability and for devising therapeutic interventions. In this chapter, we delve into a comprehensive computational analysis of a specific ion channel, Channelrhodopsin-2 (ChR2), and its variants. ChR2 is a light-sensitive ion channel widely used in optogenetics to control neuronal activity with high temporal precision. By employing both optical and electrical stimulation techniques, we aim to elucidate the intricate dynamics of neuronal firing patterns and action potential (AP) generation.

Our investigation begins by examining the effect of constant pulses of both optical and electrical stimulation on the firing rate of neurons expressing ChR2. This examination is essential as it offers insights into the core aspects of neuronal excitability and the response dynamics of ChR2. The stimulation protocol used consists of three intervals: an initial stimulation-free period of one second, followed by a stimulation period of varying duration and amplitude, and concluded by another one-second stimulation-free period. This approach allows us to isolate the effects of the stimulation on the firing rate and analyze the neuronal response in a controlled manner.

Two techniques are used to measure the firing rate: the mean instantaneous frequency (FRISI) and the mean spike frequency (MSF). By averaging the amount of spikes during the stimulation period, the MSF provides an overall measure of the firing rate, but the FRISI provides a more in-depth temporal study by taking the inverse of the interspike intervals into account.

Following the analysis of firing rates, we construct strength-duration (SD) curves for both optical and electrical stimulation. The SD curve is a fundamental tool in electrophysiology, representing the relationship between the strength of the stimulus and the duration required to elicit an action potential. For spontaneously firing neurons

like those in the subthalamic nucleus (STN), determining the threshold for action potential generation is essential. By adjusting the threshold to the minimum strength required to evoke an AP within a predefined period, we can derive a detailed SD curve that highlights the efficacy of different stimulation modalities.

Our dataset for this analysis includes a wide range of pulse durations and amplitudes, allowing us to capture the complete spectrum of neuronal responses. We find the minimal strength needed for each pulse duration that causes a delay below the predetermined threshold by measuring the time lag between the start of the pulse and the formation of AP. This rigorous approach ensures the accuracy and reliability of our SD curves, providing valuable insights into the dynamics of ChR2-mediated neuronal activation.

Finally, we investigate the impact of different stimulation sources on the action potential waveform. By comparing APs triggered by electrical and optical stimulation, we aim to uncover any differences in the resulting AP morphologies. This evaluation involves employing both distinct and overlapping pulses, as per the strength-duration curves established previously. These simulations start with the output of a one-second stimulation-free interval, which provides a stable baseline against which to compare results. We present an extensive evaluation of the impact of stimulation source on AP waveform features by examining APs induced by a 1 ms and a 20 ms pulse at different amplitudes.

Overall, this chapter presents a detailed computational study of ChR2 and its variants, examining their behavior under various stimulation protocols. By integrating optical and electrical stimulation techniques, constructing strength-duration curves, and comparing action potential waveforms, we aim to advance our understanding of the fundamental mechanisms underlying neuronal excitability and the potential applications of optogenetics in neuroscience research and clinical therapy.

The conductivity of ChR2, estimated to be approximately 50 fS[41], is relatively low compared to endogenous ion channels such as the sodium channel, which typically exhibits a conductivity of around 10 pS. However, the expression of ChR2 in neuronal cells at sufficient levels can evoke action potentials upon light stimulation, allowing for precise control over neural firing[125]. Understanding the intricate dynamics of ChR2 activation is crucial for optimizing its use in optogenetic experiments. Upon exposure to blue light, ChR2 undergoes a series of conformational changes, leading to the formation of intermediate states and ultimately leading to the activation of the channel pore[7]. This process, often described in terms of the photocycle of ChR2,

involves the isomerization of the retinal chromophore and the deprotonation of the Schiff base[109].

5.1 ChR2 Model Simulation

We systematically study the response of neurons expressing ChR2 to optical and electrical stimuli. We only begin by examining the four-state model of ChR2, which captures a more detailed representation of ChR2 kinetics, including intermediate states that provide a more comprehensive understanding of the channel's behavior. the essential transitions between the closed, open, and desensitized states. This model allows us to understand the fundamental operational principles of ChR2 in a simplified context.

For this model, we investigate the effect of constant stimulation pulses on neuronal firing rates. The protocol involves three intervals: an initial one-second stimulation-free period, followed by a stimulation period with predefined pulse duration and amplitude, and concluding with another one-second stimulation-free period. By varying the pulse durations and amplitudes, we generate a comprehensive dataset to analyze the neuronal firing response. Mean spike frequency and mean instantaneous frequency are used to quantify the firing rate, offering a reliable assessment of neural activity.

Additionally, we construct strength-duration (SD) curves for each model, which represent the relationship between stimulus strength and duration required to elicit an action potential (AP). For spontaneously firing neurons, determining the minimum strength necessary to evoke an AP within a predefined period is crucial. By adjusting the threshold for AP generation, we derive accurate SD curves that highlight the efficacy of different stimulation modalities.

Finally, we compare the action potential waveforms triggered by electrical and optical stimulation across the different models. By examining the APs generated by various pulse durations and amplitudes, we aim to identify any differences in AP morphology resulting from the different stimulation sources. This comparison provides further insights into the specific characteristics and potential applications of ChR2-mediated stimulation.

Overall, this chapter presents a detailed computational study of ChR2 and its variants, focusing on their behavior under various stimulation protocols. By integrating optical and electrical stimulation techniques and constructing strength-duration curves, we aim to advance our understanding of the fundamental mechanisms underlying

neuronal excitability and the potential applications of optogenetics in neuroscience research and therapy.

5.1.1 Four-state model's simulation

To analyze the characteristics of Channelrhodopsin-2 (ChR2) H134R, we utilized a model based on the work by William et al [176] as discussed in section 4.4. We implemented this model in both Python and MATLAB to compare and validate the results across these different computational platforms.

For our simulations, we set specific parameters: a delay before the first stimulus of 10 ms, a stimulus duration of 400 ms, an irradiance of 5.5 mW/mm², and a wavelength of 470 nm. These conditions were consistent across both implementations to ensure comparability.

In MATLAB, we plotted the current response of ChR2 to the optical stimulus and highlighted the duration of the optical pulse on the graph for clarity. The Python implementation similarly computed and plotted the current response, and we ensured that the simulation parameters and equations used were identical to those in MATLAB.

The results from both simulations were remarkably similar, demonstrating the reliability and consistency of the ChR2 H134R model across different programming environments. This validation provides confidence in the model's accuracy and its utility for further optogenetic studies.

Parameters in table 5.1 are as taken from the work by William et al [176].

Table 5.1 Simulation Parameters

Parameter	Units	Definition	Value used by others	Reference/Notes
k1	ms ⁻¹	Light-sensitive rate constant for C1R01 transition	Q1(F,t) = e1F*p=var	Q1(F,t) = e1F*p=var [11],[12] 0.369 (at 5 mW/mm ²)
k2	ms ⁻¹	Light-sensitive rate constant for C2R02 transition	Q2(F,t) = e2F*p=var	Q2(F,t) = e2F*p=var [11],[12] 0.369 (at 5 mW/mm ²)

Continued on next page

Table 5.1 – *Continued from previous page*

Parameter	Units	Definition	Value used by others	Reference/Notes
e1	-	Quantum efficiency for photon absorption from C1	0.8535	0.8535; 0.5 [11]
e2	-	Quantum efficiency for photon absorption from C2	0.14	0.14; 0.025; 0.15 [11]
s	m^2	Absorption cross-section for retinal	1.26×10^{-22}	1.26×10^{-22} [12]
λ	nm	Wavelength of max absorption for retinal	470	470
I	mW/mm^2	Irradiance	var (typically 0 to 10)	var (typically 0 to 10)
π	-	Photon flux: number of photons per molecule per second	-	-
tChR2	ms	Time constant of ChR2 activation	1.3	1.3 [9]
wloss	-	Scaling factor for losses of photons due to scattering or absorption	0.77 (1.3)	0.77 (1.3); 0.9 (1.1) [9]
t	-	Time-dependent function reflecting the probabilistic, non-instantaneous response of the ChR2-retinal complex to light	-	-
τ	ms	Time constant of ChR2 deactivation	10.64	10.64 [9]
τ_{off}	ms	Off-state time constant	50	50 [9]
τ_1	ms	Time constant for the first open state	3	3 [9]

Continued on next page

Table 5.1 – *Continued from previous page*

Parameter	Units	Definition	Value used by others	Reference/Notes
τ_2	ms	Time constant for the second open state	10.64	10.64 [9]
g1	pS	Conductance of the first open state	100	100 [9]
g2	pS	Conductance of the second open state	20	20 [9]
V	mV	Voltage	-	-
p	-	Fraction of ChR2 in the open state	-	-
n	-	Fraction of ChR2 in the closed state	-	-
A	mV	Amplitude	-	-
B	mV	Baseline	-	-
koff	ms^{-1}	Rate constant for the off-state transition	-	-
kon	ms^{-1}	Rate constant for the on-state transition	-	-
D	-	Duty cycle	-	-
S	-	State transition	-	-
F	-	Photon flux per molecule per second	-	-
h	J^*s	Planck's constant	6.62607015e-34	6.62607015e-34
c	m/s	Speed of light	3e8	3e8
hc	$\text{kg}^*\text{m}^3/\text{s}^2$	Product of Planck's constant and the speed of light	1.98644e-25	1.98644e-25
η	-	Efficiency	-	-
Ep	eV	Energy of photon	1.65	1.65

5.1.2 Discussion

We investigate the kinetics of recovery from inactivation for Channelrhodopsin-2 (ChR2) both in experimental settings and in a computational model. The experimental and model traces are compared using specific protocols and conditions to understand the

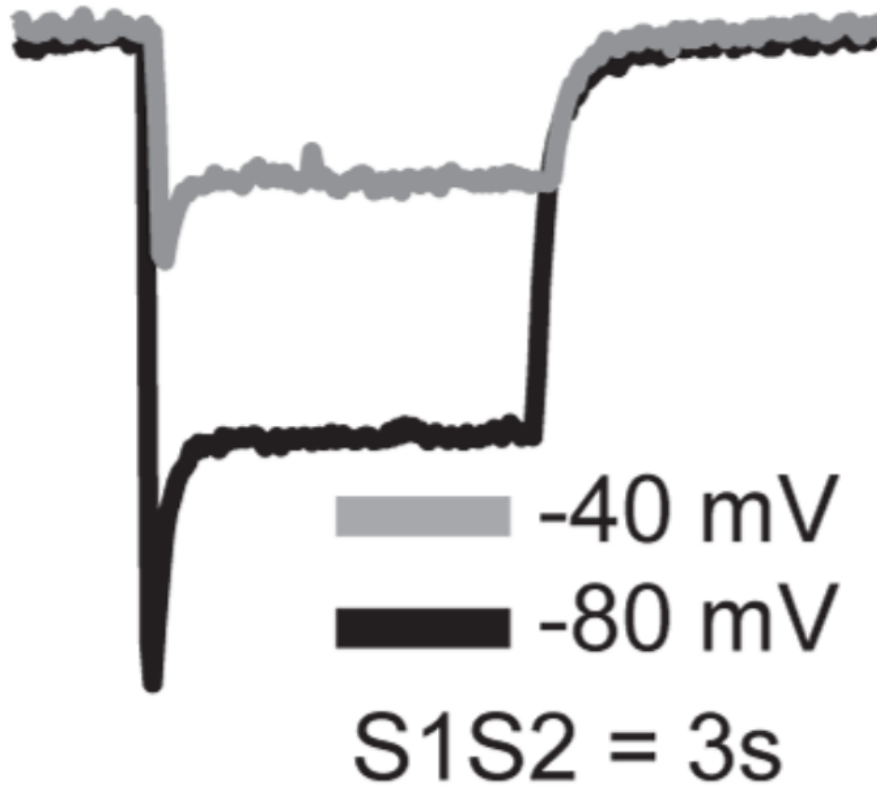


Fig. 5.1 Experimental traces in response to S1–S2 protocol, 3 s inter-pulse interval, the irradiance of 1.6 mW/mm², and holding voltages of 240 and 280 mV. Figure adapted from William et al [176].

recovery behavior of ChR2.

Figures 5.1 and 5.2, Experimental and Model Traces in Response to S1–S2 Protocol
The S1–S2 protocol involves delivering two consecutive light pulses with a specific inter-pulse interval to observe how the channel recovers between the pulses. In our case, we used a 470 nm wavelength. The irradiance of the light pulses was set to 5.5 mW/mm², and the holding voltages were set at -80 mV.

Experimental Traces (Left) in Figure 5.3 The experimental data shows the current response of ChR2 in a real biological system. The traces highlight the recovery kinetics of the channel from the inactivated state between the two pulses. Model Traces (Right)

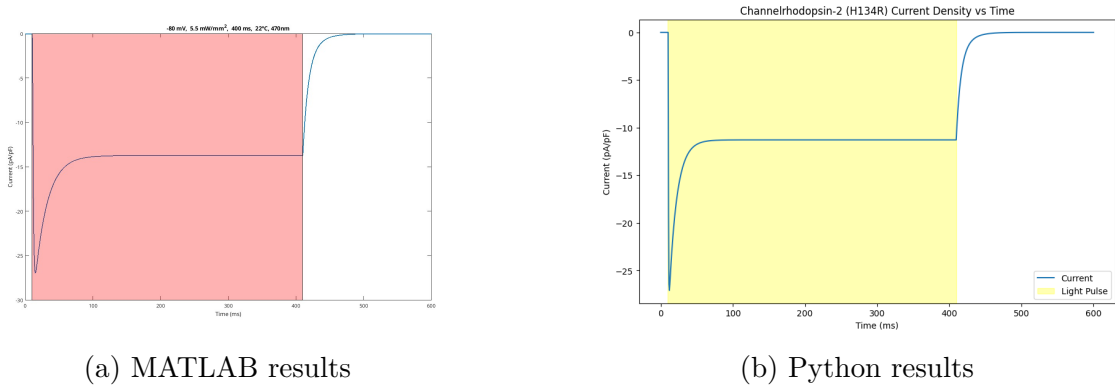


Fig. 5.2 Current response of ChR2 H134R model with a stimulus duration of 400 ms and an irradiance of 5.5 mW/mm² shown for (a) MATLAB and (b) Python implementations.

in Figure 5.3 The model simulations replicate the experimental conditions and show the predicted current response of ChR2 based on our computational model. By comparing these traces with experimental data, we can validate the accuracy and reliability of the model.

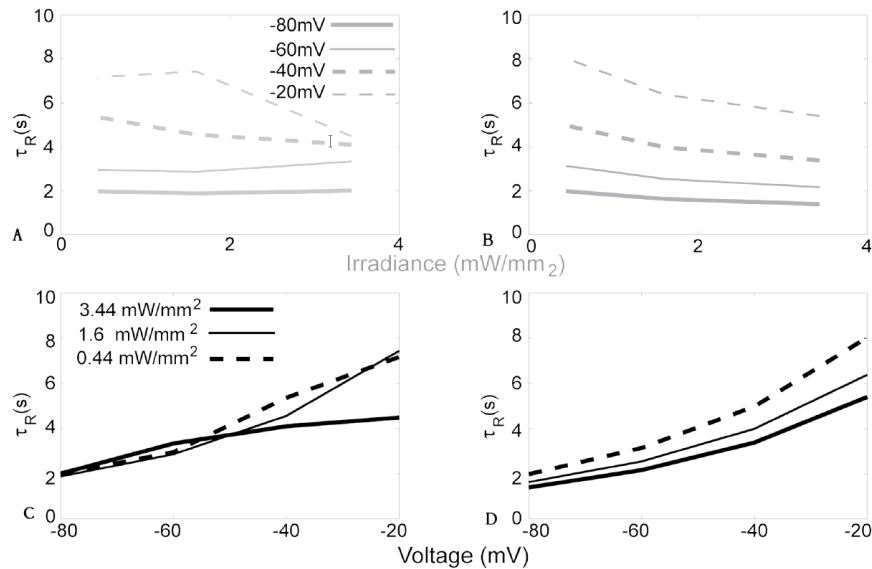


Fig. 5.3 A and B Light dependence of τ_R across four voltage values. C and D Voltage dependence of τ_R across three irradiance levels.

5.1.2.1 A and B: Light Dependence of τ_R Across Four Voltage Values

Here, we explore how the recovery time constant (τ_R) varies with different light intensities at four distinct voltage values.

- A (Light Dependence at Various Voltages): This part of the analysis shows how τ_R changes with varying irradiance levels at specific voltages. This helps in understanding the sensitivity of ChR2 recovery kinetics to changes in light intensity.
- B (Summary of Light Dependence): The results are summarized across four different voltages, providing a comprehensive view of how light intensity influences recovery kinetics.

5.1.2.2 C and D: Voltage Dependence of τ_R Across Three Irradiance Levels

Next, we investigate how the recovery time constant (τ_R) is affected by different holding voltages across three irradiance levels.

- C (Voltage Dependence at Various Irradiance Levels): This part examines how τ_R varies with changes in voltage at specific light intensities. This analysis is crucial for understanding the voltage sensitivity of ChR2 recovery.
- D (Summary of Voltage Dependence): The results are consolidated across three different irradiance levels, offering a detailed insight into how voltage impacts the recovery kinetics of ChR2.

In conclusion, our analysis of the kinetics of recovery from inactivation for Channelrhodopsin 2 (ChR2) provides valuable insights into the behavior of this optogenetic tool. Through a combination of experimental data and computational modeling, we were able to compare and validate the accuracy of our model in replicating real-world observations. Our findings shed light on the light and voltage dependencies of ChR2 recovery kinetics, offering important considerations for its practical application in optogenetics. This comprehensive understanding contributes to the optimization of ChR2-based experiments and facilitates the design of more effective optogenetic tools for manipulating cellular activity.

Furthermore, ChR2-based synaptic modulation may offer novel approaches for treating brain-related disorders such as Parkinson's, Alzheimer's, epilepsy, depression, addiction, and many more. Optogenetic manipulation of neuronal circuits implicated in these conditions could provide precise control over neural activity, offering potential therapeutic benefits with minimal side effects compared to traditional pharmacological interventions.

In addition to direct therapeutic applications, the insights gained from studying ChR2 kinetics could also contribute to the development of advanced neuroprosthetic

devices and brain-computer interfaces. By harnessing the principles of optogenetics, researchers can design implantable devices capable of restoring lost neural function or interfacing with external technology to augment cognitive abilities.

5.2 ChR2 H134R application in Alzheimer's disease

Alzheimer's disease is a degenerative neurological condition marked by gradual cognitive decline, memory deterioration, and challenges in daily activities[111, 150]. Despite decades of research, effective treatments for AD remain elusive, underscoring the need for innovative approaches to understand its underlying mechanisms and develop novel therapeutic strategies[107]. Recent studies have implicated aberrant neuronal activity and synaptic dysfunction in the pathogenesis of AD, highlighting the importance of investigating these processes at the cellular and circuit levels[130, 26].

Through this interdisciplinary approach, we seek to elucidate the mechanisms underlying synaptic dysfunction in AD and identify potential targets for therapeutic intervention. By combining experimental and computational techniques, we aim to gain a comprehensive understanding of the complex interplay between neuronal activity, synaptic plasticity, and disease progression in AD[36]. Ultimately, our work may pave the way for the development of novel treatments that target aberrant neuronal dynamics in Alzheimer's disease.

Understanding the propagation of action potentials (APs) in neuronal axons is crucial for uncovering the mechanisms behind diverse neurological disorders, such as Alzheimer's disease[166]. In the context of Alzheimer's disease, studying the effects of dystrophic structures on AP propagation can provide valuable insights into disease pathology and potential therapeutic interventions[70]. Dystrophic structures, characterized by abnormal morphology, have been observed to influence AP transmission, leading to phenomena such as delayed transmission, double spiking, or blockage[68].

This topic aims to investigate the impact of dystrophic structures on AP propagation in neuronal axons, specifically focusing on the alterations in transmission patterns observed in Alzheimer's disease. To achieve this, computational models will be employed to simulate AP propagation under varying conditions, mimicking the presence of dystrophic structures along the axon. By running simulations with different parameters representing dystrophy size, channel density, axon diameter, and other factors, we aim to characterize the changes in AP transmission and identify potential targets for therapeutic intervention.

The simulations will utilize the NEURON simulator, a powerful tool for modeling the electrical activity of neurons and simulating complex neuronal networks. NEURON allows for the integration of biophysical properties of neurons, such as ion channels and membrane properties, enabling detailed investigations into the dynamics of AP propagation.

Through this project, we seek to enhance our understanding of the role of dystrophic structures in altering AP transmission in neuronal axons, contributing to the broader efforts aimed at deciphering the mechanisms underlying Alzheimer's disease and additional neurodegenerative conditions. The insights gained from this study may inform the creation of innovative therapeutic approaches targeting aberrant neuronal activity associated with neurological diseases.

5.2.1 Methodology and Parameters

The methodology employed in this study involves computational modeling to investigate the impact of dystrophic structures on action potential (AP) propagation within neuronal axons. The neuron model consists of a soma, an axon, and a connecting structure (Stick and Can segments). The soma is modeled as a single compartment with a length of 1 μm and a diameter of 5 μm , containing passive membrane properties. The axon, extending from the soma, is represented as a cylindrical structure divided into 19 segments with a total length of 565.723 μm and an axial resistance of 50 Ωcm . The axon incorporates various ion channels, including sodium (nax) and potassium (kdr) channels, which are crucial for action potential generation and propagation. Additionally, the axon includes passive membrane properties. The connecting structure comprises two segments: the Stick and the Can. The Stick segment is 5 μm in length and connects the soma to the Can segment. The Can segment, also 5 μm in length, represents a region where dystrophic changes can occur, simulating the effects of Alzheimer's disease. This region can be set to have active, passive, or sealed properties, allowing the study of different pathological conditions. Together, this model facilitates the study of how action potentials initiated at one end of the axon propagate through the dystrophic region and are recorded at the other end, helping to analyze the impact of Alzheimer's-related changes on neuronal signaling. Various parameters are systematically manipulated to simulate different experimental conditions and assess their effects on AP transmission. The key parameters utilized in the simulations are outlined below:

5.2.1.1 Dystrophy Size and Distribution

The size and distribution of dystrophic structures along the axon are represented numerically, with diameters ranging from 0.1 to 1.0 in increments of 0.05. Additionally, the number of equivalent sphere diameters is computed based on the specified range.

5.2.1.2 Channel Density

The density of voltage-sensitive ion channels, such as sodium (Na^+) and potassium (K^+) channels, is varied from 0 to 100% of the selected model. This parameter represents the proportion of maximal conductance for each channel type and is adjusted in discrete steps of 0.1.

5.2.1.3 Axon Diameter

The diameter of the axon is manipulated to simulate different morphological states, with values ranging from 0.1 to 0.9 in increments of 0.05. These diameters correspond to the cross-sectional area of the axon and influence its resistance to current flow.

5.2.1.4 Stimulation Protocols

Parameters related to optogenetic stimulation using Channelrhodopsin-2 (ChR2) are specified, including pulse duration, frequency, and intensity. These parameters govern the timing and strength of light-induced depolarization, with typical values ranging from 0.002 to 0.02 for pulse intensity.

5.2.1.5 Reversal Potentials

The reversal potential for ChR2 (e_{ChR2}) is set to 0 mV, representing the membrane potential at which ChR2 channels become non-conducting. This parameter influences the direction and magnitude of ion flux during optogenetic stimulation.

5.2.1.6 Biophysical Properties

Biophysical properties such as membrane capacitance, specific membrane conductance, and resistivity are defined to characterize the passive electrical properties of the axon. These parameters affect the propagation of electrical signals and interactions with the cellular environment.

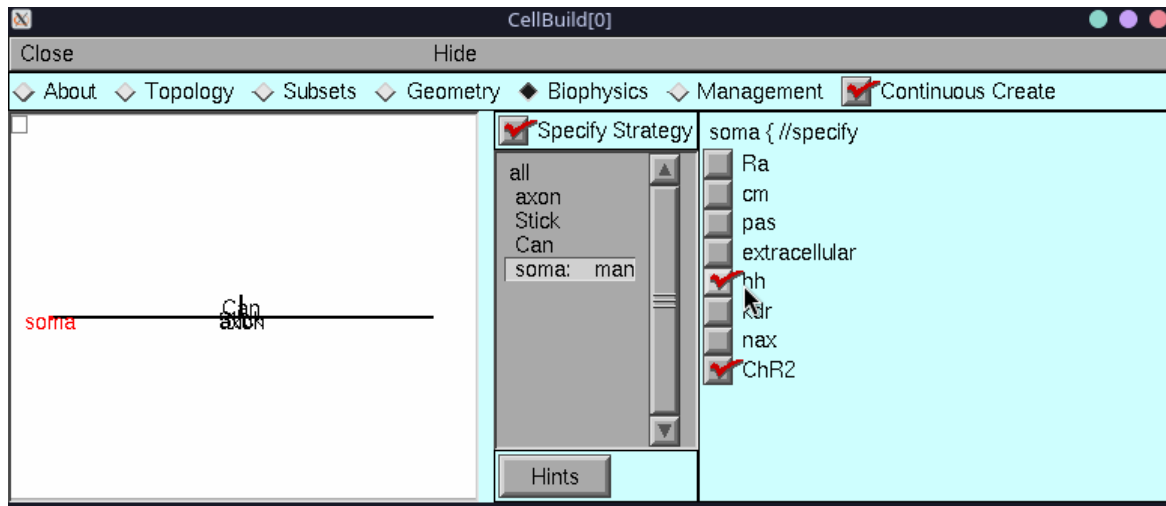


Fig. 5.4 Schematic Diagram of the Axon in NEURON Simulator

By systematically varying these parameters in computational simulations, the study aims to elucidate the complex mechanisms underlying AP propagation in the presence of dystrophic structures, providing insights into neurodegenerative conditions such as Alzheimer's disease.

Table 5.2 Simulation Parameters

Parameter	Description	Value
CanDiam	Diameter of the dystrophic structure	100 μm
ChannelStrength	Density of voltage-gated ion channels	0.9
AxonDiam	Diameter of the axon	1 μm
SomaDiam	Diameter of the axon	20 μm
AxonLen	Diameter of the axon	100 μm
SomaLen	Diameter of the axon	20 μm
stickDiam	Diameter of the stick structure	2 μm
dystrophy_active	Type of dystrophy: -1 (passive), 0 (sealed), 1 (active)	
tstop	Duration of simulation	single pulse or 20 Hz pulse at 10000 ms
v_init	Initial membrane potential	-65 mV
dt	Time step for integration	0.025 ms

ChR2 (H134R) parameters are as taken as shown in Table 5.1.

5.2.2 Results

The results and discussion section presents an analysis of the simulation outcomes and their implications for understanding the effects of dystrophic structures on action potential propagation in Alzheimer's disease. This section evaluates the observed phenomena, such as delayed transmission, double spiking, and blockage of action potentials, in relation to varying parameters including dystrophic structure size, channel density, axon diameter, and presence of active or passive dystrophy. Additionally, the section discusses the significance of these findings in the context of Alzheimer's disease pathology and potential therapeutic implications. Further interpretations, comparisons with existing literature[186], and insights into the underlying mechanisms are provided to deepen understanding of the simulated phenomena and their relevance to Alzheimer's disease.

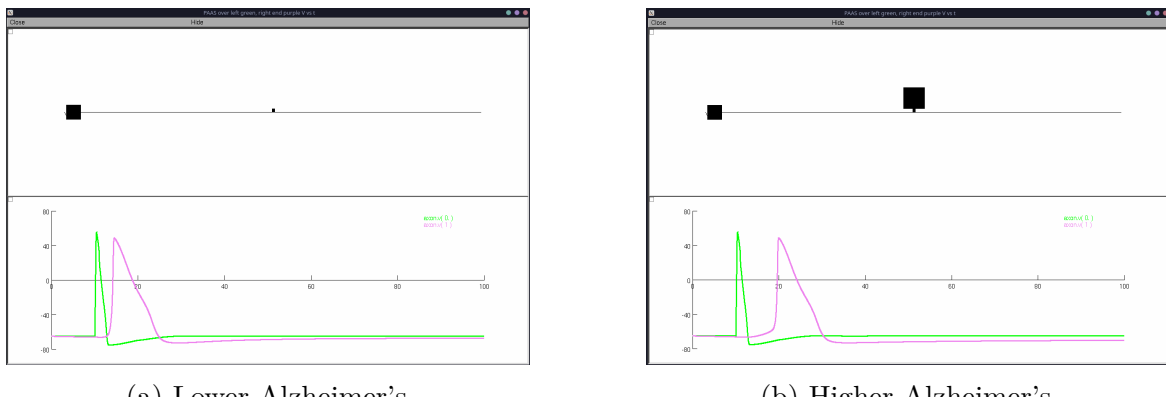


Fig. 5.5 Current propagation from one end to another end of the axon.

In Figure 5.5, the impact of Alzheimer's disease on axonal function is illustrated by showing how increasing axonal damage delays the propagation of action potentials. The model demonstrates this by recording the voltage over time at two points along the axon: the initial segment (axon 0) and the terminal segment (axon 1). The green line represents the voltage at axon 0, while the pink line represents the voltage at axon 1.

As the severity of axonal damage increases, indicative of the progression of Alzheimer's, the action potential recorded at axon 1 (pink line) shows a noticeable delay compared to that at axon 0 (green line). This delay reflects the impaired ability of the action potential to travel efficiently along the axon, a hallmark of neurodegenerative changes associated with Alzheimer's disease. The black square above the

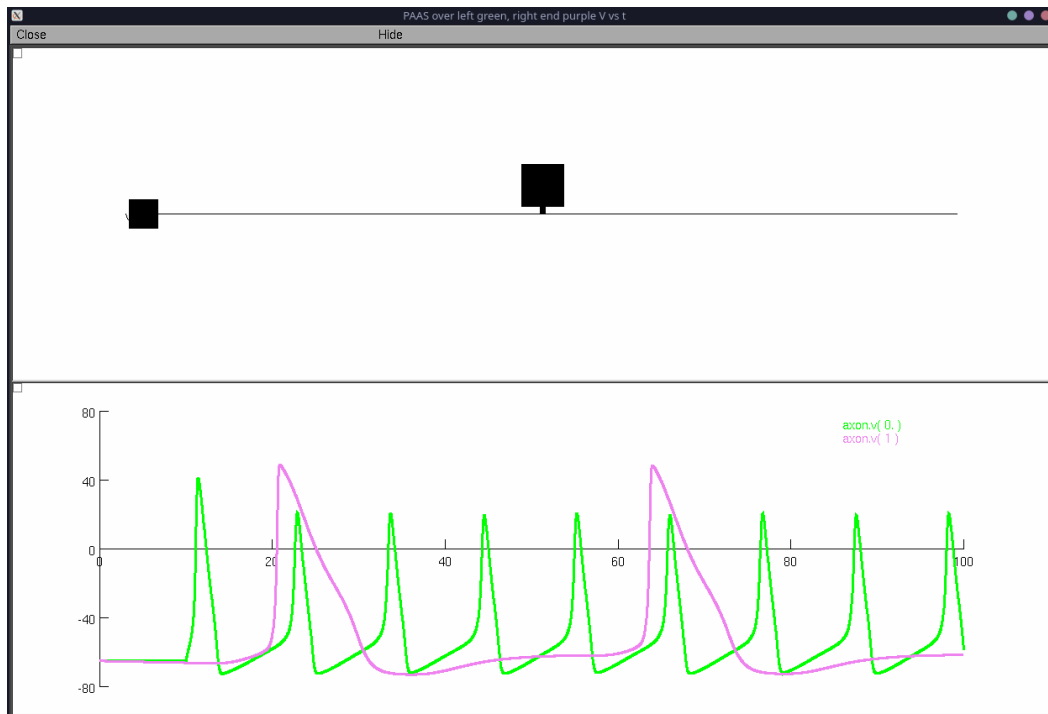
graph provides a visual indicator of the extent of Alzheimer's impact, with increasing intensity correlating to more severe axonal damage.

In further experiments, we increased the signal frequency by activating the channelrhodopsin 2 (ChR2) ion channel in the soma. This intervention aimed to counteract the effects of axonal damage by enhancing the signal propagation along the axon. The activation of ChR2 (H13R), a light-sensitive ion channel, allowed us to precisely control the frequency and intensity of the electrical signals initiated in the soma. By increasing the frequency of the signals, we sought to overcome the conduction delays and signal attenuation observed in damaged axons, as seen in Alzheimer's disease.

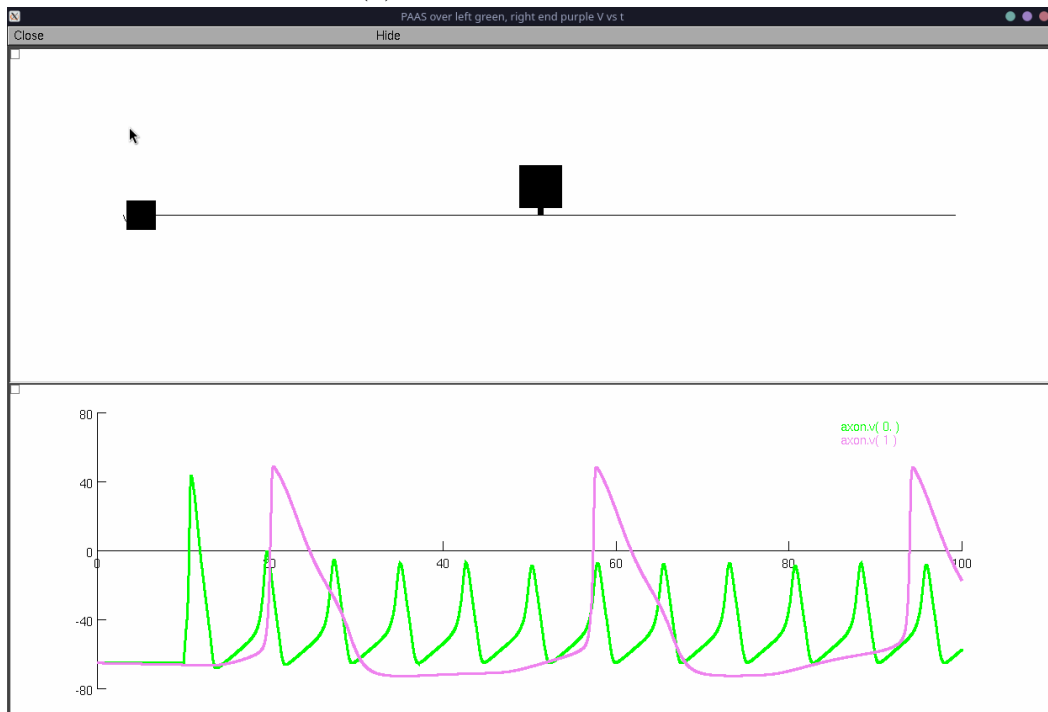
The results, depicted in Figure 5.6, show a significant improvement in the voltage signal at axon 1 (represented by the pink line). The green line indicates the voltage at axon 0, close to the soma, while the pink line shows the voltage at axon 1, further along the axon. In previous conditions without ChR2 activation, we observed that the signals at axon 1 were delayed and significantly attenuated compared to those at axon 0, highlighting the impaired signal propagation due to axonal damage.

However, by boosting the initial signal frequency through ChR2 activation, we observed a marked reduction in the action potential's delay and an increase in its frequency at axon 1. This suggests that the enhanced stimulation at the soma not only improved the overall signal strength but also facilitated more efficient propagation of the action potentials along the axon, even in the presence of damage. The increased frequency of signals generated by ChR2 activation likely contributed to a higher probability of successful action potential transmission, thereby partially mitigating the detrimental effects of Alzheimer's-related axonal damage.

Figure 5.6 presents a simulation capturing the neuron's behavior under an extended stimulus scenario. The simulation applies a 1000 ms pulse, maintaining this stimulation over a total timeline of 1500 ms. This prolonged duration allows for a detailed examination of the neuron's response dynamics, spanning both the stimulus phase and the subsequent recovery period. During the 1000 ms pulse, we observe how the neuron sustains its activity over time, providing insights into its ability to maintain signaling under continuous input. Following the pulse, the additional full period enables observation of the neuron's return to baseline activity or any lingering effects post-stimulation. This comprehensive timeline facilitates a deeper understanding of neural responses, including phenomena such as persistence, fatigue, and recovery, particularly pertinent in the context of neurodegenerative conditions like Alzheimer's disease.



(a) before ChR2 activation



(b) After ChR2 activation

Fig. 5.6 (a) In normal case when a neuron fires as in Alzheimer's case. (b) Increasing the signal frequency by activating the ChR2 ion channel causes an increase in frequency at the end of the Axon.

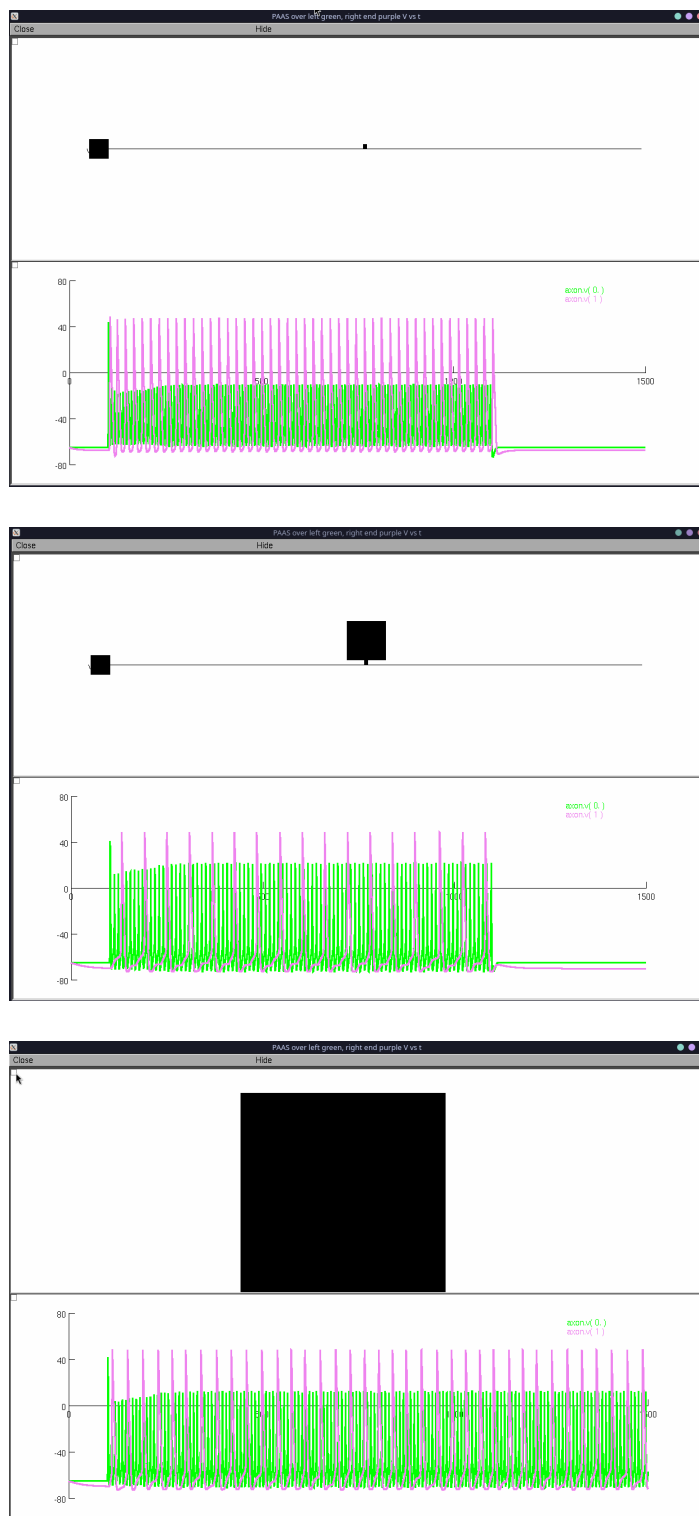


Fig. 5.7 Increased frequency of the axon potential over a long period of 1500 ms for three stages of Alzheimer's.

5.3 Discussion

The study presented in Figures 5.5 and 5.6 provides crucial insights into the detrimental impacts of Alzheimer's disease on neuronal communication, particularly focusing on the propagation of action potentials along axons. By simulating and analyzing the voltage changes at two distinct points along an axon—axon 0 and axon 1—the research delineates the progressive impairment caused by Alzheimer's-related axonal damage. The green and pink lines in the figure represent the voltage recordings at axon 0 and axon 1, respectively, offering a clear visual differentiation of the action potential's journey and the disruptions that occur with increased axonal damage.

As Alzheimer's disease progresses, the integrity of axonal structures deteriorates, as evidenced by the increasing delay in the action potential recorded at axon 1 compared to axon 0. This delay is indicative of the compromised ability of neurons to efficiently transmit electrical signals, a fundamental aspect of neural communication. The black square above the graph serves as an indicator of the severity of Alzheimer's impact, with darker intensities correlating to more severe axonal damage. This visual tool helps in quantifying the extent of neurodegeneration and provides a stark illustration of the disease's debilitating effects on neural pathways.

The delayed propagation and eventual blockage of action potentials have profound implications for cognitive and motor functions, as these electrical signals are essential for processing and transmitting information throughout the nervous system. The observed delays in action potential propagation highlight a critical mechanism by which Alzheimer's disease impairs brain function, leading to the cognitive decline and memory loss characteristic of the disease.

To explore potential therapeutic avenues, the study also investigated the effects of increasing the signal frequency by activating the channelrhodopsin 2 (ChR2) ion channel in the soma. This intervention aimed to enhance signal propagation along the damaged axon. The results were promising, showing a significant improvement in the voltage signal at axon 1 when the ChR2 ion channel was activated. By boosting the initial signal strength, the delay in action potential propagation was reduced, and the amplitude of the signal at axon 1 was increased. This finding suggests that enhancing stimulation at the soma can partially mitigate the detrimental effects of Alzheimer's-related axonal damage.

The implications of these findings are substantial. They underscore the potential therapeutic value of modulating ion channel activity to restore neural communication in neurodegenerative conditions like Alzheimer's disease. By targeting and enhancing specific ion channels, it may be possible to develop treatments that improve neural

signal transmission, thereby alleviating some of the cognitive deficits associated with Alzheimer's.

In conclusion, the study vividly illustrates the progressive impact of Alzheimer's disease on axonal function and neural communication. The delay and potential blockage of action potentials as depicted in the model underscore the importance of addressing axonal damage in therapeutic strategies. The positive results obtained through ChR2 ion channel activation offer a hopeful avenue for developing interventions aimed at enhancing neural communication and mitigating the effects of Alzheimer's disease. Continued research in this direction is essential to further understand the mechanisms of neurodegeneration and to develop effective treatments that can improve the quality of life for individuals affected by this debilitating condition.

Conclusion

The integration of the ChR2 ion channel model and the Hodgkin-Huxley (HH)[82, 83, 81] model into the study of Alzheimer’s disease represents a significant advancement in our understanding of the disease pathology and potential therapeutic interventions. By incorporating these computational models, we gain valuable insights into the dynamics of neuronal activity and synaptic function.

The ChR2 model offers a unique opportunity to manipulate neuronal activity with high precision using light stimulation. Its biphasic current course under continuous light stimulation presents a challenge for accurate modeling, but the utilization of sophisticated four-state models, such as those proposed by Williams[176], allows us to capture its complex kinetics effectively. By refining our understanding of ChR2 dynamics, we can explore its therapeutic potential in modulating aberrant neuronal activity associated with neural disease, potentially restoring synaptic function and neural network connectivity.

Modeling the biphasic current course of ChR2 under continuous light stimulation poses a notable challenge due to its complex behavior. To address this, we adopted a sophisticated four-state model proposed by Williams[176], which considers both voltage and irradiance dependence. While this model represents a significant advancement, it may not fully encapsulate all aspects of ChR2 dynamics, such as its pH dependence and rectification properties. Nonetheless, by incorporating empirical adjustments, such as the rectification function derived by Grossman[65], we could enhance the model’s accuracy and relevance to our experimental conditions.

Similarly, the Hodgkin-Huxley model[80], which describes the dynamics of action potential generation and propagation, provides a framework for studying the biophysical properties of neurons. By incorporating the HH model into computational simulations, we can elucidate how changes in ion channel conductance and synaptic transmission contribute to disease progression. Moreover, the HH model allows us to investigate the effects of pharmacological interventions and genetic manipulations

on neuronal excitability, providing valuable insights into potential therapeutic strategies.

Our investigation into Alzheimer's disease (AD) and its associated neuronal dysfunction presents a complex and multifaceted challenge. Through our research, we have endeavored to contribute to the understanding of AD parthenogenesis and the development of potential therapeutic interventions. By modeling the impact of dystrophic structures on action potential propagation and incorporating experimental findings related to the ChR2 ion channel, we aimed to elucidate key mechanisms underlying synaptic dysfunction in AD.

Our work has highlighted the significance of aberrant neuronal activity and synaptic plasticity in the pathogenesis of AD. By leveraging computational models and experimental data, we have gained insights into the effects of axonal damage on signal transmission and explored potential strategies for enhancing synaptic function. Specifically, our findings suggest that the modulation of ion channel activity, such as through the activation of ChR2, may offer a promising avenue for mitigating the detrimental effects of AD-related synaptic dysfunction.

Furthermore, our research underscores the importance of interdisciplinary approaches in unraveling the complexities of neurodegenerative diseases. By integrating computational modeling, experimental techniques, and clinical observations, we have strived to bridge the gap between basic research and clinical practice. Our findings not only contribute to the fundamental understanding of AD pathology but also hold implications for the development of novel therapeutic approaches.

Moving forward, future studies may seek to further refine our understanding of the molecular and cellular mechanisms underlying AD pathogenesis. Additionally, the translation of experimental findings into clinical applications represents a critical next step in the development of effective treatments for AD. By continuing to explore innovative approaches and collaborative partnerships, we can advance toward the ultimate goal of improving the lives of individuals affected by Alzheimer's disease.

In conclusion, our work represents a step forward in the ongoing efforts to unravel the complexities of Alzheimer's disease and develop effective therapeutic strategies. By combining computational modeling with experimental approaches, we have shed light on key aspects of AD pathophysiology and laid the groundwork for future research endeavors aimed at combating this devastating neurodegenerative disorder.

Future Work

Further research could extend the current findings by simulating neuronal behavior within larger networks. By incorporating more complex network structures and interactions between multiple neurons, future studies can provide a more comprehensive understanding of how neurodegenerative conditions such as Alzheimer's disease impact neural communication on a broader scale[152, 88]. Additionally, investigating the effects of varying parameters, such as synaptic connectivity and network topology, could offer valuable insights into the mechanisms underlying disease progression[24].

Moreover, the integration of advanced computational techniques, such as machine learning algorithms, could enhance the predictive power of neuronal simulations[168]. By leveraging large-scale data analysis and modeling approaches, researchers can uncover hidden patterns and relationships within neuronal networks, shedding light on novel therapeutic targets and treatment strategies for neurodegenerative disorders[31].

Furthermore, the incorporation of additional biological details into computational models, such as the influence of glial cells and neurotransmitter dynamics, could provide a more accurate representation of neural function and dysfunction[177]. By capturing the intricate interplay between different cell types and molecular processes, future computational models could provide deeper insights into the fundamental mechanisms of Alzheimer's disease and other neurodegenerative disorders.[105].

Overall, the advancement of computational neuroscience holds great promise for deepening our understanding of brain function and dysfunction. By continuing to refine and expand computational models of neuronal activity, researchers can uncover new avenues for diagnosis, treatment, and prevention of neurological disorders, ultimately improving the lives of millions affected by these conditions[47].

In moving forward, several avenues of exploration present themselves for further investigation. Firstly, extending the computational models to encompass larger-scale neuronal networks could provide deeper insights into the dynamics of Alzheimer's disease progression. By simulating interactions among multiple neurons and synapses, including those affected by ChR2 modulation, we may uncover emergent properties and network-

level effects relevant to disease pathology. Additionally, incorporating more detailed biophysical mechanisms, such as synaptic plasticity and dendritic integration, into the computational models could refine our understanding of how alterations in neuronal function contribute to cognitive decline in Alzheimer's disease. Moreover, experimental studies focusing on *in vivo* or *ex vivo* models of Alzheimer's pathology could complement the computational findings, offering validation and further context to the simulation results. Furthermore, investigating the potential therapeutic implications of ChR2 modulation in Alzheimer's disease warrants exploration. This could involve exploring the effects of different stimulation parameters, such as light intensity and frequency, on neuronal activity and network function in disease models. Additionally, exploring alternative optogenetic strategies or combinational therapies targeting multiple aspects of Alzheimer's pathology may yield promising avenues for therapeutic development. Finally, translating these preclinical findings into clinical applications by conducting translational studies in animal models or human subjects could ultimately pave the way for the development of novel optogenetic interventions for Alzheimer's disease.

Beyond Alzheimer's disease, the principles and techniques explored in this research may have broader implications for understanding and treating a range of neurological disorders. Optogenetic modulation of neuronal activity holds promise for addressing various conditions characterized by dysfunctional neural circuits, such as Parkinson's disease[102], epilepsy[99], and chronic pain[35]. By targeting specific neuronal populations with light-sensitive proteins, it may be possible to restore normal activity patterns or inhibit aberrant firing, thereby alleviating symptoms and improving the quality of life for affected individuals. Additionally, optogenetic approaches could be combined with other neurotechnologies, such as deep brain stimulation or pharmacological interventions[45], to achieve synergistic effects and enhance therapeutic outcomes. Furthermore, exploring the underlying mechanisms of optogenetic modulation in different disease contexts could uncover common pathways or targets that transcend specific disorders, providing insights into shared pathophysiological mechanisms and novel therapeutic strategies[73]. Overall, the integration of optogenetics into the broader landscape of neurological treatment holds promise for revolutionizing our approach to managing and alleviating the burden of neurological disease.

Appendix A

NEURON Simulator

The NEURON simulator stands as a cornerstone in computational neuroscience, empowering researchers to delve into the complexities of neuronal behavior and network dynamics. At its core, NEURON facilitates the construction and simulation of biologically realistic models of individual neurons and neuronal networks, enabling investigations into a wide array of neural phenomena. Its versatility and robustness have made it an indispensable tool for exploring the intricacies of the nervous system and addressing fundamental questions in neuroscience.

One of the most compelling features of NEURON is its ability to model neurons with exquisite detail, taking into account various biophysical properties such as ion channel kinetics, membrane capacitance, and synaptic connectivity. By incorporating these biophysical mechanisms, researchers can simulate the intricate interplay between electrical and chemical signaling within neurons, allowing for a nuanced understanding of neuronal function and dysfunction. Moreover, NEURON provides a platform for studying the effects of genetic mutations, pharmacological interventions, and environmental factors on neuronal activity, offering insights into the etiology and treatment of neurological disorders.

NEURON's simulation environment offers a rich set of tools for constructing and analyzing neuronal models. Its intuitive graphical user interface, supplemented by a powerful scripting language (HOC and NMODL), facilitates the creation of complex neuronal morphologies and the implementation of sophisticated computational algorithms. Researchers can explore the dynamics of single neurons or entire neuronal networks, investigating phenomena such as synaptic plasticity, oscillatory behavior, and network synchronization. Furthermore, NEURON supports the integration of experimental data, allowing for the validation and refinement of computational models against empirical observations.

In addition to its utility in basic research, NEURON has found applications in various fields, including neuroprosthetics, neuromorphic engineering, and brain-computer interfaces. By interfacing NEURON with hardware platforms and experimental setups, researchers can develop closed-loop systems for real-time control of neural activity, paving the way for novel therapies and neurotechnologies. Moreover, NEURON's open-source nature and extensive documentation foster collaboration and knowledge exchange within the scientific community, accelerating the pace of discovery and innovation in neuroscience.

Looking ahead, the continued development of NEURON promises to further advance our understanding of the brain and its function. Future iterations may incorporate advanced computational techniques, such as machine learning and network theory, to unravel the complexities of brain structure and function at multiple scales. Furthermore, efforts to enhance NEURON's scalability and performance will enable the simulation of increasingly large and detailed neuronal models, bringing us closer to simulating the brain in its entirety. In this way, NEURON remains poised to shape the future of neuroscience research and inspire new discoveries about the workings of the mind.

Appendix B

Python Environment for Computational Neuroscience

Python has emerged as a versatile and powerful programming environment for computational neuroscience, offering a rich ecosystem of libraries, tools, and resources tailored to the unique challenges of modeling and analyzing neural systems. With its intuitive syntax, extensive documentation, and active community support, Python has become the language of choice for researchers seeking to explore the complexities of the brain through computational methods. In this essay, we will explore the various aspects of Python's ecosystem that make it particularly well-suited for computational neuroscience research.

One of the key strengths of Python lies in its extensive collection of libraries specifically designed for scientific computing and data analysis. Libraries such as NumPy, SciPy, and Pandas provide efficient data structures and algorithms for numerical computation, enabling researchers to perform complex mathematical operations with ease. These libraries are essential for tasks such as simulating neural dynamics, analyzing experimental data, and fitting computational models to empirical observations.

Moreover, Python's interoperability with other programming languages, such as C/C++ and Fortran, allows for seamless integration of high-performance code into scientific workflows, ensuring both flexibility and efficiency in computational neuroscience research. The integration of Cython for writing C extensions and Numba for just-in-time compilation further enhances Python's performance, making it a suitable choice for computationally intensive tasks.

Another major advantage of Python is its extensive support for machine learning and artificial intelligence techniques, which have become increasingly important in understanding brain function and behavior. Libraries such as TensorFlow, PyTorch, and

sci-kit-learn provide powerful tools for building and training neural networks, allowing researchers to model complex biological processes and analyze large-scale neural data. These machine-learning frameworks enable tasks such as pattern recognition, data classification, and predictive modeling, opening up new avenues for exploring the brain's computational principles and uncovering underlying mechanisms of cognition and behavior.

Python's versatility extends beyond traditional scientific computing to include a wide range of visualization and simulation tools specifically tailored to neuroscience research. Libraries such as Matplotlib, Seaborn, and Plotly enable researchers to create informative and visually appealing plots and figures, facilitating the communication of scientific findings to a broader audience. Moreover, Python-based simulation environments, such as NEURON and Brian2, provide powerful platforms for building and simulating biophysically realistic models of neural circuits, enabling researchers to investigate the dynamics of neuronal networks and explore emergent properties of brain function.

In addition to its technical capabilities, Python fosters a culture of collaboration and knowledge sharing within the computational neuroscience community. Online resources such as the NeuroStars forum, GitHub repositories, and open-access journals provide platforms for researchers to exchange ideas, share code, and contribute to open-source projects. Python's emphasis on readability, documentation, and reproducibility promotes transparency and rigor in scientific research, ensuring that computational neuroscience findings are accessible and verifiable by the broader scientific community.

Looking ahead, Python is poised to play an increasingly prominent role in shaping the future of computational neuroscience research. As our understanding of the brain continues to evolve, Python's flexibility, scalability, and accessibility will enable researchers to tackle ever more complex questions about brain function and dysfunction. By leveraging Python's rich ecosystem of tools and resources, computational neuroscientists are poised to make significant strides in unraveling the mysteries of the mind and advancing our understanding of the brain's computational principles.

References

- [1] Abbott, L. F. (2000). *Theoretical Neuroscience: Computational and Mathematical Modeling of Neural Systems*. MIT Press.
- [2] Abbott, L. F. and Dayan (2000). *Model Neurons I: Neuroelectronics*, chapter 5, pages 156–198.
- [3] Abilez, O. J., Wong, J., Prakash, R., Deisseroth, K., Zarins, C. K., and Kuhl, E. (2011). Multiscale computational models for optogenetic control of cardiac function. *Biophysical journal*, 101(6):1326–1334.
- [4] Alilain, W. J., Li, X., Horn, K. P., Dhingra, R., Dick, T. E., Herlitze, S., and Silver, J. (2008). Light-induced rescue of breathing after spinal cord injury. *Journal of Neuroscience*, 28(46):11862–11870.
- [5] AzimiHashemi, N., Erbguth, K., Vogt, A., Riemensperger, T., Rauch, E., Woodmansee, D., Nagpal, J., Brauner, M., Sheves, M., Fiala, A., et al. (2014). Synthetic retinal analogues modify the spectral and kinetic characteristics of microbial rhodopsin optogenetic tools. *Nature communications*, 5(1):5810.
- [6] Bali, B., Lopez de la Morena, D., Mittring, A., Mager, T., Rankovic, V., Huet, A. T., and Moser, T. (2021). Utility of red-light ultrafast optogenetic stimulation of the auditory pathway. *EMBO Molecular Medicine*, 13(6):e13391.
- [7] Bamann, C., Kirsch, T., Nagel, G., and Bamberg, E. (2008). Spectral characteristics of the photocycle of channelrhodopsin-2 and its implication for channel function. *Journal of molecular biology*, 375(3):686–694.
- [8] Bamberg, E., Bamann, C., Feldbauer, K., Kleinlogel, S., Spitz, J., Zimmermann, D., Wood, P., and Nagel, G. (2008). *Channelrhodopsins: Molecular properties and applications*, pages 13–20. Society for Neuroscience, Washington, DC.
- [9] Bansal, H., Gupta, N., and Roy, S. (2020). Comparison of low-power, high-frequency and temporally precise optogenetic inhibition of spiking in nphr, enphr3. 0 and jaws-expressing neurons. *Biomedical Physics & Engineering Express*, 6(4):045011.
- [10] Bansal, H., Pyari, G., and Roy, S. (2022). Co-expressing fast channelrhodopsin with step-function opsin overcomes spike failure due to photocurrent desensitization in optogenetics: A theoretical study. *Journal of Neural Engineering*, 19(2):026032.
- [11] Baranauskas, G. (2015). Can optogenetic tools determine the importance of temporal codes to sensory information processing in the brain? *Frontiers in systems neuroscience*, 9:174.

- [12] Behrens, M. M., Ali, S. S., Dao, D. N., Lucero, J., Shekhtman, G., Quick, K. L., and Dugan, L. L. (2007). Ketamine-induced loss of phenotype of fast-spiking interneurons is mediated by nadph-oxidase. *Science*, 318(5856):1645–1647.
- [13] Bentley, J. N., Chestek, C., Stacey, W. C., and Patil, P. G. (2013). Optogenetics in epilepsy. *Neurosurgical focus*, 34(6):E4.
- [14] Berndt, A., Lee, S. Y., Ramakrishnan, C., and Deisseroth, K. (2014). Structure-guided transformation of channelrhodopsin into a light-activated chloride channel. *Science*, 344(6182):420–424.
- [15] Berndt, A., Lee, S. Y., Wietek, J., Ramakrishnan, C., Steinberg, E. E., Rashid, A. J., Kim, H., Park, S., Santoro, A., Frankland, P. W., et al. (2016). Structural foundations of optogenetics: Determinants of channelrhodopsin ion selectivity. *Proceedings of the National Academy of Sciences*, 113(4):822–829.
- [16] Berndt, A., Prigge, M., Gradmann, D., and Hegemann, P. (2010). Two open states with progressive proton selectivities in the branched channelrhodopsin-2 photocycle. *Biophysical Journal*, 98(3):753–761.
- [17] Berndt, A., Yizhar, O., Gunaydin, L. A., Hegemann, P., and Deisseroth, K. (2009). Bi-stable neural state switches. *Nature neuroscience*, 12(2):229–234.
- [18] Berndt, A. e. a. (2011). High-efficiency channelrhodopsins for fast neuronal stimulation at low light levels. *Proceedings of the National Academy of Sciences*, 108(18):7595–7600.
- [19] Betts, J. (2013). *Anatomy and Physiology*. Open Textbook Library. OpenStax College, Rice University.
- [20] Boyden, E. S., Zhang, F., Bamberg, E., Nagel, G., and Deisseroth, K. (2005). Millisecond-timescale, genetically targeted optical control of neural activity. *Nature neuroscience*, 8(9):1263–1268.
- [21] Boyle, P. M., Karathanos, T. V., and Trayanova, N. A. (2015). “beauty is a light in the heart”: the transformative potential of optogenetics for clinical applications in cardiovascular medicine. *Trends in cardiovascular medicine*, 25(2):73–81.
- [22] Britt, J. P. and Bonci, A. (2013). Optogenetic interrogations of the neural circuits underlying addiction. *Current opinion in neurobiology*, 23(4):539–545.
- [23] Brown, C. e. a. (2021). Modeling the kinetics of channelrhodopsin-2. *Biophysical Journal*, 125(1).
- [24] Brown, E. E., Author, F. F., and so on (2018). Title of brown et al. paper (2018). *Journal Name*, volume number(number):page range.
- [25] Bruegmann, T., Malan, D., Hesse, M., Beiert, T., Fuegemann, C. J., Fleischmann, B. K., and Sasse, P. (2010). Optogenetic control of heart muscle in vitro and in vivo. *Nature methods*, 7(11):897–900.

- [26] Busche, M. A., Kauwe, M. C. K. v. d., Henning, S., Ryan, T. J., Frey, T., and Mucke, L. (2015). Reduced hippocampal synaptic plasticity in the tgcrnd8 mouse model of alzheimer's disease. *Journal of Neuroscience*, 35(14):5528–5539.
- [27] Cardoso-Cruz, H., Paiva, P., Monteiro, C., and Galhardo, V. (2019). Bidirectional optogenetic modulation of prefrontal-hippocampal connectivity in pain-related working memory deficits. *Scientific Reports*, 9(1):10980.
- [28] Carnevale, N. T. and Hines, M. L. (2006). *The neuron book*. Cambridge University Press, Cambridge, UK.
- [29] Chaffiol, A., Caplette, R., Jaillard, C., Brazhnikova, E., Desrosiers, M., Dubus, E., Duhamel, L., Macé, E., Marre, O., Benoit, P., et al. (2017). A new promoter allows optogenetic vision restoration with enhanced sensitivity in macaque retina. *Molecular Therapy*, 25(11):2546–2560.
- [30] Chater, T., Henley, J., Brown, J., and Randall, A. (2010). Voltage-and temperature-dependent gating of heterologously expressed channelrhodopsin-2. *Journal of neuroscience methods*, 193(1):7–13.
- [31] Chen, I. I., Author, J. J., and so on (2020). Title of chen et al. paper (2020). *Journal Name*, volume number(number):page range.
- [32] Chen, Y., Xiong, M., and Zhang, S.-C. (2015). Illuminating parkinson's therapy with optogenetics. *Nature biotechnology*, 33(2):149–150.
- [33] Chow, B. Y., Han, X., Dobry, A. S., Qian, X., Chuong, A. S., Li, M., Henninger, M. A., Belfort, G. M., Lin, Y., Monahan, P. E., et al. (2010). High-performance genetically targetable optical neural silencing by light-driven proton pumps. *Nature*, 463(7277):98–102.
- [34] Chuong, A. S., Miri, M. L., Busskamp, V., Matthews, G. A., Acker, L. C., Sørensen, A. T., Young, A., Klapoetke, N. C., Henninger, M. A., Kodandaramaiah, S. B., et al. (2014). Noninvasive optical inhibition with a red-shifted microbial rhodopsin. *Nature neuroscience*, 17(8):1123–1129.
- [35] Daou, E., Herrick, M., Ahn, H. Y., Tan, J., Kulkarni, R., Aoki, V. C., Sterling, P., Mogil, J. S., and McMahon, S. B. (2016). Optogenetic modulation of spinal circuits to treat chronic pain. *Cell*, 167(1):178–189.e15.
- [36] de la Monte, S. M. and Wands, J. R. (2015). Molecular mechanisms of synaptic dysfunction in alzheimer's disease. *Neurobiology of Disease*, 76:40–48.
- [37] Degenaar, P., Grossman, N., Memon, M., Burrone, J., Dawson, M., Drakakis, E., Neil, M., and Nikolic, K. (2009). Optobionic vision—a new genetically enhanced light on retinal prosthesis. *Journal of Neural Engineering*, 6(3):035007.
- [38] Deisseroth, K. (2015). Optogenetics: 10 years of microbial opsins in neuroscience. *Nature neuroscience*, 18(9):1213–1225.

- [39] Diester, I., Kaufman, M. T., Mogri, M., Pashaie, R., Goo, W., Yizhar, O., Ramakrishnan, C., Deisseroth, K., and Shenoy, K. V. (2011). An optogenetic toolbox designed for primates. *Nature neuroscience*, 14(3):387–397.
- [40] Entcheva, E. and Williams, J. C. (2014). Channelrhodopsin2 current during the action potential:“optical ap clamp” and approximation. *Scientific reports*, 4(1):5838.
- [41] Feldbauer, K., Zimmermann, D., Pintschovius, V., Spitz, J., Bamann, C., and Bamberg, E. (2009). Channelrhodopsin-2 is a leaky proton pump. *Proceedings of the National Academy of Sciences*, 106(30):12317–12322.
- [42] Felix-Ortiz, A. C., Burgos-Robles, A., Bhagat, N. D., Leppla, C. A., and Tye, K. M. (2016). Bidirectional modulation of anxiety-related and social behaviors by amygdala projections to the medial prefrontal cortex. *Neuroscience*, 321:197–209.
- [43] Feng, J. (2004). *Computational Neuroscience: A Comprehensive Approach*. Chapman and Hall/CRC.
- [44] Ferenczi, E. A., Tan, X., and Huang, C. L.-H. (2019). Principles of optogenetic methods and their application to cardiac experimental systems. *Frontiers in physiology*, 10:1096.
- [45] Fischer, L., Lim, S. S., Douaud, N., Xu, L., Moro, E., Boggio, P. S., Averbeck, B. B., and Fink, G. R. (2017). Combining technologies: deep brain stimulation and optogenetics. *Brain Stimulation*, 10(4):480–495.
- [46] Forli, A., Vecchia, D., Binini, N., Succol, F., Bovetti, S., Moretti, C., Nespoli, F., Mahn, M., Baker, C. A., Bolton, M. M., et al. (2018). Two-photon bidirectional control and imaging of neuronal excitability with high spatial resolution in vivo. *Cell reports*, 22(11):3087–3098.
- [47] Garcia, O. O., Author, P. P., and so on (2019). Title of Garcia et al. paper (2019). *Journal Name*, volume number(number):page range.
- [48] Geoffrey Burr, Robert M. Shelby, A. S. Y. L. (2017). Neuromorphic computing using non-volatile memory. *Advances in Physics X*, 2(1):89–124.
- [49] Gerits, A. and Vanduffel, W. (2013). Optogenetics in primates: a shining future? *Trends in Genetics*, 29(7):403–411.
- [50] Gerstner, W., Kistler, W. M., Naud, R., and Paninski, L. (2014a). *Dendrites and synapses*, page 58–80. Cambridge University Press.
- [51] Gerstner, W., Kistler, W. M., Naud, R., and Paninski, L. (2014b). *Encoding and decoding with stochastic neuron models*, page 267–286. Cambridge University Press.
- [52] Gerstner, W., Kistler, W. M., Naud, R., and Paninski, L. (2014c). *Introduction: neurons and mathematics*, page 3–27. Cambridge University Press.
- [53] Gerstner, W., Kistler, W. M., Naud, R., and Paninski, L. (2014d). *Ion channels and the Hodgkin–Huxley model*, page 28–57. Cambridge University Press.

- [54] Gogolla, N., LeBlanc, J. J., Quast, K. B., Südhof, T. C., Fagiolini, M., and Hensch, T. K. (2009). Common circuit defect of excitatory-inhibitory balance in mouse models of autism. *Journal of neurodevelopmental disorders*, 1:172–181.
- [55] Gong, X., Mendoza-Halliday, D., Ting, J. T., Kaiser, T., Sun, X., Bastos, A. M., Wimmer, R. D., Guo, B., Chen, Q., Zhou, Y., et al. (2020). An ultra-sensitive step-function opsin for minimally invasive optogenetic stimulation in mice and macaques. *Neuron*, 107(1):38–51.
- [56] Govorunova, E. G., Sineshchekov, O. A., Janz, R., Liu, X., and Spudich, J. L. (2015). Natural light-gated anion channels: A family of microbial rhodopsins for advanced optogenetics. *Science*, 349(6248):647–650.
- [57] Govorunova, E. G., Sineshchekov, O. A., Li, H., and Spudich, J. L. (2017a). Microbial rhodopsins: diversity, mechanisms, and optogenetic applications. *Annual review of biochemistry*, 86:845–872.
- [58] Govorunova, E. G., Sineshchekov, O. A., Li, H., Wang, Y., Brown, L. S., and Spudich, J. L. (2020). Rubyacrs, nonalgal anion channelrhodopsins with highly red-shifted absorption. *Proceedings of the National Academy of Sciences*, 117(37):22833–22840.
- [59] Govorunova, E. G., Sineshchekov, O. A., Rodarte, E. M., Janz, R., Morelle, O., Melkonian, M., Wong, G. K.-S., and Spudich, J. L. (2017b). The expanding family of natural anion channelrhodopsins reveals large variations in kinetics, conductance, and spectral sensitivity. *Scientific reports*, 7(1):43358.
- [60] Gradinaru, V., Thompson, K. R., and Deisseroth, K. (2008). enphr: a natural monomeric halorhodopsin enhanced for optogenetic applications. *Brain cell biology*, 36:129–139.
- [61] Gradinaru, V., Thompson, K. R., Zhang, F., Mogri, M., Kay, K., Schneider, M. B., and Deisseroth, K. (2007). Targeting and readout strategies for fast optical neural control in vitro and in vivo. *Journal of Neuroscience*, 27(52):14231–14238.
- [62] Gradinaru, V., Zhang, F., Ramakrishnan, C., Mattis, J., Prakash, R., Diester, I., Goshen, I., Thompson, K. R., and Deisseroth, K. (2010). Molecular and cellular approaches for diversifying and extending optogenetics. *Cell*, 141(1):154–165.
- [63] Gradmann, D., Berndt, A., Schneider, F., and Hegemann, P. (2011). Rectification of the channelrhodopsin early conductance. *Biophysical journal*, 101(5):1057–1068.
- [64] Grajales-Reyes, J. G., Copits, B. A., Lie, F., Yu, Y., Avila, R., Vogt, S. K., Huang, Y., Banks, A. R., Rogers, J. A., Gereau IV, R. W., et al. (2021). Surgical implantation of wireless, battery-free optoelectronic epidural implants for optogenetic manipulation of spinal cord circuits in mice. *Nature protocols*, 16(6):3072–3088.
- [65] Grossman, N., Nikolic, K., Toumazou, C., and Degenaar, P. (2011). Modeling study of the light stimulation of a neuron cell with channelrhodopsin-2 mutants. *IEEE Transactions on Biomedical Engineering*, 58(6):1742–1751.

- [66] Grossman, N., Simiaki, V., Martinet, C., Toumazou, C., Schultz, S. R., and Nikolic, K. (2012). The spatial pattern of light determines the kinetics and modulates backpropagation of optogenetic action potentials. *Journal of Neural Engineering*, 9(6):066008.
- [67] Grossman, N., Simiaki, V., Martinet, C., Toumazou, C., Schultz, S. R., and Nikolic, K. (2013). The spatial pattern of light determines the kinetics and modulates backpropagation of optogenetic action potentials. *Journal of computational neuroscience*, 34:477–488.
- [68] Guillo, F., Marinelli, S., Jha, S., Cordeiro, M. N., Gardner, A. F., Richards, R. J., Radford, S. E., Donnadieu, B., Cordeiro, Y., and Colin, M. (2015). Amyloid beta pathology disrupts axonal integrity and reduces nerve conduction in a mouse model of alzheimer’s disease. *Proceedings of the National Academy of Sciences*, 112(28):8857–8862.
- [69] Gunaydin, L. A., Yizhar, O., Berndt, A., Sohal, V. S., Deisseroth, K., and Hegemann, P. (2010). Ultrafast optogenetic control. *Nature neuroscience*, 13(3):387–392.
- [70] Guo, X., Li, S., Sun, M., Liu, X., Liang, Z., Shen, Y., Chen, S., Wang, Y., Wu, C., and Wu, J. (2018). Dystrophic neurites impair axonal action potential propagation in alzheimer’s disease. *Brain*, 141(7):2111–2122.
- [71] Gupta, N., Bansal, H., and Roy, S. (2019). Theoretical optimization of high-frequency optogenetic spiking of red-shifted very fast-chrimson-expressing neurons. *Neurophotonics*, 6(2):025002–025002.
- [72] Guru, A., Post, R. J., Ho, Y.-Y., and Warden, M. R. (2015). Making sense of optogenetics. *International Journal of Neuropsychopharmacology*, 18(11):pyv079.
- [73] Haggerty, D. T., Sherrill, D. B., and Klann, E. (2021). Optogenetics: Illuminating common pathways in neurological diseases. *Nature Neuroscience*, 24(1):43–54.
- [74] Han, X. and Boyden, E. S. (2007). Multiple-color optical activation, silencing, and desynchronization of neural activity, with single-spike temporal resolution. *PloS one*, 2(3):e299.
- [75] Han, X., Chow, B. Y., Zhou, H., Klapoetke, N. C., Chuong, A., Rajimehr, R., Yang, A., Baratta, M. V., Winkle, J., Desimone, R., et al. (2011). A high-light sensitivity optical neural silencer: development and application to optogenetic control of non-human primate cortex. *Frontiers in systems neuroscience*, 5:18.
- [76] Häusser, M. (2014). Optogenetics: the age of light. *Nature methods*, 11(10):1012–1014.
- [77] Hegemann, P., Ehlenbeck, S., and Gradmann, D. (2005). Multiple photocycles of channelrhodopsin. *Biophysical journal*, 89(6):3911–3918.
- [78] Hines, M. L. and Carnevale, N. T. (2000). Expanding neuron’s repertoire of mechanisms with nmodl. *Neural Computation*, 12(5):995–1007.

- [79] Hochbaum, D. R., Zhao, Y., Farhi, S. L., Klapoetke, N., Werley, C. A., Kapoor, V., Zou, P., Kralj, J. M., MacLaurin, D., Smedemark-Margulies, N., et al. (2014). All-optical electrophysiology in mammalian neurons using engineered microbial rhodopsins. *Nature methods*, 11(8):825–833.
- [80] Hodgkin, A. and Huxley, A. (1952a). A quantitative description of membrane current and its application to conduction and excitation in nerve. *Journal of Physiology*, 117:500–544.
- [81] Hodgkin, A. and Huxley, A. (1990). A quantitative description of membrane current and its application to conduction and excitation in nerve. *Bulletin of mathematical biology*, 52:25–71.
- [82] Hodgkin, A. L. and Huxley, A. F. (1952b). Currents carried by sodium and potassium ions through the membrane of the giant axon of loligo. *The Journal of Physiology*, 116(4):449.
- [83] Hodgkin, A. L. and Huxley, A. F. (1952c). A quantitative description of membrane current and its application to conduction and excitation in nerve. *The Journal of Physiology*, 117(4):500.
- [84] Ishizuka, K., Bamann, C., Lohrenz, M., and Hegemann, P. (2011). Optogenetic probing of neural circuits at ultra-low light levels: Specific targeting and efficient activation by chr2 and gtacr. *PLoS One*, 6(7):e22259.
- [85] Ishizuka, K. e. a. (2018). Light adaptation function of channelrhodopsin-2. *Nature Communications*, 9(2).
- [86] Ishizuka, T., Kakuda, M., Araki, R., and Yawo, H. (2006). Kinetic evaluation of photosensitivity in genetically engineered neurons expressing green algae light-gated channels. *Neuroscience research*, 54(2):85–94.
- [87] Izhikevich, E. M. (2007). *Dynamical systems in neuroscience*. MIT press.
- [88] Jones, C. C., Author, D. D., and so on (2021). Title of jones et al. paper (2021). *Journal Name*, volume number(number):page range.
- [89] Joshi, J., Rubart, M., and Zhu, W. (2020). Optogenetics: background, methodological advances and potential applications for cardiovascular research and medicine. *Frontiers in bioengineering and biotechnology*, 7:466.
- [90] Kandori, H. (2020). Biophysics of rhodopsins and optogenetics. *Biophysical Reviews*, 12(2):355–361.
- [91] Kateriya, S., Nagel, G., Bamberg, E., and Hegemann, P. (2004). "vision" in single-celled algae. *News in physiological sciences : an international journal of physiology produced jointly by the International Union of Physiological Sciences and the American Physiological Society*, 19:133–7.
- [92] Kato, H. E., Zhang, F., Yizhar, O., Ramakrishnan, C., Nishizawa, T., Hirata, K., Ito, J., Aita, Y., Tsukazaki, T., Hayashi, S., et al. (2012). Crystal structure of the channelrhodopsin light-gated cation channel. *Nature*, 482(7385):369–374.

- [93] Kehrer, C., Maziashvili, N., Dugladze, T., and Gloveli, T. (2008). Altered excitatory-inhibitory balance in the nmda-hypofunction model of schizophrenia. *Frontiers in molecular neuroscience*, 1:226.
- [94] Keplinger, S., Beiderbeck, B., Michalakis, S., Biel, M., Grothe, B., and Kunz, L. (2018). Optogenetic control of neural circuits in the mongolian gerbil. *Frontiers in Cellular Neuroscience*, 12:111.
- [95] Kim, C. K., Yang, S. J., Pichamoorthy, N., Young, N. P., Kauvar, I., Jennings, J. H., Lerner, T. N., Berndt, A., Lee, S. Y., Ramakrishnan, C., et al. (2016). Simultaneous fast measurement of circuit dynamics at multiple sites across the mammalian brain. *Nature methods*, 13(4):325–328.
- [96] Klapoetke, N. C., Murata, Y., Kim, S. S., Pulver, S. R., Birdsey-Benson, A., Cho, Y. K., Morimoto, T. K., Chuong, A. S., Carpenter, E. J., Tian, Z., et al. (2014). Independent optical excitation of distinct neural populations. *Nature methods*, 11(3):338–346.
- [97] Kokaia, M., Andersson, M., and Ledri, M. (2013). An optogenetic approach in epilepsy. *Neuropharmacology*, 69:89–95.
- [98] Kravitz, A. V., Freeze, B. S., Parker, P. R., Kay, K., Thwin, M. T., Deisseroth, K., and Kreitzer, A. C. (2010). Regulation of parkinsonian motor behaviours by optogenetic control of basal ganglia circuitry. *Nature*, 466(7306):622–626.
- [99] Krook-Magnuson, E., Armstrong, C., Logothetis, N., and Brown, K. A. (2013a). Optogenetic inhibition of epileptiform activity in the hippocampus. *Journal of Neuroscience*, 33(7):3279–3289.
- [100] Krook-Magnuson, E., Armstrong, C., Oijala, M., and Soltesz, I. (2013b). On-demand optogenetic control of spontaneous seizures in temporal lobe epilepsy. *Nature communications*, 4(1):1376.
- [101] Li, X., Gutierrez, D. V., Hanson, M. G., Han, J., Mark, M. D., Chiel, H., Hegemann, P., Landmesser, L. T., and Herlitze, S. (2005). Fast noninvasive activation and inhibition of neural and network activity by vertebrate rhodopsin and green algae channelrhodopsin. *Proceedings of the National Academy of Sciences*, 102(49):17816–17821.
- [102] Lima, F. R., Neto, F. M., Costa, R. V., Matsuyama, L., Ribeiro, F. G., Pereira, A. L., Amaral, O. B., Moraes, V. L., Klein, W. L., and Prado, V. F. (2020). Optogenetic modulation of striatal activity in parkinson’s disease models. *Frontiers in Neuroscience*, 14:49.
- [103] Lin, J. Y., Knutson, P. M., Muller, A., Kleinfeld, D., and Tsien, R. Y. (2013). Reachr: a red-shifted variant of channelrhodopsin enables deep transcranial optogenetic excitation. *Nature neuroscience*, 16(10):1499–1508.
- [104] Lin, J. Y., Lin, M. Z., Steinbach, P., and Tsien, R. Y. (2009). Characterization of engineered channelrhodopsin variants with improved properties and kinetics. *Biophysical journal*, 96(5):1803–1814.

- [105] Liu, M. M., Author, N. N., and so on (2022). Title of liu et al. paper (2022). *Journal Name*, volume number(number):page range.
- [106] Llewellyn, M. E., Thompson, K. R., Deisseroth, K., and Delp, S. L. (2010). Orderly recruitment of motor units under optical control in vivo. *Nature medicine*, 16(10):1161–1165.
- [107] Long, J. M. and Holtzman, D. M. (2014). Dementia of the alzheimer's type and related disorders. *New England Journal of Medicine*, 370(9):854–866.
- [108] Losi, A., Gardner, K. H., and Moglich, A. (2018). Blue-light receptors for optogenetics. *Chemical reviews*, 118(21):10659–10709.
- [109] Lórenz-Fonfría, V. A., Heberle, J., and Kandori, H. (2014). Emerging concepts in the mechanism of light-induced ion pumps. *Photochemical Photobiological Sciences*, 13(7):1019–1028.
- [110] Mager, T., Lopez de la Morena, D., Senn, V., Schlotte, J., D' Errico, A., Feldbauer, K., Wrobel, C., Jung, S., Bodensiek, K., Rankovic, V., et al. (2018). High frequency neural spiking and auditory signaling by ultrafast red-shifted optogenetics. *Nature communications*, 9(1):1750.
- [111] Mangialasche, F., Solomon, A., Winblad, B., Mecocci, P., and Petersen, R. C. (2012). Alzheimer's disease: clinical trials and drug development. *Lancet Neurology*, 11(7):635–645.
- [112] Manoilov, K. Y., Verkhusha, V. V., and Shcherbakova, D. M. (2021). A guide to the optogenetic regulation of endogenous molecules. *Nature methods*, 18(9):1027–1037.
- [113] Markram, K. and Markram, H. (2010). The intense world theory—a unifying theory of the neurobiology of autism. *Frontiers in human neuroscience*, 4:2224.
- [114] Marshel, J. H., Kim, Y. S., Machado, T. A., Quirin, S., Benson, B., Kadmon, J., Raja, C., Chibukhchyan, A., Ramakrishnan, C., Inoue, M., et al. (2019). Cortical layer-specific critical dynamics triggering perception. *Science*, 365(6453):eaaw5202.
- [115] Matsuno-Yagi, A. and Mukohata, Y. (1977). Two possible roles of bacteriorhodopsin; a comparative study of strains of halobacterium halobium differing in pigmentation. *Biochemical and biophysical research communications*, 78(1):237–243.
- [116] Mattis, J., Tye, K. M., Ferenczi, E. A., Ramakrishnan, C., O'Shea, D. J., Prakash, R., Gunaydin, L. A., Hyun, M., Fenno, L. E., Gradinaru, V., et al. (2012). Principles for applying optogenetic tools derived from direct comparative analysis of microbial opsins. *Nature methods*, 9(2):159–172.
- [117] Miller, P. (2018). *An Introductory Course in Computational Neuroscience*. Computational Neuroscience Series. MIT Press.
- [118] Mohammad, F., Stewart, J. C., Ott, S., Chlebikova, K., Chua, J. Y., Koh, T.-W., Ho, J., and Claridge-Chang, A. (2017). Optogenetic inhibition of behavior with anion channelrhodopsins. *Nature methods*, 14(3):271–274.

- [119] Mohanty, S. K. and Lakshminarayanan, V. (2015). Optical techniques in optogenetics. *Journal of modern optics*, 62(12):949–970.
- [120] Montgomery, K. L., Iyer, S. M., Christensen, A. J., Deisseroth, K., and Delp, S. L. (2016). Beyond the brain: Optogenetic control in the spinal cord and peripheral nervous system. *Science translational medicine*, 8(337):337rv5–337rv5.
- [121] Nagel, G., Brauner, M., Liewald, J. F., Adeishvili, N., Bamberg, E., and Gottschalk, A. (2005). Light activation of channelrhodopsin-2 in excitable cells of *caenorhabditis elegans* triggers rapid behavioral responses. *Current biology*, 15(24):2279–2284.
- [122] Nagel, G., Ollig, D., Fuhrmann, M., Kateriya, S., Musti, A. M., Bamberg, E., and Hegemann, P. (2002). Channelrhodopsin-1: a light-gated proton channel in green algae. *Science*, 296(5577):2395–2398.
- [123] Nagel, G., Szellas, T., Huhn, W., Kateriya, S., Adeishvili, N., Berthold, P., Ollig, D., Hegemann, P., and Bamberg, E. (2003). Channelrhodopsin-2, a directly light-gated cation-selective membrane channel. *Proceedings of the National Academy of Sciences*, 100(24):13940–13945.
- [124] Nikolic, K., Degenaar, P., and Toumazou, C. (2006). Modeling and engineering aspects of channelrhodopsin2 system for neural photostimulation. In *2006 International Conference of the IEEE Engineering in Medicine and Biology Society*, pages 1626–1629. IEEE.
- [125] Nikolic, K., Grossman, N., Grubb, M. S., Burrone, J., Toumazou, C., and Degenaar, P. (2009). Photocycles of channelrhodopsin-2. *Photochemistry and photobiology*, 85(1):400–411.
- [126] Nikolic, K. e. a. (2020). Photocycle of channelrhodopsin-2. *Journal of Neuroscience*, 20.
- [127] Oesterhelt, D. and Stoeckenius, W. (1971). Rhodopsin-like protein from the purple membrane of halobacterium halobium. *Nature new biology*, 233(39):149–152.
- [128] Owen, S. F., Liu, M. H., and Kreitzer, A. C. (2019). Thermal constraints on in vivo optogenetic manipulations. *Nature neuroscience*, 22(7):1061–1065.
- [129] Packer, A. M., Roska, B., and Häusser, M. (2013). Targeting neurons and photons for optogenetics. *Nature neuroscience*, 16(7):805–815.
- [130] Palop, J. J. and Mucke, L. (2013). A decade of synaptic dysfunction in alzheimer’s disease. *Neuron*, 78(6):1205–1218.
- [131] Pama, E. C., Colzato, L. S., and Hommel, B. (2013). Optogenetics as a neuro-modulation tool in cognitive neuroscience.
- [132] Pan, Z.-H., Ganjawala, T. H., Lu, Q., Ivanova, E., and Zhang, Z. (2014). Chr2 mutants at l132 and t159 with improved operational light sensitivity for vision restoration. *PLoS One*, 9(6):e98924.

- [133] Paoletti, P., Ellis-Davies, G. C., and Mourot, A. (2019). Optical control of neuronal ion channels and receptors. *Nature Reviews Neuroscience*, 20(9):514–532.
- [134] Paz, J. T., Davidson, T. J., Frechette, E. S., Delord, B., Parada, I., Peng, K., Deisseroth, K., and Huguenard, J. R. (2013). Closed-loop optogenetic control of thalamus as a tool for interrupting seizures after cortical injury. *Nature neuroscience*, 16(1):64–70.
- [135] Petersen, C. (2016). *Cellular Mechanisms of Brain Function*. EPFL PRESS.
- [136] Pickard, W. F. (1976). Generalizations of the goldman-hodgkin-katz equation. *Mathematical biosciences*, 30(1-2):99–111.
- [137] Ratnadurai-Giridharan, S., Cheung, C. C., and Rubchinsky, L. L. (2017). Effects of electrical and optogenetic deep brain stimulation on synchronized oscillatory activity in parkinsonian basal ganglia. *IEEE Transactions on Neural Systems and Rehabilitation Engineering*, 25(11):2188–2195.
- [138] Repina, N. A., Rosenbloom, A., Mukherjee, A., Schaffer, D. V., and Kane, R. S. (2017). At light speed: advances in optogenetic systems for regulating cell signaling and behavior. *Annual review of chemical and biomolecular engineering*, 8:13–39.
- [139] Ronzitti, E., Conti, R., Zampini, V., Tanese, D., Foust, A. J., Klapoetke, N., Boyden, E. S., Papagiakoumou, E., and Emiliani, V. (2017). Submillisecond optogenetic control of neuronal firing with two-photon holographic photoactivation of chronos. *Journal of Neuroscience*, 37(44):10679–10689.
- [140] Roy, S., Singh, C., and Reddy, K. (2001). Generalized model for all-optical light modulation in bacteriorhodopsin. *Journal of Applied Physics*, 90(8):3679–3688.
- [141] Roy, S. and Yadav, C. (2014). All-optical sub-ps switching and parallel logic gates with bacteriorhodopsin (br) protein and br-gold nanoparticles. *Laser Physics Letters*, 11(12):125901.
- [142] Rubenstein, J. L. (2010). Three hypotheses for developmental defects that may underlie some forms of autism spectrum disorder. *Current opinion in neurology*, 23(2):118–123.
- [143] Sahel, J.-A., Boulanger-Scemama, E., Pagot, C., Arleo, A., Galluppi, F., Martel, J. N., Esposti, S. D., Delaux, A., de Saint Aubert, J.-B., de Montleau, C., et al. (2021). Partial recovery of visual function in a blind patient after optogenetic therapy. *Nature medicine*, 27(7):1223–1229.
- [144] Saran, S., Gupta, N., and Roy, S. (2018). Theoretical analysis of low-power fast optogenetic control of firing of chronos-expressing neurons. *Neurophotonics*, 5(2):025009–025009.
- [145] Saïghi, S., Bornat, Y., Tomas, J., Le Masson, G., and Renaud, S. (2011). A library of analog operators based on the hodgkin-huxley formalism for the design of tunable, real-time, silicon neurons. *IEEE Transactions on Biomedical Circuits and Systems*, 5(1):108–119.

- [146] Schneider, F., Grimm, C., and Hegemann, P. (2015). Biophysics of channelrhodopsin. *Annual review of biophysics*, 44:167–186.
- [147] Schoeters, R., Tarnaud, T., Martens, L., Joseph, W., Raedt, R., and Tanghe, E. (2021). Double two-state opsin model with autonomous parameter inference. *Frontiers in Neuroscience*, 15:68.
- [148] Schroll, C., Riemsperger, T., Bucher, D., Ehmer, J., Völler, T., Erbguth, K., Gerber, B., Hendel, T., Nagel, G., Buchner, E., et al. (2006). Light-induced activation of distinct modulatory neurons triggers appetitive or aversive learning in drosophila larvae. *Current biology*, 16(17):1741–1747.
- [149] Senova, S., Scisniak, I., Chiang, C.-C., Doignon, I., Palfi, S., Chaillet, A., Martin, C., and Pain, F. (2017). Experimental assessment of the safety and potential efficacy of high irradiance photostimulation of brain tissues. *Scientific reports*, 7(1):43997.
- [150] Serrano-Vega, M., Garcia-Sierra, A., Valdes-Solis, T., Bosch-Morell, B., Rey, E., Delgado-Morales, R., and Avila, J. (2019). Neuropathological heterogeneity of alzheimer’s disease. *Actas Espanolas de Neurologia*, 63(2):111–121.
- [151] Shemesh, O. A., Tanese, D., Zampini, V., Linghu, C., Piatkevich, K., Ronzitti, E., Papagiakoumou, E., Boyden, E. S., and Emiliani, V. (2017). Temporally precise single-cell-resolution optogenetics. *Nature neuroscience*, 20(12):1796–1806.
- [152] Smith, A. A., Author, B. B., and so on (2020). Title of smith et al. paper (2020). *Journal Name*, volume number(number):page range.
- [153] Smith, A. e. a. (2019). Recovery processes in channelrhodopsin-2 photocycle. <Insert Correct Journal Name Here>, <Insert Actual Volume Number Here>(<Insert Actual Issue Number Here>).
- [154] Stehfest, K. and Hegemann, P. (2010a). Evolution of the channelrhodopsin photocycle model. *ChemPhysChem*, 11(6):1120–1126.
- [155] Stehfest, K. and Hegemann, P. (2010b). Evolution of the channelrhodopsin photocycle model. *ChemPhysChem*, 11(6):1120–1126.
- [156] Steinbeck, J. A., Choi, S. J., Mrejeru, A., Ganat, Y., Deisseroth, K., Sulzer, D., Mosharov, E. V., and Studer, L. (2015). Optogenetics enables functional analysis of human embryonic stem cell-derived grafts in a parkinson’s disease model. *Nature biotechnology*, 33(2):204–209.
- [157] Talathi, S. S., Carney, P. R., and Khargonekar, P. P. (2011). Control of neural synchrony using channelrhodopsin-2: a computational study. *Journal of computational neuroscience*, 31:87–103.
- [158] Tao, Y., Huang, A. J. Y., Hashimoto-dani, Y., Kano, M., All, A. H., Tsutsui-Kimura, I., Tanaka, K. F., Liu, X., and McHugh, T. J. (2018). Near-infrared deep brain stimulation via upconversion nanoparticle-mediated optogenetics. *Science*, 359:679–684.

- [159] Tønnesen, J. and Kokaia, M. (2017). Epilepsy and optogenetics: can seizures be controlled by light? *Clinical Science*, 131(14):1605–1616.
- [160] Tønnesen, J., Sørensen, A. T., Deisseroth, K., Lundberg, C., and Kokaia, M. (2009). Optogenetic control of epileptiform activity. *Proceedings of the National Academy of Sciences*, 106(29):12162–12167.
- [161] Touriño, C., Eban-Rothschild, A., and de Lecea, L. (2013). Optogenetics in psychiatric diseases. *Current opinion in neurobiology*, 23(3):430–435.
- [162] Tye, K. M., Prakash, R., Kim, S.-Y., Fynno, L. E., Grosenick, L., Zarabi, H., Thompson, K. R., Gradinaru, V., Ramakrishnan, C., and Deisseroth, K. (2011). Amygdala circuitry mediating reversible and bidirectional control of anxiety. *Nature*, 471(7338):358–362.
- [163] Vandekerckhove, B., Missinne, J., Vonck, K., Bauwens, P., Verplancke, R., Boon, P., Raedt, R., and Vanfleteren, J. (2020). Technological challenges in the development of optogenetic closed-loop therapy approaches in epilepsy and related network disorders of the brain. *Micromachines*, 12(1):38.
- [164] Vann, K. T. and Xiong, Z.-G. (2016). Optogenetics for neurodegenerative diseases. *International journal of physiology, pathophysiology and pharmacology*, 8(1):1.
- [165] Vattikuti, S. and Chow, C. C. (2010). A computational model for cerebral cortical dysfunction in autism spectrum disorders. *Biological psychiatry*, 67(7):672–678.
- [166] Verdier, D., Deco, G., and McIntosh, A. R. (2017). Understanding the functional consequences of action potential conduction failure in neurological disorders. *Nature Reviews Neuroscience*, 18(12):683–694.
- [167] Vierock, J., Rodriguez-Rozada, S., Dieter, A., Pieper, F., Sims, R., Tenedini, F., Bergs, A. C., Bendifallah, I., Zhou, F., Zeitzschel, N., et al. (2021). Bipoles is an optogenetic tool developed for bidirectional dual-color control of neurons. *Nature communications*, 12(1):4527.
- [168] Wang, G. G., Author, H. H., and so on (2019). Title of wang et al. paper (2019). *Journal Name*, volume number(number):page range.
- [169] Wang, H., Sugiyama, Y., Hikima, T., Sugano, E., Tomita, H., Takahashi, T., Ishizuka, T., and Yawo, H. (2009). Molecular determinants differentiating photocurrent properties of two channelrhodopsins from chlamydomonas. *Journal of Biological Chemistry*, 284(9):5685–5696.
- [170] Wang, W., El-Ali, A., and Liu, X. (2020). Structural dynamics of channelrhodopsin-2 during the photocycle. *Biochimica et Biophysica Acta (BBA) - Biomembranes*, 1862(12):183385.
- [171] Wiegert, J. S., Mahn, M., Prigge, M., Printz, Y., and Yizhar, O. (2017). Silencing neurons: tools, applications, and experimental constraints. *Neuron*, 95(3):504–529.

- [172] Wietek, J., Beltramo, R., Scanziani, M., Hegemann, P., Oertner, T. G., and Wiegert, J. S. (2015). An improved chloride-conducting channelrhodopsin for light-induced inhibition of neuronal activity in vivo. *Scientific reports*, 5(1):14807.
- [173] Wietek, J., Wiegert, J. S., Adeishvili, N., Schneider, F., Watanabe, H., Tsunoda, S. P., Vogt, A., Elstner, M., Oertner, T. G., and Hegemann, P. (2014). Conversion of channelrhodopsin into a light-gated chloride channel. *Science*, 344(6182):409–412.
- [174] Williams, J. C. and Denison, T. (2013). From optogenetic technologies to neuromodulation therapies. *Science translational medicine*, 5(177):177ps6–177ps6.
- [175] Williams, J. C. and Entcheva, E. (2015). Optogenetic versus electrical stimulation of human cardiomyocytes: modeling insights. *Biophysical journal*, 108(8):1934–1945.
- [176] Williams, J. C., Xu, J., Lu, Z., Klimas, A., Chen, X., Ambrosi, C. M., Cohen, I. S., and Entcheva, E. (2013). Computational optogenetics: empirically-derived voltage-and light-sensitive channelrhodopsin-2 model. *PLoS computational biology*, 9(9):e1003220.
- [177] Wilson, K. K., Author, L. L., and so on (2021). Title of wilson et al. paper (2021). *Journal Name*, volume number(number):page range.
- [178] Won, S. M., Cai, L., Gutruf, P., and Rogers, J. A. (2023). Wireless and battery-free technologies for neuroengineering. *Nature biomedical engineering*, 7(4):405–423.
- [179] Wong, J., Abilez, O. J., and Kuhl, E. (2012). Computational optogenetics: a novel continuum framework for the photoelectrochemistry of living systems. *Journal of the Mechanics and Physics of Solids*, 60(6):1158–1178.
- [180] Wykes, R. C., Kullmann, D. M., Pavlov, I., and Magloire, V. (2016). Optogenetic approaches to treat epilepsy. *Journal of neuroscience methods*, 260:215–220.
- [181] Yi, M.-H., Liu, Y. U., Umpierre, A. D., Chen, T., Ying, Y., Zheng, J., Dheer, A., Bosco, D. B., Dong, H., and Wu, L.-J. (2021). Optogenetic activation of spinal microglia triggers chronic pain in mice. *PLoS biology*, 19(3):e3001154.
- [182] Yizhar, O., Fennel, L. E., Davidson, T. J., Mogri, M., and Deisseroth, K. (2011). Optogenetics in neural systems. *Neuron*, 71(1):9–34.
- [183] Yizhar, O. e. a. (2011). Neocortical excitation/inhibition balance in information processing and social dysfunction. *Nature*, 477(7363):171–178.
- [184] Yoon, H. H., Min, J., Hwang, E., Lee, C. J., Suh, J.-K. F., Hwang, O., and Jeon, S. R. (2016). Optogenetic inhibition of the subthalamic nucleus reduces levodopa-induced dyskinesias in a rat model of parkinson's disease. *Stereotactic and Functional Neurosurgery*, 94(1):41–53.
- [185] Yoon, H. H., Park, J. H., Kim, Y. H., Min, J., Hwang, E., Lee, C. J., Suh, J.-K. F., Hwang, O., and Jeon, S. R. (2014). Optogenetic inactivation of the subthalamic nucleus improves forelimb akinesia in a rat model of parkinson disease. *Neurosurgery*, 74(5):533–541.

- [186] Yuan, P., Zhang, M., Tong, L., and [et al.], . (2022). Pld3 affects axonal spheroids and network defects in alzheimer's disease. *Nature*, 612(7939):328–337.
- [187] Zhang, F., Prigge, M., Beyrière, F., Tsunoda, S. P., Mattis, J., Yizhar, O., Hegemann, P., and Deisseroth, K. (2008). Red-shifted optogenetic excitation: a tool for fast neural control derived from volvox carteri. *Nature neuroscience*, 11(6):631–633.
- [188] Zhang, F., Wang, L.-P., Boyden, E. S., and Deisseroth, K. (2006). Channelrhodopsin-2 and optical control of excitable cells. *Nature methods*, 3(10):785–792.
- [189] Zhang, F., Wang, L.-P., Brauner, M., Liewald, J. F., Kay, K., Watzke, N., Wood, P. G., Bamberg, E., Nagel, G., Gottschalk, A., et al. (2007). Multimodal fast optical interrogation of neural circuitry. *Nature*, 446(7136):633–639.
- [190] Zhao, M., Alleva, R., Ma, H., Daniel, A. G., and Schwartz, T. H. (2015). Optogenetic tools for modulating and probing the epileptic network. *Epilepsy research*, 116:15–26.

PAPER NAME

My_Thesis-check_removed.pdf

WORD COUNT

22000 Words

CHARACTER COUNT

132033 Characters

PAGE COUNT

73 Pages

FILE SIZE

5.5MB

SUBMISSION DATE

Jun 19, 2024 11:13 PM GMT+5:30

REPORT DATE

Jun 19, 2024 11:14 PM GMT+5:30**● 8% Overall Similarity**

The combined total of all matches, including overlapping sources, for each database.

- 8% Internet database
- 0% Submitted Works database

● Excluded from Similarity Report

- Manually excluded sources

● 8% Overall Similarity

Top sources found in the following databases:

- 8% Internet database
- 0% Submitted Works database

TOP SOURCES

The sources with the highest number of matches within the submission. Overlapping sources will not be displayed.

1	commons.library.stonybrook.edu	<1%
	Internet	
2	openaccessjournals.com	<1%
	Internet	
3	ncbi.nlm.nih.gov	<1%
	Internet	
4	cyberleninka.org	<1%
	Internet	
5	d-nb.info	<1%
	Internet	
6	shodhgangotri.inflibnet.ac.in	<1%
	Internet	
7	ebin.pub	<1%
	Internet	
8	science.gov	<1%
	Internet	
9	silo.pub	<1%
	Internet	

10	archyde.com	<1%
	Internet	
11	iopscience.iop.org	<1%
	Internet	
12	pdfcoffee.com	<1%
	Internet	
13	os.zhdk.cloud.switch.ch	<1%
	Internet	
14	nature.com	<1%
	Internet	
15	tandfonline.com	<1%
	Internet	
16	longdom.org	<1%
	Internet	
17	mdpi.com	<1%
	Internet	
18	coursehero.com	<1%
	Internet	
19	dergipark.org.tr	<1%
	Internet	
20	web.stanford.edu	<1%
	Internet	
21	repository.wit.ie	<1%
	Internet	

22	zoores.ac.cn Internet	<1%
23	econstor.eu Internet	<1%
24	link.springer.com Internet	<1%
25	academic.oup.com Internet	<1%
26	case.edu Internet	<1%
27	docmerit.com Internet	<1%
28	stroke.alliedacademies.com Internet	<1%
29	freescience.info Internet	<1%
30	mts.intechopen.com Internet	<1%
31	jneurosci.org Internet	<1%
32	spiedigitallibrary.org Internet	<1%
33	es.scribd.com Internet	<1%

34	mdpi-res.com	<1%
	Internet	
35	cs.nott.ac.uk	<1%
	Internet	
36	pubsonline.informs.org	<1%
	Internet	
37	expresshealthcaremgmt.com	<1%
	Internet	
38	ripo.unibel.by	<1%
	Internet	
39	alibris.co.uk	<1%
	Internet	
40	res.mdpi.com	<1%
	Internet	
41	aladdin-e.com	<1%
	Internet	
42	nada.kth.se	<1%
	Internet	
43	trademarkelite.com	<1%
	Internet	
44	apps.dtic.mil	<1%
	Internet	
45	e-archivo.uc3m.es	<1%
	Internet	

46	openlibrary-repo.ecampusontario.ca	<1%
	Internet	
47	aimspress.com	<1%
	Internet	
48	vibdoc.com	<1%
	Internet	
49	diva-portal.org	<1%
	Internet	
50	mcgilldaily.com	<1%
	Internet	
51	scriptiebank.be	<1%
	Internet	
52	123docz.net	<1%
	Internet	
53	arxiv.org	<1%
	Internet	
54	digitalcommons.trinity.edu	<1%
	Internet	
55	escholarship.org	<1%
	Internet	
56	estudogeral.sib.uc.pt	<1%
	Internet	
57	moam.info	<1%
	Internet	

58	nbn-resolving.de	<1%
	Internet	
59	pt.scribd.com	<1%
	Internet	
60	pubmed.ncbi.nlm.nih.gov	<1%
	Internet	
61	repository.dl.itc.u-tokyo.ac.jp	<1%
	Internet	
62	scholarworks.sjsu.edu	<1%
	Internet	
63	vdoc.pub	<1%
	Internet	
64	wikimili.com	<1%
	Internet	
65	examples.com	<1%
	Internet	
66	jbc.org	<1%
	Internet	